University of Southern Queensland

Faculty of Engineering & Survey

Safety risks associated with HV electrical equipment at the point of imminent failure.

A dissertation submitted by

Mr Chase Matthew Richardson

In fulfilment of the requirements of

ENG4111/4112 Research Project

Towards the degree of

Bachelor of Engineering (Honours) (Electrical & Electronic)

Submitted: October 2023

ABSTRACT

The risk of an electrical arc blast or explosion and subsequent pressure waves are a major concern with high voltage (HV) equipment that is at risk of imminent failure (ERF). Projectiles caused by the fragmentation of an ERF, and the distances that they can travel, present challenges when trying to maintain safety. This paper investigates the relationship between the available energy during an arc blast event and the distance that projectiles can travel by simulating a gapless porcelain surge arrestor failure.

The current Energy Queensland Limited (EQL) procedures for enabling ERF to remain energised is based on the Network Access Restriction (NAR). It outlines the controls that must be adhered to in order to maintain risks to As Low As Reasonably Practical (ALARP). A key component of a NAR is the establishment of a Risk Management Hazard Zone (RMHZ) which is an exclusion zone around the ERF. The current outdoor distance settings for RMHZ are typically 25 metres when there is a potential of projectiles, though this is yet to be fully rationalised.

Initial research used a primitive porcelain cylinder filled with TNT explosive to represent the surge arrestor during a simulated arc blast explosion. Advanced computational modelling, using hydrocode, were used to simulate the energy, pressure, and time required to fragment the cylinder. Modelling solutions were compared to a physics based projectile model script, which considered the available energy, drag, height, and distance a porcelain fragment could travel. The collated data from these models were analysed to determine the accuracy of each one against a known incident/event.

The time for fragmentation to occur was identified as a critical component, which through observation, closely relates to initial pressure rise. This led to an investigation into the vaporisation of internal material as a potential cause of the pressure rise. Copper was used for this analysis due to both the availability of its material properties and its common use within electrical equipment. It was identified that only a small amount of copper mass was required to be vaporised to exceed the tensile strength of a HV porcelain shell.

An electrical arc blast explosion is a nonlinear explicit time event with the projectiles expelled early in the event. This presented several challenges when attempting to predict the amount of energy available to a projectile, which modelling indicates would be hazardous during the entire flight path. It is recommended that further research, including physical testing in a controlled environment, would benefit network owners, power workers, and the public.

Chase Richardson [redacted]

University of Southern Queensland

Faculty of Engineering and Surveying

ENG4111/2 Research Project

Limitations of Use

The Council of the University of Southern Queensland, its Faculty of Engineering and Surveying, and the staff of the University of Southern Queensland, do not accept any responsibility for the truth, accuracy, or completeness of material contained within or associated with this dissertation.

Persons using all or any part of this material do so at their own risk, and not at the risk of the Council of the University of Southern Queensland, its Faculty of Engineering and Surveying or the staff of the University of Southern Queensland.

This dissertation reports an educational exercise and has no purpose or validity beyond this exercise. The sole purpose of the course pair entitled “Research Project” is to contribute to the overall education within the student’s chosen degree program. This document, the associated hardware, software, drawings, and other material set out in the associated appendices should not be used for any other purpose: if they are so used, it is entirely at the risk of the user.

Dean

Faculty of Health, Engineering & Sciences

Certification of Dissertation

I certify that the ideas, designs, and experimental work, results, analyses, and conclusion set out in this dissertation are entirely my own effort, except where otherwise indicated and acknowledged.

I further certify that the work is original and has not been previously submitted for assessment in any other course or institution, except where specifically stated.

Chase Matthew Richardson

[redacted]

_____

Signature: [redacted]

_____

Date: October 2023

Acknowledgements

The journey to this point has not been straightforward or smooth. I would like to thank everyone who has guided me, supported me and those non-believers, without all of you I would not have made it to this point. There are many people that I have met and assisted me in reaching this point, but a few special mentions are:

Firstly, my loving wife Ashlee and our absolutely awesome kids Aimee and Blake, you guys make all the struggles to this point worthwhile.

Secondly, Tony Ahfock, your support of this dissertation has furthered my understanding of the topic and supported my development towards becoming an electrical engineer, thank-you.

Lastly the two industry leaders who gave me the idea to conduct the research, Dan Warne and Matthew Ridgely.

Chase Richardson

University of Southern Queensland

October 2023

CONTENTS

LIST OF FIGURES

LIST OF TABLES

NOMENCLATURE

ALARP	As Low As Reasonably Practical
ASB	Area of Solid Bases
CB	Circuit Breaker
CD	Coefficient of Drag
DMP	Defect Management Plan
EOS	Equation of State
EQL	Energy Queensland Limited
ERF	Equipment at Risk of imminent Failure
ESA	External Surface Area
FMEA	Failure Modes and Effects Analysis
GUI	Graphical User Interface
HV	High voltage
IDE	Integrated Development Environment
IEEE	Institute of Electrical and Electronics Engineers
ISA	Internal Surface Area
KE	Kinetic Energy
kJ	kilo Joules
kV	kilo Volt
LSA	Lateral Surface Area
MJ	Mega Joule
MOSA	Metal-Oxide Surge Arrester
MPa	Mega Pascal
MVA	Mega Volt Amps
NAR	Network Access Restriction
PPE	Personal Protective Equipment
QRA	Quantitative Risk Assessments
RMHZ	Risk Management Hazard Zone

RREQ	Registered Professional Engineers Queensland
SiC	Silicon Carbide
TNT	Tri Nitro Toluene
TSA	Total Surface Area
VScode	Visual Studio Code
ZnO	Zinc Metal Oxide
2D	Two-Dimensional
3D	Three-Dimensional

NOTATION

a	acceleration in m/s
a_x	Acceleration in the x direction in m/s
b	Mass flow rate in kg/s
C	Specific heat in kJ/kg.K
d	Depth / thickness
D	Distance in metres
E	Energy in m^2/s^2 or Joules
F	Force in N
g	Gravitational acceleration in m/s^2
h	Height in metres
I	Current in ampere
I_{arc}	Arc Current in kilo Amps
L	Latent heat in kJ
m	mass in kg
ms	milliseconds
P	Pressure in pascal (Pa)
t	Time in seconds
v	Voltage in volts
V	Volume in m^3
V_0	Initial velocity in m/s
$V_{Terminal}$	Terminal velocity in m/s
V_x	Velocity in the x direction with respect to time in m/s
V_{x0}	Initial velocity in the x direction with respect to time in m/s
V_y	Velocity in the y direction with respect to time in m/s
V_{y0}	Initial velocity in the y direction with respect to time in m/s
Q	Energy in Joules
R	Gas Constant
r	Radius
ρ	Density

1 INTRODUCTION

1.1 INTRODUCTION

Sudden failure of High Voltage (HV) equipment can cause injury or death to employees or members of the public. Operators of HV transmission and distribution networks are responsible for maintaining electrical supply to customers while ensuring the highest standards of safety are met. In developed nations, like Australia, the reliable supply of electricity is fast becoming more than an expectation and can be perceived as a human right. This places additional pressure on electrical networks to maintain electricity supply especially for important infrastructure and services.

Gulski et al. (2005) identifies that network operators are required to maintain a robust reliable network while keeping within a given budget. This presents a challenge when deciding what type of HV equipment are kept on hand as strategic spares. Problems arise when equipment types or models outside of stock holdings are exposed to fault conditions or deterioration has occurred quicker than expected. In these situations, where it is safe to do so, operators may be required to leave the equipment at risk of imminent failure (ERF) energised while awaiting maintenance or replacement.

In accordance with Energy Queensland Limited's (EQL) Network Risk Framework (2021), a risk assessment is performed to decide whether to keep the ERF energised. Current practices within EQL require experienced electrical engineers that hold the Registered Professional Engineers Queensland (RPEQ) credentials to assess and provide direction as to whether it is possible to leave the ERF energised. If the risk is deemed acceptable, a Network Access Restriction (NAR) will be issued which details what controls are to be put in place to allow the ERF to remain energised.

A major part of the NAR process is determining the Risk Management Hazard Zone (RMHZ). This is the area in which it is deemed unsafe for people to be within due to the possibility of electrical arc blasts or explosions and the subsequent pressure waves. The current practice at EQL when setting the RMHZ is to use a 25-metre zone for an ERF (EQL 2022) that is constructed from materials that have the potential to fragment during an electrical explosion. The 25-metre zone reduces the risk of hazardous projectiles, though historical incidents have identified that projectiles have travelled beyond 25 metres.

1.2 THE PROBLEM

Currently, there is a gap in the knowledge as to what constitutes a safe distance in relation to protecting personnel from electrical arc blasts and the pressure waves in the open environment. In the event of a blast, fragments of the ERF become projectiles; porcelain materials being of most concern due to the brittle nature of the material. The current practise (EQL 2022) is to mitigate potential hazards, including projectiles, by establishing an RMHZ around the ERF. The effectiveness of the RMHZ distances have not been thoroughly quantified by theoretical calculation, simulation, or practical testing. This risk is realised when materials used to construct the ERF form part of the hazard within the arc blast danger area in the form of projectiles.

Utilising historical incident data, a porcelain insulated gapless surge arrester was chosen for the modelling of the electrical arc blast. The internal components of the surge arrester are Zinc Metal Oxide (ZnO) and aluminium tube spacers. These materials are exposed to the extreme temperature changes during a HV electrical fault, creating a rapid temperature and pressure change (Australian Energy Council 2019).

The three-dimensional nature of the explosion and the explicit time frames involved prohibits hand calculation and restricts mathematically scripted models using software packages including MatLab or Python. The amount of computation required to obtain an initial understanding of this event, and the resultant fragmentation of the outer porcelain insulation shell required nonlinear explicit dynamic modelling to be carried out (Century-Dynamics 2005).

1.3 RESEARCH OBJECTIVES

The aim of this research is to attempt to quantify the hazardous area around a given piece of HV equipment. This will allow for the expansion of the EQL NAR management processes with the initial focus on analysing the electrical arc blast and discharge potential created by the pressure change within the ERF. This requires:

- Computational analysis of incident energy from a known EQL event using formulae from literature.
- Simulation of the porcelain gapless surge arrester in the open environment using a nonlinear explicit dynamic model using Ansys software suites.

- Physics based projectile trajectory modelling using the MatLab scripting software.

The findings of the modellings can then be applied to several other simulation configurations including equipment mounted on a wall, ground, and similar combinations. The outcomes from the modelling can be utilised in the design of a future risk calculator for RMHZ within the automated NAR process tool. The final objective is to provide further evidence around safe distances that engineers can consider when developing the settings of RMHZ as part of an NAR.

1.4 SUMMARY

The simulation of the electrical arc blast using the incident energy from a known EQL incident has been conducted. The fragmentation of a gapless porcelain surge arrester has been partially simulated using the explicit dynamic suite within Ansys software. A second projectile modelling technique using physics-based formulae was also developed to enable comparison and, where possible, validation.

The outcome from this research has the potential to improve safety practices in situations where HV electrical equipment are known to have reached ERF. The results will provide EQL with a foundation to improve the RMHZ as well as improving the future design and construction of HV installations. These improvements will benefit both employees who work on and around HV equipment as well as assist engineers in making informed decisions about a given situation. The danger or hazard will still be present, but the goal is to reduce the risk level to the lowest possible level while still ensuring safety and continuity of supply to the community.

2 CONSEQUENCES AND ETHICS

2.1 CONSEQUENTIAL EFFECTS

Research into this project topic was selected to gather further information to assist with the quantification of the RMHZ. The current standard for setting the RMHZ requires RPEQ registered engineers to conduct bespoke assessments for the identified HV equipment to determine the size the exclusion zone. Consequences of these decisions have a direct impact on the safety of the electrical supply network and when personnel have cause to be in the vicinity. Making these decisions can be particularly difficult when trying to maintain electricity supply with legacy designs and equipment where RMHZ was not considered. Outcomes from this research should assist the engineers responsible to make a better-informed decision regarding required RMHZ distances.

2.2 ETHICAL RESPONSIBILITIES

This undergraduate dissertation utilises both private and publicly available information to examine the electrical arc blast phenomena. The use of EQLs private electrical incident investigation reports and the associated data has enabled the formulation of a set of initial parameters to base both mathematical and simulation models on. To use this private information ethical standards were required to be upheld, to maintain the privacy of that information which is not publicly available. This is achieved by not divulging any information about incidents other than the fault data required to calculate the potential incident energy, HV equipment type, and construction.

The publicly available information used within this research is collated from electronic sources accessed via the university's library website or general internet searches. This information is collected responsibly with all reference material and associated citations continually updated into the referencing software package EndNote. The sources for formulae and supporting ideas are documented throughout the dissertation in accordance with ethical responsibility of academic writings using citations.

3 LITERATURE REVIEW

3.1 CHAPTER OVERIEW

The available knowledge of electrical hazards associated with electrical arc flashes and blasts has been investigated. The initial stages of this research were conducted while completing the research proposal for ENG4110 – Research Methodology. The literature review also evaluates risk-based analysis, EQL's risk framework, EQL's NAR, the standards associated with arc flash and blasts, HV equipment construction types, pressure waves analysis, projectile modelling, surge arrester devices, the analysis modelling software package Ansys Explicit Dynamics, and Autodyn, explicit time and vaporisation of materials. These topic areas enable a better understanding of the challenges that exist in quantifying the risks associated with HV equipment failure.

3.2 LITERATURE

3.2.1 Risk Assessment

Risk assessment and management has been employed in the power industry for many years. This was highlighted by Muhr and Sumereder (2008) who discussed the four steps of risk management which includes risk identification, risk analysis and evaluation, risk handling and finally risk control. When it comes to the analyses of a given hazardous HV situation the NAR process follows these same steps. By doing so the risks can be identified and managed to ensure where possible they are eliminated or reduced to As Low As Reasonably Practicable (ALARP).

The risk assessment process is also required to be aligned with the Australian Standard, Risk management: Principles and guidelines AS/NZS ISO 31000:2009 (2004). This standard describes the processes and techniques that are required to identify and evaluate a threat or hazard. These methods include: qualitative, for ranking from low to high; semi quantitative, for likelihood; and Quantitative Risk Assessments (QRA), for consideration of the probability. The equations that form part of these assessments are as follows:

$$Qualitative = Low, Medium\ or\ High \quad (1)$$

$$Semi - Quantitative\ Risk = Consequence * Likelihood \quad (2)$$

$$Quantitative\ Risk = Probability\ of\ stated\ Consequence \quad (3)$$

The QRA that will be applied to this research will be the Failure Modes and Effects Analysis (FMEA), which is commonly used in maintenance planning (*Network Risk Framework* 2021).

3.2.2 Network Access Restriction (NAR)

To ensure the safety of electrical workers that work on and around the HV transmission and distribution network, the NAR tool was developed by EQL. It provides information about the hazards and the controls that exist at a particular site location when invoked. (*Guide to Preparing Network Access Restriction Documentation* 2015) These controls are developed using the risk assessment process where risk mitigations are applied to the hazard. This includes the establishment of a RMHZ and the reconfiguration of the actual network where applicable. The NAR is currently developed by a minimum of three engineers to ensure that electrical workers can safely work around electrical plant and equipment at risk of imminent failure.

3.2.3 Arc-Flash Hazard Standards

The Institute of Electrical and Electronics (IEEE) have produced a standard for the calculation of arc flashes and hazard calculation (*IEEE Std 1584-2018 (Revision of IEEE Std 1584-2002): IEEE Guide for Performing Arc-Flash Hazard Calculations* 2018). Within this standard, extensive work has been conducted to establish the danger area from several theoretical and practical tests. These studies assisted with the development of formulae for the computational analysis of this research.

The investigation of electrical arc flash and the distance it can travel from the source was carried out by Ralph Lee in the 1980's (Hoagland et al. 2016). Arc flash calculations have been proposed by other researchers, including the study 'Predicting incident energy to better manage the electric arc hazard on 600-V power distribution systems' (Doughty et al. 2000), who provided calculations for arc flash on three-phase systems. The IEEE uses Lee's calculations within the standard. He developed an equation for arc flash that calculates the initial impulse

force, with Pressure (P) in lbs/ft^2, Current (I_{arc}) in kilo Amps, and Distance (D) in feet. The formula is as follows:

$$P = \frac{11.58 * I_{arc}}{D^{0.9}} \quad (4)$$

The results generated using this equation are useful for quantifying the minimum clearances required to minimise radiation burns associated with arc flash in an indoor environment and especially in the vicinity of a switchboard.

The other standard that is quoted within the study of arc flash and blast is the electrical safety code manual also known as the NFPA70E (Keller 2010). The term energy incident is detailed through calculation and the formula to determine the distance (D_c) from an energy source. The variables within the equation are Power in Mega Volt Amps (MVA), and time (t). The formula is as follows:

$$D_c = [53 * MVA * t]^{\frac{1}{2}} \quad (5)$$

Time is the variable which has the most effect on the distance for this equation which is an important consideration when carrying out energy and fault calculations. Other formulae outlined within the NFPA70E include:

$$Energy\ (E) = Power(P) * Time(t) \quad (6)$$

$$Power\ (P) = Volts(V) * Amps(I) \quad (7)$$

$$Calories(E) = Volts(V) * Amps(I) * Time(t) \quad (8)$$

$$1\ Calorie = 4.1868\ watts\ per\ second \quad (9)$$

$$1\ Joule = 1\ watt\ per\ second \quad (10)$$

These formulae apply physics fundamentals to demonstrate the connections between power, energy, and time. These parameters were used to further develop a theoretical hazardous distance for different equipment locations.

3.2.4 HV Equipment

A wide variety of HV equipment is required to operate a distribution or transmission network. The construction and insulation types associated with this equipment also varies requiring a mixture of maintenance approaches. According to Reindel and Steger (2010) this requires testing and inspection schedules to be adjusted to suit individual equipment types in order to maximise their service life. Often the equipment is divided into insulation types which include mineral oil, oil impregnated paper, bitumen, porcelain, SF6 gas, and synthetics.

These variations in insulation types were a major consideration for this research as their construction type forms part of the hazard. As noted previously, the potential for the insulation type to become a projectile that can be expelled by an electrical discharge or explosion is of concern. The distances that a given projectile will travel will vary, depending on type. This adds additional complexity when attempting to quantify the RMHZ around a given piece of HV equipment.

When investigating potential faults, it was highlighted by Ward (2021) that Partial Discharge (PD) is one of the indicators that the likelihood of equipment failure was increasing. PD can be identified in several ways depending on the equipment construction type. For equipment that uses oil as part of its insulation, oil sample testing is used. Other methods employed include visual inspection as well as listening for the audible sounds that can be emitted from the equipment as it approaches failure.

3.2.5 Pressure waves

The research of electrical pressure waves lacks the extensive knowledge base of arc flashes, according to Neal and Parry (2005). In ‘Pressures developed by Arcs’, the authors tried to raise the importance of electrical blast or pressure waves as worthy of targeted research (Lee & Nailen 1987). They argued that the amount of damage to nearby structures can be correlated proportionally with the distance for a given current. The graph for pressure versus distance that was developed by Lee and Nailen can be viewed in Figure 3 - 1. The work undertaken by Lee

in this field has not been fully accepted according to Hoagland et al. (2016). It is theorised that the peak of a wave is directly related to the amount of current and the length of time that the explosion occurs. The Lee equation does provide a starting point for the research even though it could be considered overly conservative.

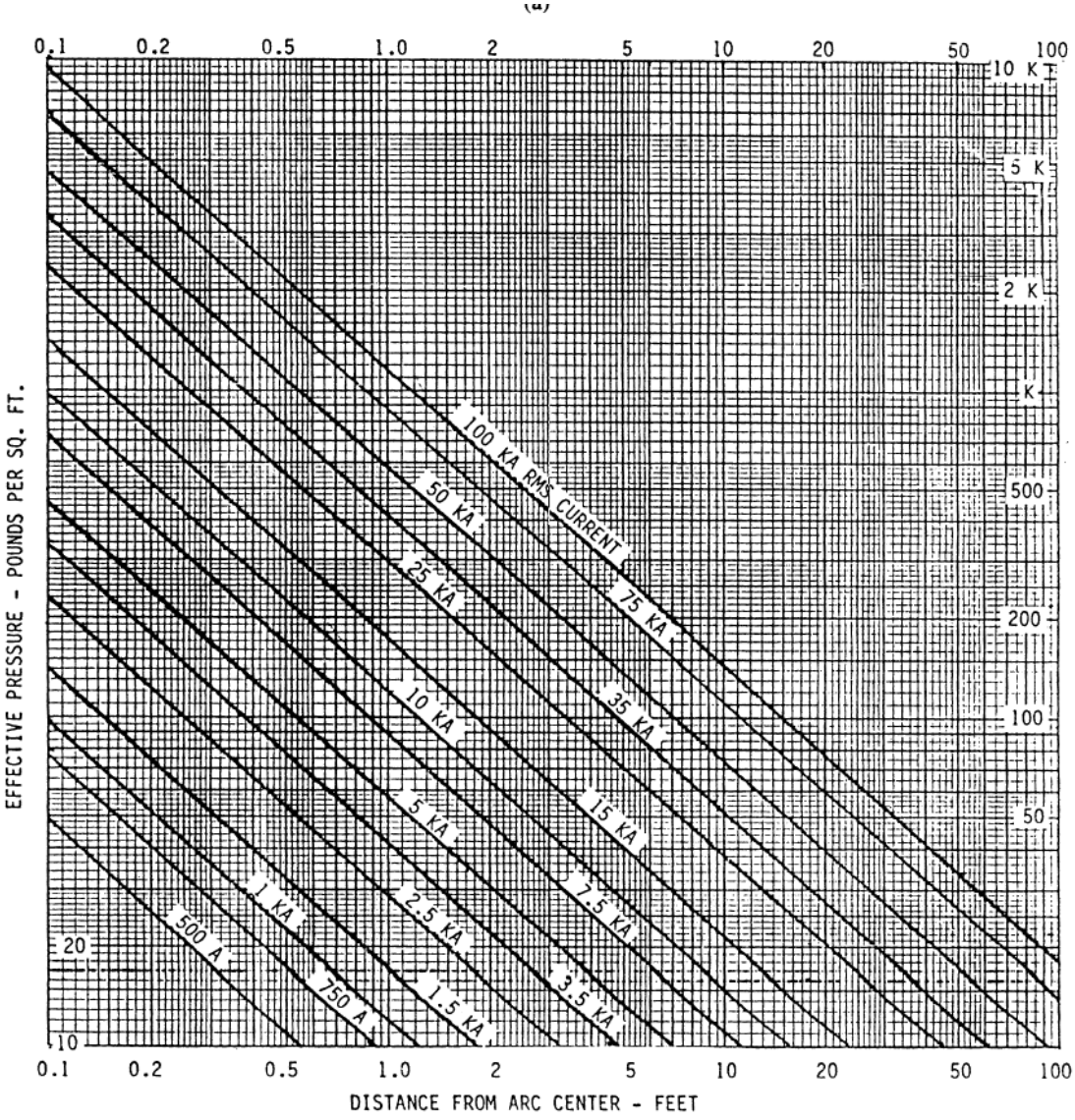

Figure 3 - 1: Pressure versus distance from arc

Beyond the electrical literature, the area of research in the field of defence has investigated pressure waves for military applications. Researchers Xue et al. (2019) have studied explosions in free-fields and have argued that there is more than one component to a pressure wave. The study observes that one component contains a positive zone, and the other contains a negative zone. The wave decayed across both zones in an oscillating pattern following the initial overpressure peak. These findings assisted with the development of an assumption for the length of time that the pressure or force from an explosion will be maintained.

3.2.6 Projectile motion

The study of projectile motion has been conducted for many centuries with the classical cases around ballistics still performed today (Packel & Yuen 2004). The resistive medium in which a projectile is travelling through greatly effects its trajectory (Jahangir et al. 2020). In the case of this research the projectile is in free space, with the forces applied assumed to be gravity and air density. The other considerations are the height of the ignition and the trajectory angle. The time required for the projectile to reach the ground is directly related to the peak height reached by the projectile. The angle, initial height of projectile and air resistance simulations are quantified as part of the simulated analysis.

It is accepted by Neal and Parry (2005) that shrapnel produced in an electrical arc flash or blast event is difficult to quantify. They postulate that there is a correlation between the pressure wave, the arc current, and possibly even electro-magnetic fields on the velocity of shrapnel produced in an electrical discharge or explosion. The forces produced during an arc flash event and resulting explosions can be estimated by calculating the Tri-Nitro-Toluene (TNT) equivalent (ARCAD_INC 2019). The vast majority of research into projectiles is focussed on military applications and personal protective equipment (PPE) requirements, based on ballistic testing (Neal & Parry 2005).

Estimating the trajectory of a projectile requires the inclusion of atmospheric forces that it would be exposed to. One method is to use Newtons second law, from which the differential equation for a projectile can be derived (Polking et al. 2022). This technique was applied by Hays (2014) using the Newtonian equations and integration to estimate the trajectory of a paintball projectile. This required the initial velocity(V_0), mass of projectile (m), mass flow rate through the atmosphere (b), and the estimated terminal velocity($V_{Terminal}$) in order to estimate the distances in both the horizontal ($_x$) and vertical planes ($_y$).

The horizontal plane:

$$\sum F_x = ma_x$$

$$ma_x = -bV_x$$

$$\frac{dV_x}{dt} = -\frac{bV_x}{m} \tag{11}$$

Solving for $$V_x(t) = V_{x0}\, e^{-\frac{bt}{m}} \tag{12}$$

Where $$V_x(0) = V_{x0} = V_0 Cos\,\theta$$

Integrating to find x,

$$x(t) = \int_0^t \left(V_{x0}\, e^{-\frac{bt}{m}}\right) dt'$$

$$= \frac{mV_{x0}}{b}\left(1 - e^{-\frac{bt}{m}}\right) \quad (13)$$

The vertical plane:

$$\sum F_y = ma_y$$

$$ma_y = -mg - bV_y$$

$$\frac{dV_y}{dt} = -g - \frac{bV_y}{m} \quad (14)$$

Solving for $V_y(t) = \left(\frac{mg}{b} + V_{y0}\right) e^{-\frac{bt}{m}} - \frac{mg}{b}$ (15)

Integrating to find y,

$$\text{y(t)} = \int_0^t \left(\left(\frac{mg}{b} + V_{y0}\right) e^{-\frac{bt}{m}} - \frac{mg}{b}\right) dt'$$

$$= \left(\frac{gm^2 + bmV_{y0}}{b^2}\right)\left(1 - e^{-\frac{bt}{m}}\right) - \frac{mg}{b}\,\text{t} \quad (16)$$

Where $V_y(0) = V_{y0} = V_0 Sin\,\theta$ (17)

Position for time (t):

$$t = \frac{m}{b}\ln\left(\frac{mV_{x0}}{mV_{x0} - bx}\right) \quad (18)$$

Trajectory equation Y:

$$Y = \left(\frac{mg\sec\theta}{bV_0} + tan\,\theta\right)x + \frac{m^2 g}{b^2}\ln\left(1 - \frac{b\sec\theta}{mV_0}\,x\right) \quad (19)$$

Where $b = \frac{mg}{V_{terminal}}$ (20)

$$V_{terminal} = \frac{\sqrt{2 * m_{ass} * g_{ravity}}}{\rho_{air} * A_{rea} * Coefficient_{Drag}} \quad (21)$$

These formulae enabled a projectile motion model to be developed for estimation of porcelain trajectories. The coefficient of drag that is used with equation 20 can have wide impact on the

projectile trajectory which, according to Cengel (2017), changes depending on the shape and what part is facing in the forward direction. The irregular shape of a porcelain fragment is difficult to quantify as can be seen below in Figure 3 - 2. The inclusion of drag forces improved the physics based projectile model that uses the incident energy calculations in equation 6 and 7.

Figure 3 - 2 : Fragment of a hollow porcelain shell. (INMR 2014)

3.2.7 Surge arrestor

The electrical surge arrester is used to protect electrical equipment during lightning events where very large but short bursts of energy are present. There are two common varieties used for reducing these lightning impulses according to Mari (2020), the metal oxide or Zinc metal Oxide (ZnO), and the Silicon Carbide (SiC). The Metal-Oxide Surge Arrester (MOSA) has nonlinear characters which can handle transient fault current and come in three types, the gapless, series-gapped, and the shunt gap. The SiC arrestors uses a nonlinear value element to quench the lightning event by using spark gaps that are design to limit the fault current from reaching earth potential.

The overvoltage of a lightning strike, or exposure to fault current, can overload a surge arrester creating large increases in pressure. The way in which the device handles or fails is dependent on the construction type and whether it incorporates a pressure relief device which can be seen in Figure 3 - 3. The internal design of the arrester and whether it is gapless or hollow tube also has an effect. If a device does not have a pressure relief, or the event is larger than it can handle, the gases and associated pressure can lead to fragmentation of the bushing or housing (Taylor 2023). The internal design of the arrester and whether it is gapless, or a hollow tube

also has an effect. If a device does not have a pressure relief, or the event is larger than it can handle, the gases and associated pressure can lead to fragmentation of the bushing or housing (Taylor 2023).

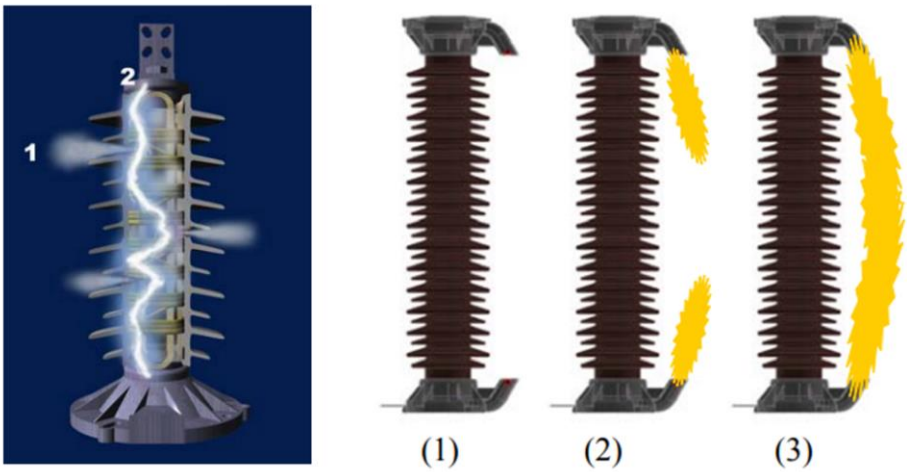

Figure 3-3: No pressure relief and pressure relief

The traditional insulation medium for bushings or housings has been porcelain, which can be converted into projectiles during an electrical explosion. A common failure mode is moisture ingress which occurs for several reasons, but most commonly from deterioration caused by weather and age, with an example being the failure of seals between the end caps and the porcelain over time. To eliminate the risk of porcelain projectiles, research into other materials has been carried out with Jonsson (2009) arguing that silicon insulation significantly reduces the projectiles hazards during electrical explosions. The results from research into silicon has led to the electrical industry moving to modern silicon polymers as the preferred insulation medium at all system voltages.

3.2.8 Ansys

The Ansys engineering simulation software is designed to support advanced physics-based analysis of the entire life cycle of a product design. To support a wide variety of engineering fields and their specific analysis, Ansys utilises a workbench platform that enables various software suites to be integrated on one program schematic (ANSYS 2023). An entire projects analysis can be coordinated in one location from the drawing of the model to the specific type and number of simulations that may be required. This improves efficiency by allowing engineering data fields to be input or simulated within one application and then easily transferred to another application on the same workbench.

To conduct analysis of a highly nonlinear, high stress, and high strain situation of an explosion requires the use of explicit methods according to Century-Dynamics (2005). The discrete time frame integration requirements of the dynamic event require numerical simulations that are continuous in more than one direction (ANSYS 2023). The equations of the conservation of mass, momentum and the energy equation are used to model the multi-dimensional nature within the simulation. This requires a significant amount of computational work to be completed simultaneously and the technique is referred to as hydrocode (Ludwig 2012). Solutions from the hydrocode are obtained by discretisation of the event at each calculation cycle. This is achieved using the geometries mesh which allows the computational analysis to be conducted on each individual cell using the initial boundary conditions or the results from the previous iteration of computations.

The generation of the mesh is completed by the algorithm solvers provided by the specific Ansys product suite. There are two types of meshing solvers available for explicit simulations and they are the Lagrangian which is used for solid materials, and the Eulerian which is used for gases or spatial substances (Ludwig 2012). The Lagrangian mesh is connected to the geometry's material, using constant mass of the material. This mass connected to the mesh can affect the hydrocode calculations by creating localised stress zones. The Eulerian mesh is set by the area of the model and is known as the Eularian virtual (ANSYS 2023) and uses constant volume within the hydrocode to calculate the material flow through the mesh. The size of the generated mesh can also affect the timesteps between cycles of individual cells when deformation becomes too small. This can cause the hydrocode to terminate before the simulation time has been reached. Both mesh types and size setting have their advantages and disadvantages making the selection of the correct mesh type critical to successful calculations and a reliable solution.

The modelling application software products from Ansys that are suited to an explicit event are the Explicit Dynamics and Autodyn suite. The Explicit Dynamics suites user interfaces are well suited to the initial setup of explicit models with all model setups and workflows very similar to the workbench itself when using Autodyn solvers within it. The Autodyn suite itself can also be used to perform the same models though has a more antiquated user interface for setting up models though Quan et al. (2006) postulate it is well suited to fragmentation analysis.

3.2.9 Explicit dynamic time

The phenomena of a HV electrical explosion can occur at any point in time once an electrical plants insulation medium starts to deteriorate. The time involved in an explosion is within an explicit dynamic time frame which according to Century-Dynamics (2005) is in the order of microseconds. The explicit time frame when compared to other similar explosions, like a bomb is argued by Quan et al. (2006) to have a blast phase and fragment phase. These phases are plotted in Figure 3- 4. The plot displays Kinetic Energy (KE) against time in microseconds and implies that KE does not significantly increase beyond the fragmentation phase. This suggests that the time associated with KE transfer to a projectile can be limited due to the very short period.

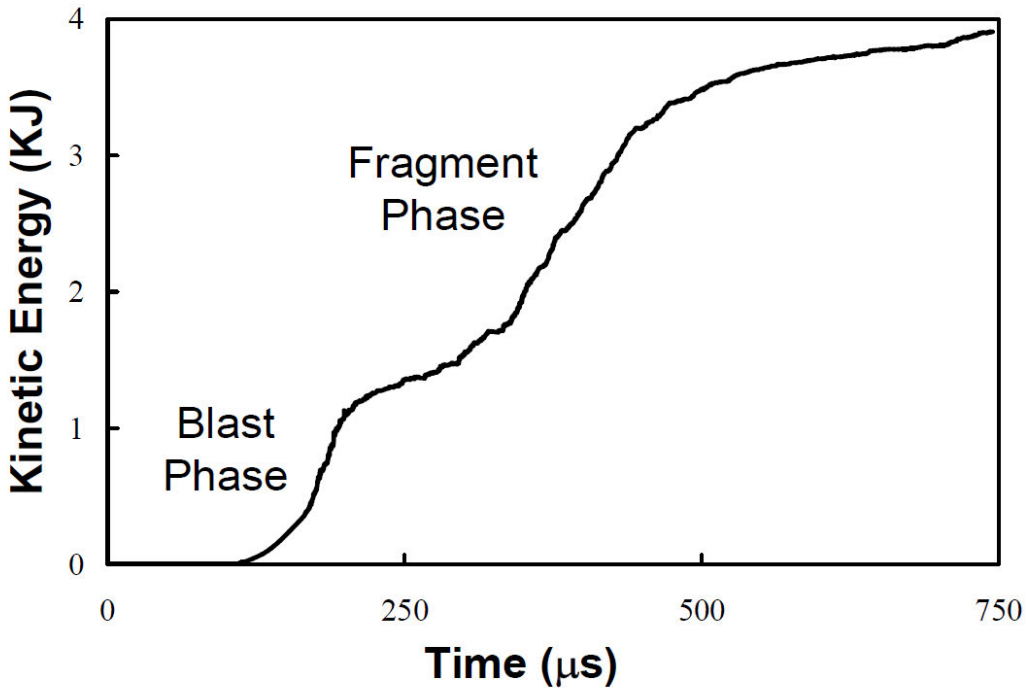

Figure 3 - 4: Time history of kinetic energy from a pipe bomb simulation

Additionally, the explosion of porcelain requires the consideration of the tensile strength and the time in which it can be assumed that it can withstand pressure build up. The failure of ceramics is known to initiate with very small cracks before transitioning into fragments. Analysis by Tasdemirci and Hall (2007) identified that the time required for the ceramics to fragment under pressure would be during the initial stress applied to the ceramic.

3.2.10 Vaporisation and pressure

The process of vaporisation of a material requires the phase transitions from a solid to a gas or vapour achieved through heating (Cengel 2017). The latent heat of fusion is the first phase and converts the solid material to a liquid. The second phase is the latent heat of vaporisation which above this temperature the material begins to boil and vaporise into a gas. The phase change process can be viewed in Figure 3 - 5.

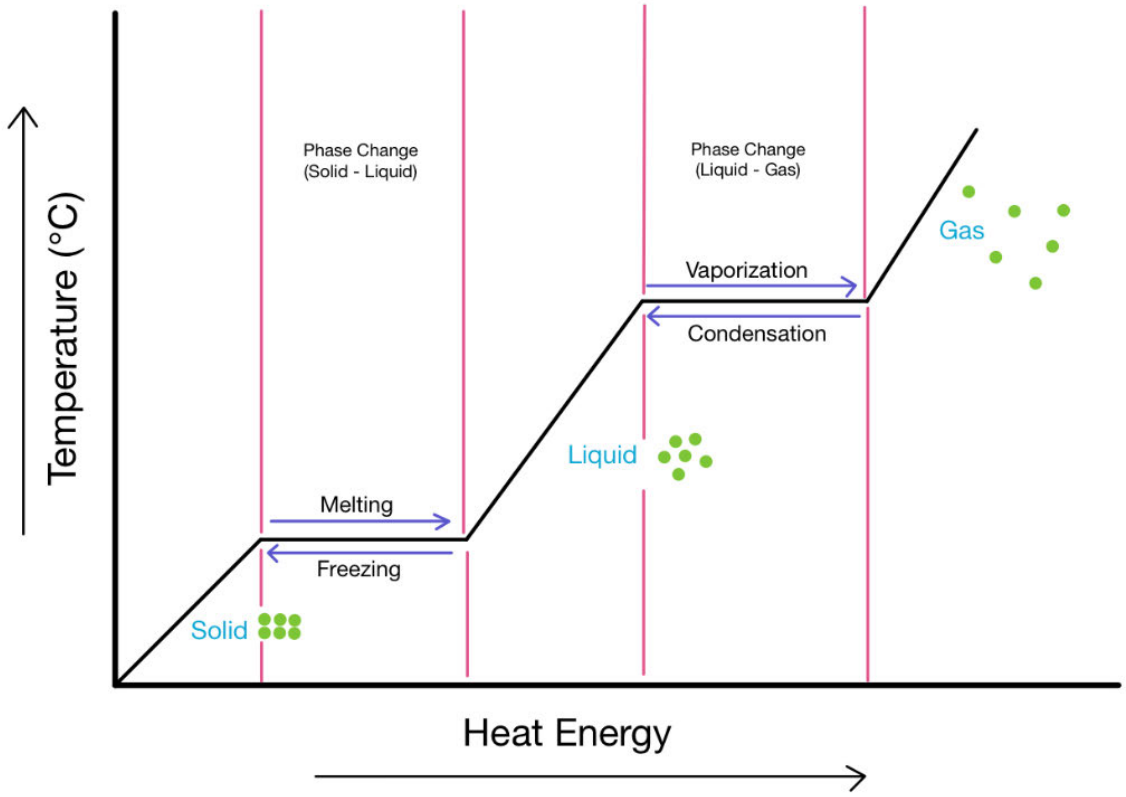

Figure 3 - 5: Phase change diagram (Expii 2016)

The entire process can require a significant amount of energy depending on the material that is being vapourised. The vaporisation process, according to Speight (2019) results in a vapor pressure that can be above standard atmospheric pressure and along with an increase in vapor temperature. The high temperatures associated with an electrical arc explosion is argued by Kadivar et al. (2021) to cause high-density plasma. According to the Australian Energy Council (2019), see Figure 3 - 6, the arc plasma is ejected from the fault location and is estimated to be in the region of 20,000 ^{o}C.

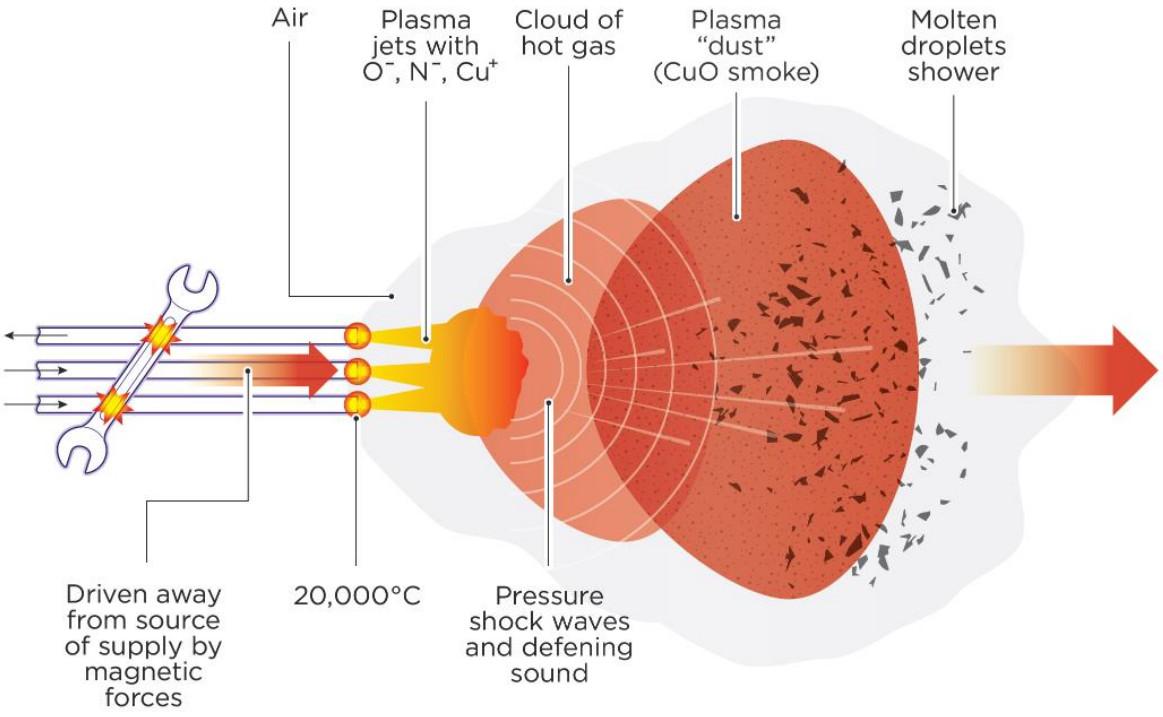

Figure 3 - 6: Arc – Flash Diagram (Australian Energy Council)

3.3 SUMMARY

The literature review has provided a detailed overview of risk analysis and of the electrical hazards associated with an electrical arc explosion. This included the various construction types of the porcelain surge arrestor along with the Ansys advance computational modelling software packages. Finally, the explicit time that is association with fragmentation as well as the vaporisation and pressure from an electrical arc are summarised.

4 CURRENT PRACTICES

4.1 CHAPTER OVERIEW

The current EQL process for maintaining the integrity of its electrical network requires the expertise of experienced electrical engineers and the effective use of risk management processes. Risk assessments are conducted when a piece of electrical plant is identified to have reached ERF. A Defect Management Plan (DMP) is developed and when required a NAR is also invoked. The NAR adds additional controls around an ERF when there is a possibly of catastrophic failure with the potential to cause harm to anyone in the vicinity of it at the time of failure.

4.2 CURRENT PROCESSES

The risk management of the health and safety of electrical workers, the public, and the electrical network is the responsibility of the asset management engineering department which is divided into sections aligned to particular asset types and network activities. The asset types range from conductors, cables, and reactive plant including transformers, switchgear, and protection equipment. For network activities, the operation and maintenance of the network involves electrical network connections, switching of the network for planned and unplanned operations, and work practises associated with maintaining the electrical distribution network. Where hazards are identified, the responsible engineering department is required to manage the risks associated with the hazard until it can be resolved (*Network Risk Framework* 2021).

The vast size and complexity of EQL's electrical distribution network presents a challenge for engineers when managing risk due to the various legacy networks and their designs. The process that is employed at EQL is based around the risk assessment process which is used to identify the issues and risk factors associated with a hazard. Once identified, control measures are developed to lower the risks of the hazard to ALARP (*Network Risk Framework* 2021).

4.3 ADDITIONAL CONTROLS

The NAR is used as an additional control with its own processes and documentation with the same risk assessment developed for the DMP. The additional controls are designed to limit the

physical access to electrical plant at risk of catastrophic failure. As part of the NAR development process a RMHZ is identified, and controls are created to assist in limiting both employees and the public from accessing the hazardous areas. These restrictions come in the form of formal documentation of an invoked NAR and any other specific controls recommended (*Guide to Preparing Network Access Restriction Documentation* 2015).

At the location where a NAR is invoked, the specific controls vary depending on whether the affected ERF is within an indoor or outdoor environment. Plant that is considered to be within the indoor environment, are either located inside a building or cubical enclosure, and as such the RMHZ is placed over the entirety of those locations. The outdoor environment requires additional engineering judgement due to the unrestricted nature of the location. The unpredictability of the electrical explosion, the construction type and associated materials of the ERF also affects the controls that are required.

The invoked NAR and its controls and documentation also must be reviewed on a 6 monthly basis in line with the DMP. These documents and controls will remain in place until the NAR is revoked. The engineer in charge of the specific NAR will revoke the NAR once the ERF has either been repaired, replaced, or removed from service and can no longer be connected to the EQL electrical network.

4.4 DISTANCE SETTINGS

The determination of the RMHZ distance is directly related to the composition of the ERF, with higher risks associated with the materials that can become projectiles or increase the overall size of the event during the electrical explosion. The presence of pressure relief devices allowing for rapid changes in pressures and temperatures to be released in a controlled way are included in the consideration when setting an RMHZ. The location of the ERF, whether mounted on the ground, wall, pole, or structure influences the RMHZ shape. One of the largest RMHZ distances set at EQL (2022) is currently 25 metres from the ERF, although incidents have occurred where projectile fragments have been located well beyond this zone. This can present challenges when trying to ensure the exclusion zone can be maintained and whether it will be adequate for the situation. Where it has been identified that a RMHZ distance cannot be maintained, additional controls are required which can include the installation of barriers and signage to reduce the potential hazard to ALARP.

4.5 SUMMARY

The current practice of implementing a 25 metre RMHZ reduces the risk level of exposure to any of the projectile fragments from an electrical blast. The decision to set the distance to 25 metres has not been fully quantified. This is an ongoing challenge for engineers when conducting health and safety risk assessments for ERF especially when the RMHZ is difficult to establish and maintain.

5 METHODOLOGY

5.1 CHAPTER OVERVIEW

Solving potential distances of a projectile from an ERF during an electrical explosion are well suited to advanced computational modelling techniques which cannot easily be achieved using typical two-dimensional mathematical software. The Autodyn suite within Ansys has the capability to model the nonlinear explicit dynamics of the three-dimensional explosion. The solution from Autodyn is compared to a physics based projectile model that is developed with MatLab in 2D alongside it and historical incident data. This comparison could support improvements to the NAR automation tool that is under development at EQL.

5.2 INTRODUCTION

To enhance the current processes of EQL's NAR process and the associated RMHZ involves several steps. This includes extensive research into publicly available data of HV electrical incidents and historical data from within EQL. Evaluations of the computational formulae from within the available literature and traditional formulas including for electrical fault analysis, energy, and motion are conducted. This assists in the development of the initial conditions for modelling of explicit dynamic event and the physics based 2D projectile model of porcelain fragments. A comparison analysis of these two models was conducted and the findings could be considered for inclusion in the risk matrix calculator incorporating type of equipment, voltage, current (isn't current level amperage) and clearing times associated with electrical discharge or explosion potential of a suspect ERF.

5.3 COMPONENT SELECTON AND INITIAL CONDITIONS

The review of HV incidents at EQL identified several equipment types that were suitable for initial evaluation. Each were evaluated against their makeup or construction and the amount of incident data available. A 33 kilovolt (kV) porcelain surge arrestor was selected because of the following. The specific construction type of the surge arrester was a solid design which has no gap between ZnO, aluminium spacers and the porcelain insulation housing. This reduced some of the complexity associated with other designs and equipment types which can have additional

components that add to the explosion or blast. Parameters included in the simulations to model the effects of the worst-case fault currents on projectile range/blast effects were the basic dimensions of all the components of the surge arrester, system voltage (33kV), and a substation protection relay clearing time of 150ms.

5.4 COMPUTATIONAL ANALYSIS OF FORMULAE

The review of formulae for electrical arc fault standards and energy conversion to an explosion was identified and computational analysis was conducted using the MatLab software package. The IEEE 1584 -2018 standard is suitable for electrical fault calculation of system voltages up to 15kV. For voltages above this the Lee model standard was used, see Figure 3 – 1 on page 9. The results from these calculations were then applied to the TNT equivalent formula which was developed by ARCAD_INC (2019) to estimate the amount of TNT in grams that is required to generate a similar electrical arc blast. The calculated amount of explosive was then used as part of explicit dynamic simulations. Findings could then be used in the development of the risk matrix for electrical arc flashes and associated blasts.

5.5 SIMULATION SOFTWARE

Ansys software suites were used to simulate a variety of 2D and 3D nonlinear dynamic interactions between solids and gaseous materials. The mechanical workbench user interface was used to combine the Geometry, Explicit Dynamics, and Autodyn suites. The Design Modeler program was used for drawing components in 3D see Figure 5 - 2. This initially involved drawing the outside and then each component is spliced inside the next. The overall design was then sliced for 2D analysis as required. The Explicit Dynamics program enables engineering data specific to each component's material properties to be assigned to each individual component with the geometry design. It was also able to carry out the modelling of both 2D and 3D explosions and predict the component interactions. The Autodyn suite was to be used for fragmentation generation and analysis following a successful solution of the explicit dynamic model.

5.6 2D SIMULATION

The 2D simulation was used for both familiarisation of the Ansys software environment and the reduced computational requirements of this type of modelling. The multi-material Euler simulation method was used within the Autodyn suite. Two iterations of tests were conducted with contact areas between materials within the model set to none and then enabled. The model geometry consisted of three materials, which were porcelain, air (atmospheric), and the TNT equivalent. The model was sliced along the x axis and the z axis exposing half of the x and y axis's cross-sectional face. The multi-material 2D Euler simulation uses a cartesian mesh across the x and y axis. The air box area within the geometry serves as the boundaries for fragmentation to occur during the explosive simulation with the x axis treated as an axis of symmetry further reducing computations. The Ansys Workbench workflow for 2D simulations is shown below in Figure 5 - 1.

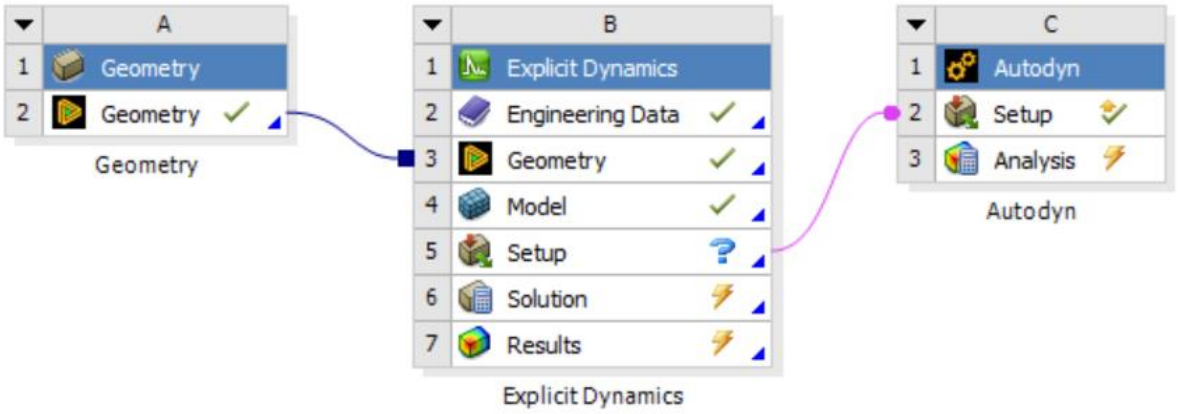

Figure 5 - 1. Ansys Workbench workflow for 2D analysis

5.6.1 Geometry

A sphere geometry within a box was selected for initial simulations to determine whether the modelled explosion would uniformly expand outwards. The dimensions of the box were 1000mm x 1000mm x 1000mm, the porcelain outer sphere section had a radius of 100mm, the middle air layer had a radius of 50mm, and the inner section of TNT had a radius of 25mm. The 3D sphere slide for 2D simulation is shown below in Figure 5 - 2.

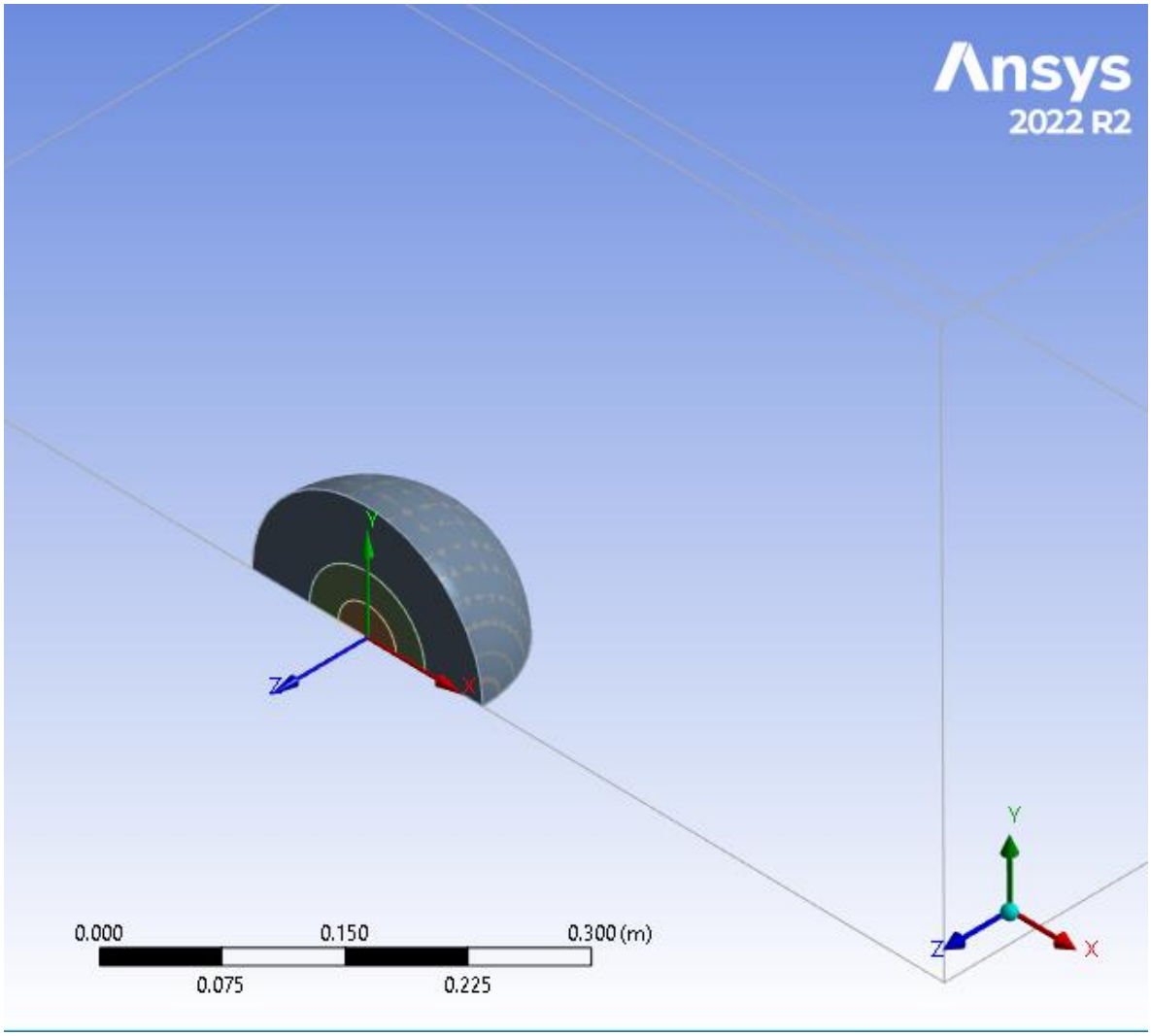

Figure 5 - 2. 3D sphere sliced for use in 2D multi-material Euler simulation in Explicit Dynamics

5.6.2 Conclusions from 2D modelling

The simulation with contacts set to none was successfully simulated within Autodyn with all material properties set to multi-material Euler. The detonation of the explosive and the resulting pressure increase within the sphere was verified though the porcelain did not fragment. The reason for the lack of fragmentation can be attributed to several factors including thickness of the porcelain compared with the amount of explosive, the use of the Euler modelling method on brittle material when the method is designed for gaseous situations and incorrect material data setting for porcelain. The simulation with contact areas enabled and the porcelain material modelling set to Lagrangian could not be analysed because the 2D multi-material Euler method does not support the porcelain material. Further development within the 2D simulation analysis was stopped because fragmentation analysis of porcelain was not supported.

5.7 3D SIMULATION

The initiation of 3D simulation was expedited due to the limitation of 2D analysis within Autodyn. The Explicit Dynamics program environment was utilised for much of the simulation modelling and solving of a variety of geometries. It provided an improved user experience when setting up models and the analysis of generated solutions. 3D simulation requires additional nodes and element meshing to complete these types of simulations. This required the use of the academic software licence which removes elements and node limitations that are restricted in student software licences.

There were two 3D primitive shapes that were used for analysis, one being the sphere, the other being a cylinder with the different materials sliced within the outer porcelain layer. The sphere was utilised initially for developing an understanding how uniform the fragmentation phase would be during the event. This provided a foundation to build from when employing the 3D cylinder primitive which also utilities different materials spliced within the porcelain outer layer. During this stage of the analysis, variations in material thickness, lengths, and internal components with and without voids are considered. These variations assisted with the iterated design of the model, enabling improvements, and understanding of both the material property interactions, and modelling software. The Ansys Workbench workflow for 3D Explicit Dynamic simulations is shown below in Figure 5 - 3.

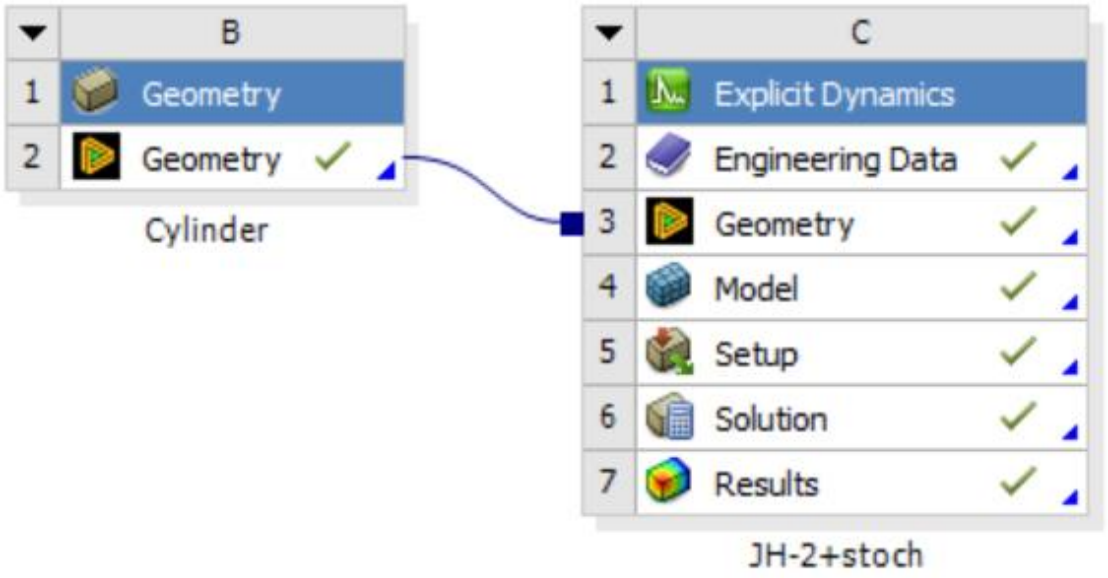

Figure 5 - 3. Ansys Workbench workflow for 3D Explicit Dynamics Analysis

The solved models that were generated for the various iterations were collated for use within the standalone Autodyn software suite, providing additional analysis of the 3D fragmentation phase of an explicit event. This software suite can assist with estimating the number of fragments and their velocities as they are expelled from the source of the event, once the solutions of the various models from the Explicit Dynamic suite are aligned. During the alignment stage it was identified that the Autodyn suite requires the linear elastic model for its analysis which is not suitable for brittle materials including porcelain. Further development of 3D fragmentation analysis using the Autodyn suite was stopped due to it not supporting the modelled solutions.

5.7.1 Geometry

The two geometries that have been used are a sphere and a cylinder with components and their sizes adjusted for a variety of configurations. The sphere uses the same overall dimensions used in 2D modelling with a radius of 100mm, though the thickness of the porcelain is adjusted and the air gap inside is replaced with TNT explosive in some iterations.

A cylinder geometry was used as a simplified representation of a surge arrester. The overall dimensions were reduced to increase the speed in which a model could be analysed. The dimensions of the airbox were 200mm x 200mm x 200mm, see figure 5-4. The outer porcelain layers length was 100mm with a radius of 50mm, the inner section of TNT explosive had a length 90mm and a radius of 45mm.

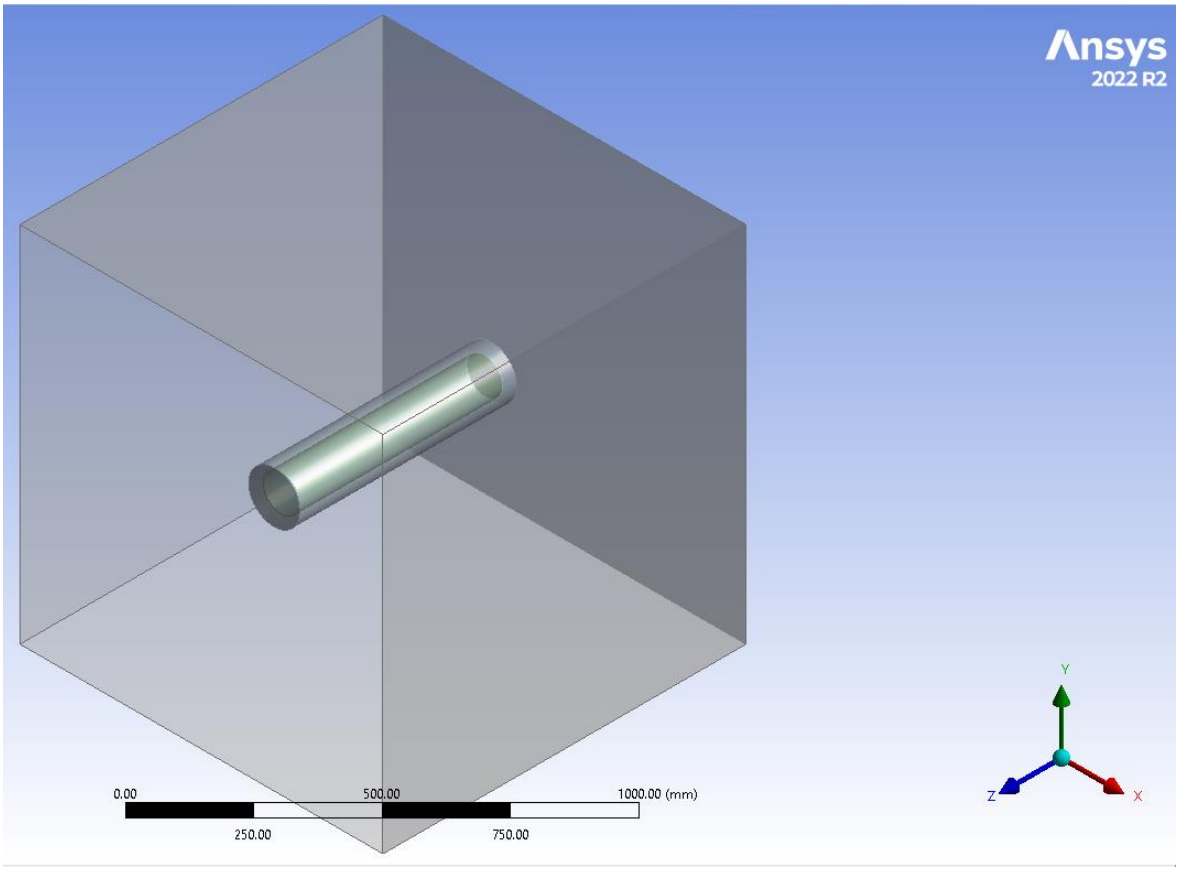

Figure 5 - 4. 3D geometry of the cylinder representation of a surge arrester inside an air box

Following the completion of the modelling of a reduced geometry a model was created which aligned closely with a 33kV surge arrestor. The dimensions of the airbox were 3000mm x 3000mm x 3000mm. The length of the outer porcelain layers was 600mm with a radius of 76mm. The thickness of the porcelain layers and the volume of TNT varied during iterations of the simulation by splicing the inner sections of the TNT with porcelain, thicknesses ranging from 10 - 25mm.

5.7.2 Meshing

The accuracy of mesh sizing of each geometry is essential for successful simulation analysis. The longer the duration of the simulation the more critical the mesh settings become. For each iteration of mesh sizing and component sizing, the run time was set to very short durations, initially to verify the model would solve. Following a successful simulation, the run time was incrementally increased until the step size between mesh node sizes became too small and the simulation terminated before the desired end time.

The initial time period analysis settings were 200 and 500 microseconds which according to Quan et al. (2006) are the blast and fragment phases. The mesh was further refined to enable analysis of the period beyond these initial phases to support further analysis of fragmentation sizes and distances. The explicit time and nonlinear nature of these events meant that analysis beyond 50 milliseconds was difficult.

5.7.3 Explicit Dynamics settings

The explicit dynamic suite provides the framework required to conduct most of the Autodyn simulations without the requirement to setup simulations inside the more complex Autodyn suite. The design and selection of engineering data, geometry, modelling, analyses setup and solutions can all be accessed within the explicit dynamic suite except for fragmentation analysis. The simulation enables materials to fracture, though once the final piece or fragment disconnects from the main geometry body it is not able to be further analysed and is represented by red dots within the 3D animation of the simulation solution images in Figure 5 - 5.

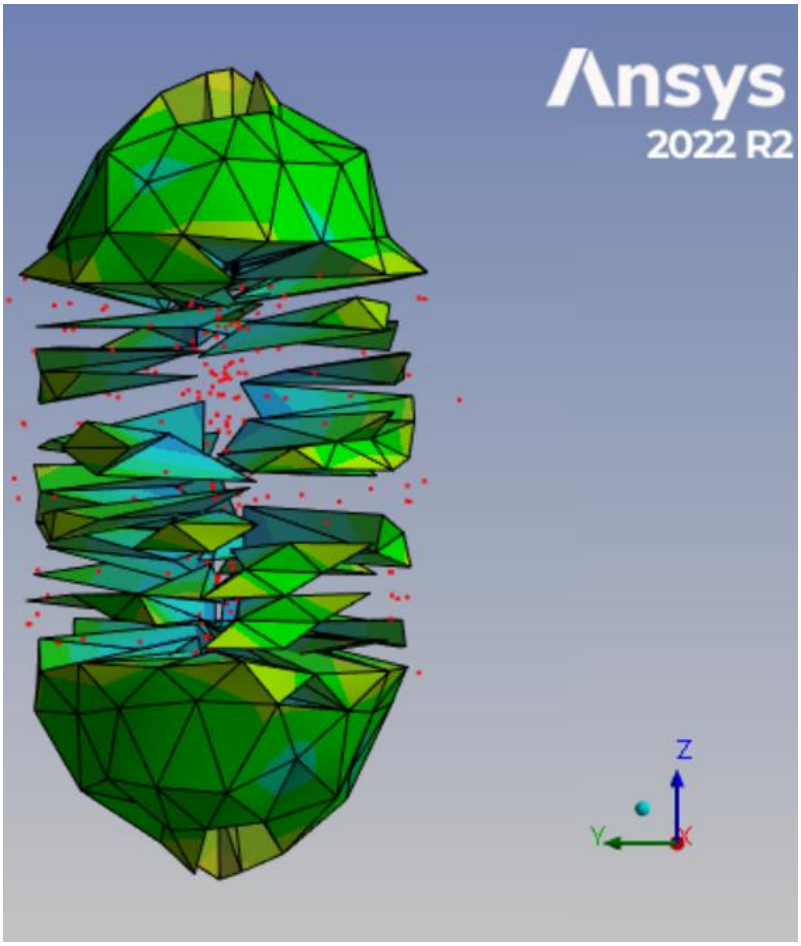

Figure 5 - 5. Disconnected porcelain fragments from explicit dynamics 3D simulation.

5.7.4 Material selection and settings

Individual materials are selected from within the engineering data suite, where material properties and models can be inserted or adjusted. The engineering data available on porcelain was limited with no pre-set brittle model, Equation of State (EOS), or strain failure parameters. The settings of these properties and parameters were sourced from similar materials using academic papers, if available. High-strength Aluminous porcelain IEC60672 Type C-130 (MakeItFrom.com 2021) was used for the mechanical properties and the Johnson-Holmquist Strength Continuous was used for brittle modelling and the Stochastic Failure for material fracture variation (Tasdemirci & Hall 2007). The porcelain model setting is shown below in Figure 5 - 6. For TNT explosive material and air (atmospheric) materials, pre-set properties and parameters in Ansys were utilised, with TNT model settings as shown below in Figure 5 - 7.

Outline of Schematic C2: Engineering Data

	A	B	C	D	E
1	Contents of Engineering Data			Source	Description
2	Material				
3	Air (Atmospher			Explicit_Materials.xml	"Thermodynamic and Transport Properties of Fluids, SI Units", GFC Rogers, YR Mayhew
4	Porcelain			Thermal_Materials.xml	
5	TNT-2			Explicit_Materials.xml	LLNL Explosives Handbook, Properties of Chemical Explosives and Explosive Simulants, B .M. Dobratz, P.C. Crawford, Jan 31 1985

Properties of Outline Row 4: Porcelain

	A	B	C	D	E
1	Property	Value	Unit		
2	Material Field Variables	Table			
3	Density	2400	kg m^-3		
4	Specific Heat Constant Pressure, C_p	1070	J kg^-1 C^-1		
5	Johnson-Holmquist Strength Continuous				
6	Failure Type	Gradual			
7	Hugoniot Elastic Limit HEL	7	GPa		
8	Intact Strength Constant A	0.88			
9	Intact Strength Exponent N	0.64			
10	Strain Rate Constant C	0.007			
11	Fracture Strength Constant B	0.45			
12	Fracture Strength Exponent m	0.6			
13	Maximum Fracture Strength Ratio SFMAX	1			
14	Damage Constant D1	0.0125			
15	Damage Constant D2	0.7			
16	Bulking Constant B	1			
17	Hydrodynamic Tensile Limit T	0.462	GPa		
18	Shear Modulus	34	GPa		
19	Polynomial EOS				
20	Parameter A1	2.31E-07	GPa		
21	Parameter A2	-1.6E-07	GPa		
22	Parameter A3	2.774E-06	GPa		
23	Parameter B0	1			
24	Parameter B1	1			
25	Parameter T1	2.31E-07	GPa		
26	Parameter T2	0	Pa		
27	Principal Strain Failure				
28	Maximum Principal Strain	0.25			
29	Maximum Shear Strain	1E+20			
30	Stochastic Failure				
31	Distribution Type	Fixed Seed			
32	Stochastic Variance γ	10			
33	Minimum Failure Fraction	0.1			

Figure 5 - 6. Porcelain settings and modelling properties for initial 3D simulations.

Outline of Schematic C2: Engineering Data

	A	B	C	D	E
1	Contents of Engineering Data			Source	Description
2	Material				
3	Air(Atmospher			Explicit_Materials.xml	"Thermodynamic and Transport Properties of Fluids, SI Units", GFC Rogers, YR Mayhew
4	Porcelain			Thermal_Materials.xml	
5	TNT-2			Explicit_Materials.xml	LLNL Explosoves Handbook, Properties of Chemical Explosives and Explosive Simulants, B .M. Dobratz, P.C. Crawford, Jan 31 1985

Properties of Outline Row 4: TNT-2

	A	B	C	D	E
1	Property	Value	Unit		
2	Material Field Variables	Table			
3	Density	1630	kg m^-3		
4	Explosive JWL				
5	Parameter A	3.712E+11	Pa		
6	Parameter B	3.231E+09	Pa		
7	Parameter R1	4.15			
8	Parameter R2	0.95			
9	Parameter W	0.3			
10	C-J Detonation Velocity	6930	m s^-1		
11	C-J Energy / unit mass	4.294E+06	J kg^-1		
12	C-J Pressure	2.1E+10	Pa		
13	Burn on compression fraction	0			
14	Pre-burn bulk modulus	0	Pa		
15	Adiabatic Constant	0			
16	Additional specific energy / unit mass	0	J kg^-1		
17	Begin Time	0	s		
18	End Time	0	s		

Figure 5 - 7. TNT settings and modelling properties for initial 3D simulations.

The specific material and reference frame was assigned to each geometry components material definition. Porcelain material component of the geometry was set to the Lagrangian reference frame to enable the modelling of the fragmentation of the brittle material. The explosive material TNT and air (atmospheric) materials had their reference frame set to Eulerian (virtual) for fluid or gases modelling. To enable both types of reference frames to interact within the same model required the setting of Euler domain controls. This included the Euler domain or interaction space display which controls where Euler assigned materials are modelled.

The size of the Euler domain is a critical component of the analysis as the domain allows materials and gases to interact within the space. As the duration of the event was increased the expansion of materials and gases increased requiring the domain to be adjusted to ensure the limits of the domain were not reached before the fragmentation of the porcelain can be analysed. The visual representation of the domain as shown within Explicit dynamics can be viewed in Figure 5 - 8.

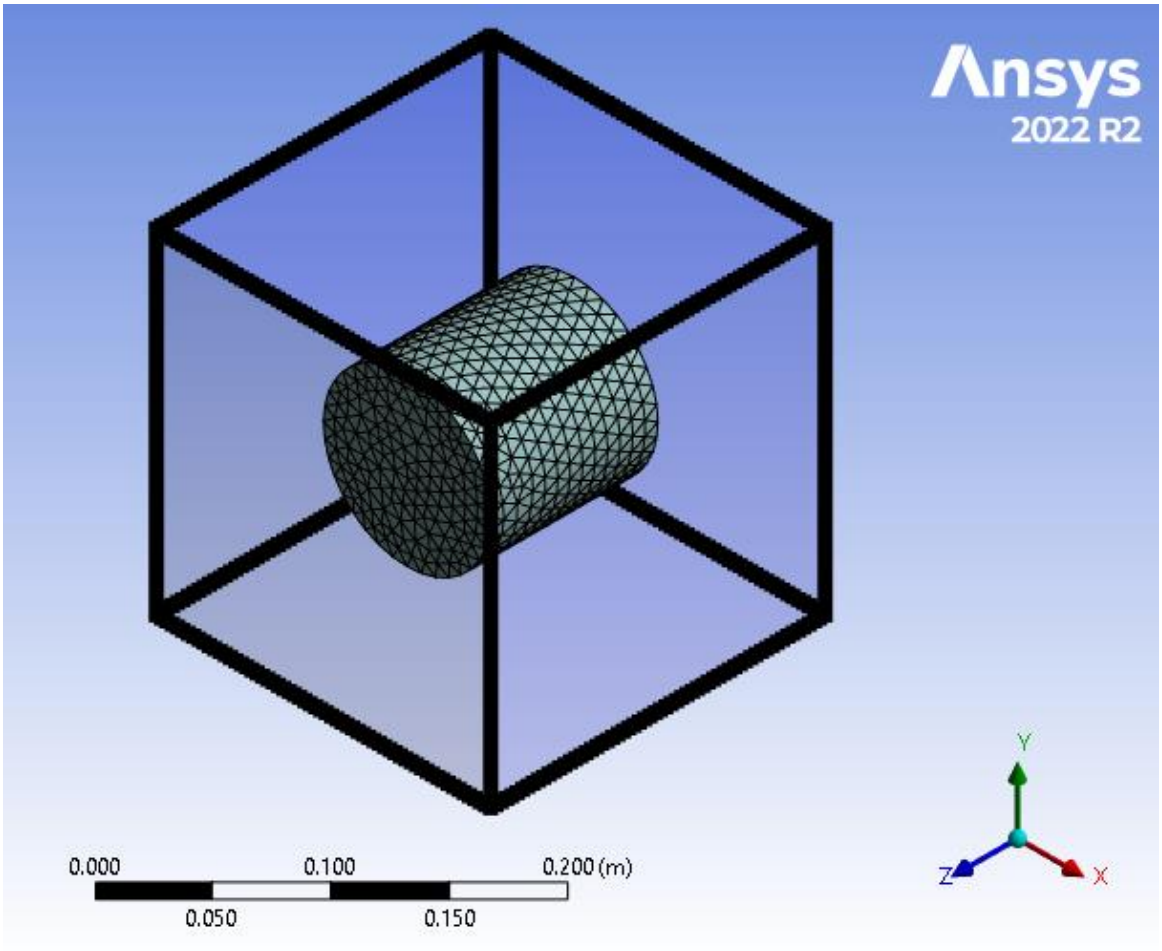

Figure 5 - 8. Euler domain space for 3D cylinder geometry.

Connection contacts between the materials are suppressed within the model as porcelain is the only Lagrangian material and located in free space. The meshing of all materials was adjusted to meet the requirements of the model. Meshing was set to default during the initial exploratory phase of the simulation analysis. The mesh settings went through several iterations to enable solutions to be generated for the desire period beyond the fragment phase, which is when porcelain elements increasingly disconnect from the main body.

5.7.5 Explicit Dynamics Model

The model sections of the explicit dynamics suite the analysis settings were configured for the modelling of the surge arrester explosion. The program provides generic settings for the analysis that require adjustment to obtain the desired modelling solution. These include:

- End time - set the length of time the modelling analysis to run.
- Time step safety factor - set to 0.5.

- Maximum velocity - set to be twice the detonation velocity of the explosive, which is approximately 14000 m/s for TNT.
- Euler domain controls.
- Output controls - set result number of points to at least 200.

5.7.6 Solution analysis

An extensive amount of data was produced from the simulation analysis within the explicit dynamic suite. The user defined results that were utilised for the cylinder geometry include:

- INT_ENERGYALL
- PRESSURE

INT_ENERGYALL results define the amount of energy in Joules per kilogram for Lagrangian bodies, of which porcelain is the only one. PRESSURE is the pressure applied to the ceramic body during the entire simulation period. The periods of the two phases of the explosion were analysed using both the INT_ENERGYALL and the PRESSURE results. The overall solutions from the simulated models were uploaded directly to Autodyn software suite for fragmentation analysis. The user defined results were also utilised within the physics based projectile model.

5.7.7 Fragmentation modelling

This analysis was intended to quantify outcomes of the porcelain fragments following their disconnection from the main geometry. Specifically investigating the velocity, energy, and distance from the source of the event or arc blast. The Autodyn suites utilises specific fragmentation simulation and analysis of a non-linear explicit error-free model solution. The suite requires the model solutions to include a Linear Elastic model or equivalent which is not suitable for materials with brittle properties. Therefore, the available modelling parameters that are available within Autodyn were not suitable.

5.7.8 Conclusions of 3D Simulation

The task of 3D simulation of porcelain fragmentation has required extensive iterations of the geometries, material properties, material parameters as well as meshing. The nonlinear explicit dynamic software enabled a detailed analysis of an arc blast event for a specified HV equipment

type. The findings provided an estimate of the forces including pressure, energy, and porcelain fragmentation as well as allowing the behaviour to be better understood. Further simulation analysis into fragmentation projectiles using the Autodyn's advanced post processing capabilities was unsuccessful.

5.8 PHYSICS BASED PROJECTILE MODEL

A physics based projectile model was developed in MatLab to provide an additional solution to verify the findings of the Ansys modelling. The electrical arc blast and HV equipment fragmentation projectile distance was analysed in free space using both the incident energy results of INT_ENERGYALL from the computational analysis and the fault data from the known EQL incident. The estimated porcelain mass of a 33kV surge arrester was also used. Simulation of projectile trajectories with air resistance was conducted using a variety of angles and heights of the events source locations. The results from this analysis are collated to provide a dataset of potential distances that fragments could travel for a given amount of energy and weight.

Assumptions for modelling the fragmentation with air resistance technique were:

1. The amount of energy was calculated using:
    a. The Ansys user defined solutions
    b. The voltage, faults current, clearing times and estimated moment of explosion identified during a known EQL incident. This provided known incident energy elements at the source of the electrical arc blast or explosion.
2. The cylinder geometry that represented the basic shape of the surge arrester was broken into either 3, 5, or 10 equal sized fragments. The decision to select 3 different amounts of fragments was from the review of historical incidents and the average number of fragments that were reported. The use of 3 fragment sizes provided a reasonable population of results for comparison analysis.
3. For terminal velocity calculations the drag coefficient was set to 0.2 to allow for a non-uniform or sharp jagged edges associated with porcelain traveling in turbulent air. For comparison, a flat plate like object would have a drag coefficient of 1 and a smooth spherical shape would be 0.5.
4. The terminal velocity of the fragments was determined by dividing the total blast energy by the number of fragments simulated. This reduced the complexity of the calculations

and there is no evidence to suggest that a single fragment of a particular group or size would have additional energy applied than any other.

5. The total area of the porcelain cylinder, including the inner surfaces, were considered when calculating the surface area of fragment. The decision to include the inner area was due the projectile's variation in shape once fragmented.
6. Air resistance on the projectile is in the opposite direction to the projectile trajectory.
7. The trajectories angles of 25 degrees and 45 degrees were chosen as they are known to provide the maximum distance with and without air (Hays 2014).
8. The pressure wave created by the arc blast was ignored for this model due to the uncertainty of a projectile's location in relation to the pressure wave at any time during the event.

The computation analysis using these assumptions provided an approximation of the distance that a fragment of porcelain for a given amount of energy and mass will travel. This required the deviation of initial velocity using the kinetic energy equation 22 and the linear air resistance differential equations 11 through 20 for both vertical and horizontal planes of motion using the terminal velocity of a projectiles mass equation 21.

$$KE = \frac{1}{2} mass * v^2 \quad (22)$$

$$velocity = \sqrt{\frac{KE}{\left(\frac{1}{2}\right) * mass}} \quad (23)$$

The weight of the porcelain fragments was estimated by calculating the mass of the hollow porcelain cylinder using the hollow cylinder or pipe, and the solid cylinder equations below:

$$Hollow = \pi * h * (r^2 - (r - d)^2) * \rho \quad (24)$$

$$End\ cap = \pi * d * ((r - d)^2) * \rho \quad (25)$$

$$mass = Hollow + (End\ cap * 2) \quad (26)$$

Where h is height, r is radius, d is diameter, and rho is density. The total area of the porcelain shell including the internal area was estimated by calculating the Lateral Surface Area (LSA) or walls, which required the addition of the External Surface Area (ESA) with the Internal

Surface Area (ISA). The Area of the Solid Bases (ASB) of the shell was multiplied by two for top and bottom. These equations enabled the Total Surface Area (TSA) to be estimated.

$$LSA = ESA + ISA \quad (27)$$

$$ESA = 2\pi r_{Total} * h \quad (28)$$

$$ISA = 2\pi r_{inner} * h \quad (29)$$

$$ASB = 2\pi r d_{thickness} + 2\pi h(r_{Total} + r_{inner}) \quad (30)$$

$$TSA = (2 * ASB) + LSA \quad (31)$$

Each of the fragment parameters, incident energy and associated velocity were utilised with a MatLab script to create the parabolic trajectory plots with the height in metres on the y axis and the distance in metres on the x axis. These plots and associated data were collated for comparison with the nonlinear 3D explicit dynamic simulation model solutions and the known incident investigations. Figure 5 - 9 below shows an example of a projectile trajectory for a given amount of energy and mass.

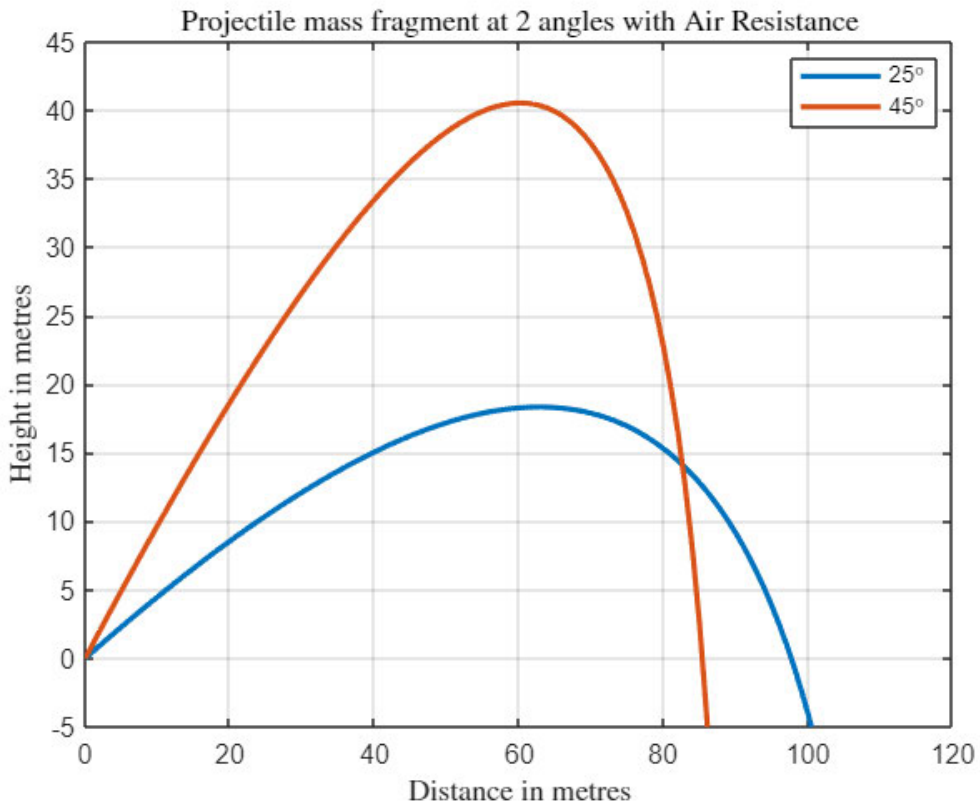

Figure 5 - 9. Projectile model example for a given amount of energy and mass.

5.9 COMPARISON OF MODELS

Two different techniques utilised the calculation of incident energy and time of the event to estimate the distance that fragmented porcelain projectiles could be expected to travel. The 3D Ansys simulation used the Stochastic Failure model to randomise the size and location of the fragmentations of the porcelain. The physics-based projectile analysis used the same dimensions of the porcelain shell with three different fragments sizes. The incident energy and time of the event from both the Ansys model and the fault data from the known incident were also compared against both electrical arc formulae from the available literature and the conventional energy equation 6 of this dissertation.

These energy values along with the estimated mass of the porcelain fragments were used within the differential projectile equations to estimate fragment trajectories. This comparison is used to support the development of a risk framework for HV equipment of the same or similar construction types. This framework could improve the existing NAR process through its inclusion in an automated NAR tool that is currently under development.

5.10 SUMMARY

The methodology chapter outlined the processes and procedures that were required to conduct theoretical research of projectile distances associated with an electrical explosion. This included presenting the material properties settings used within Ansys modelling for both Explicit dynamics and Autodyn packages. Both the 2D and 3D modelling were explored and subsequently discontinued due to software limitations associated with brittle material fragmentation analysis. For the physics based projectile model the formulae required for enabling parabolic curves caused by drag were presented, and then used to provide the initial estimates of fragments trajectory.

6 RESULTS

6.1 CHAPTER OVERVIEW

The chapter will present the results of the initial research that was undertaken based on the described methodology. It provides both visual and numerical solutions for the Ansys modelling and to further assist with interpretation of these results. The initial physics based projectile model results are plotted and points of interested are also presented. Further detailed analysis will be presented in the subsequent discussion chapter.

6.2 ANSYS MODELING RESULTS

6.2.1 2D Simulations

A primitive sphere was tested with different internal dimensional layers, one having an air gap between the TNT and the outer porcelain shell, and the other without the air gap. The TNT explosive was successfully detonated in each test, though no fragmentation of the porcelain shell was observed during the 3 milliseconds simulation runtimes. Figure 6 - 1 shows the initial conditions of the 2D model of the sphere sliced along the axis of symmetry with the air void between the TNT explosive and the porcelain shell.

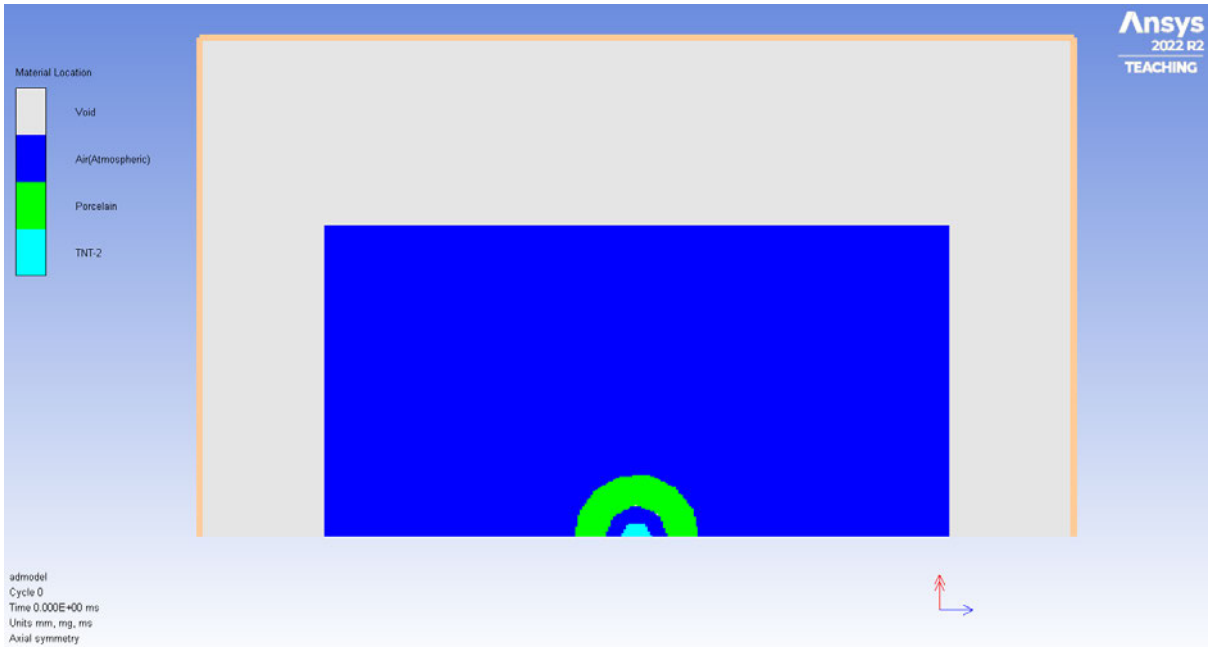

Figure 6 - 1. 2D sphere using multi-material Euler with boundary conditions set.

Figure 6 - 2 shows the results of the detonation with the TNT having expanded into the air void inside the porcelain shell. The porcelain outer shell has not fragmented during the simulation time which was approximately 40 milliseconds.

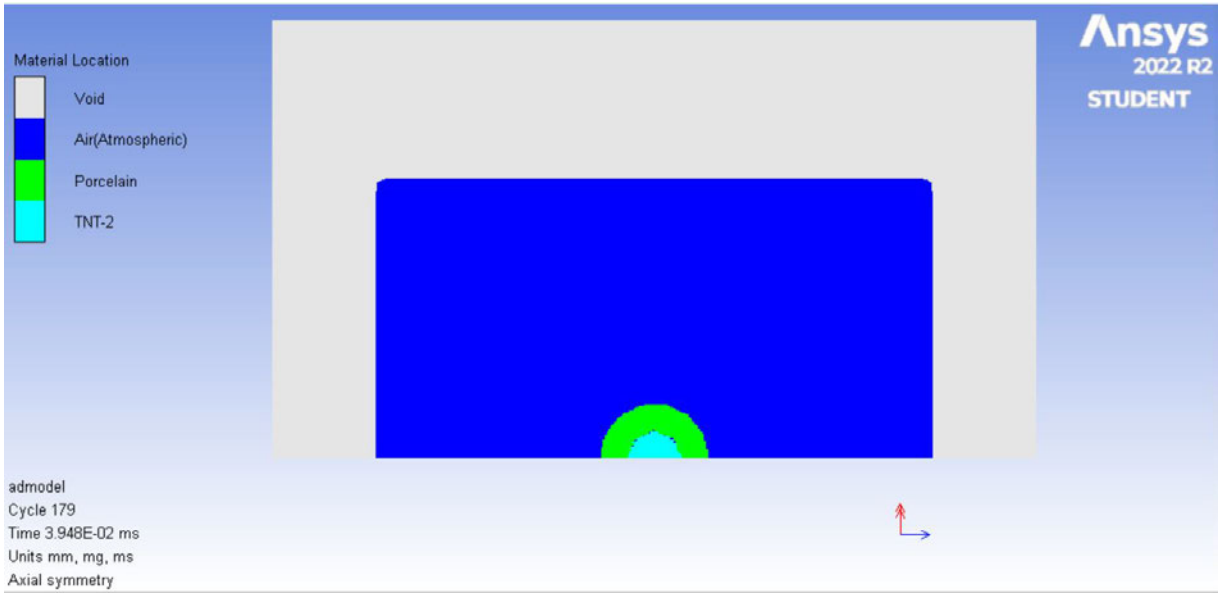

Figure 6 - 2. 2D sphere modelling results using multi-material Euler.

Adjustments to the 2D model were made to refine the brittle characteristics of porcelain material. The changes were not supported within the Ansys Autodyne software suite, resulting in no further analysis of 2D modelling being conducted.

6.2.2 3D Simulations

The primitive cylinder was used to represent the surge arrestor with dimensions and layers of materials properties tested using the explicit dynamic suite, results tabulated in Table 6 - 1.

Table 6-1. Porcelain Shell thickness fragmentation results

Porcelain Thickness (cm)	Radius TNT (cm)	Height TNT (cm)	Porcelain (kg)	TNT (kg)	Fragmentation
0.8	6.8	58.4	6.49	14.00	Yes
0.9	6.7	58.2	7.24	13.54	Yes
1	6.6	58	7.97	13.10	Yes
1.1	6.5	57.8	8.68	12.66	Yes
1.2	6.4	57.6	9.38	12.23	Yes
1.3	6.3	57.4	10.07	11.81	Yes
1.4	6.2	57.2	10.75	11.40	Yes
1.5	6.1	57	11.41	10.99	Yes
1.6	6	56.8	12.05	10.60	No
1.7	5.9	56.6	12.68	10.21	No
1.8	5.8	56.4	13.30	9.83	No
1.9	5.7	56.2	13.91	9.46	No
2	5.6	56	14.50	9.10	No

The external dimensions of the cylinder were maintained throughout testing while the thickness of the porcelain and amount of TNT explosive was adjusted to determine the maximum thickness of the porcelain required below which fragmentation occurred. Figure 6 - 3 shows a cross section of the cylinder with the identified maximum thickness of 15 mm of porcelain.

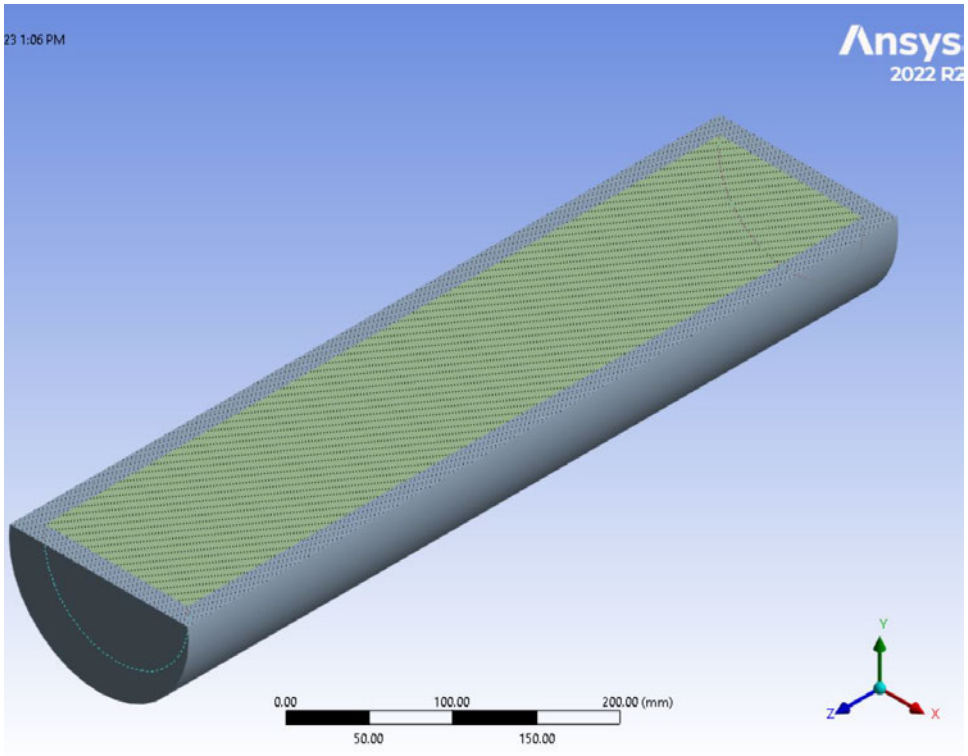

Figure 6-3. Cross section of porcelain cylinder with an internal layer of TNT explosive.

The simulation time for the model is set to 10 milliseconds for explicit nonlinear event with the screenshots of the animated solution in Figure 6 - 4 showing, from left to right, the initial condition through to the amount of fragmentation after 10 milliseconds.

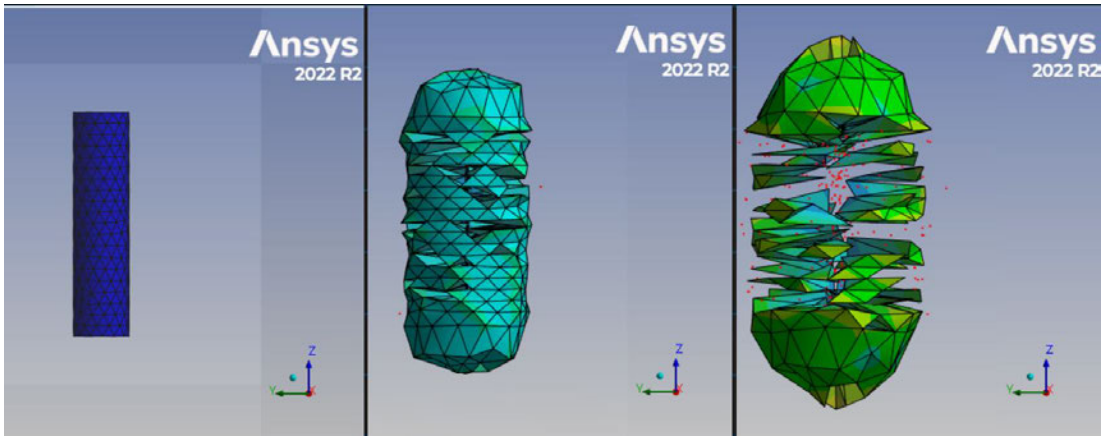

Figure 6 - 4: 3D Porcelain cylinder 10-millisecond simulation time.

The results of the 3D simulated porcelain cylinder model for incident energy 'INT_ENERGYALL' can be seen in Figure 6 - 5. The maximum amount of incident energy that the porcelain cylinder was exposed to was 3.7 MJ in 1.3 milliseconds. This represents a significant amount of energy that has been expelled in a very short amount of time. Energy continues to be available following the initial peak though the amount is reducing over the remaining time of the simulation.

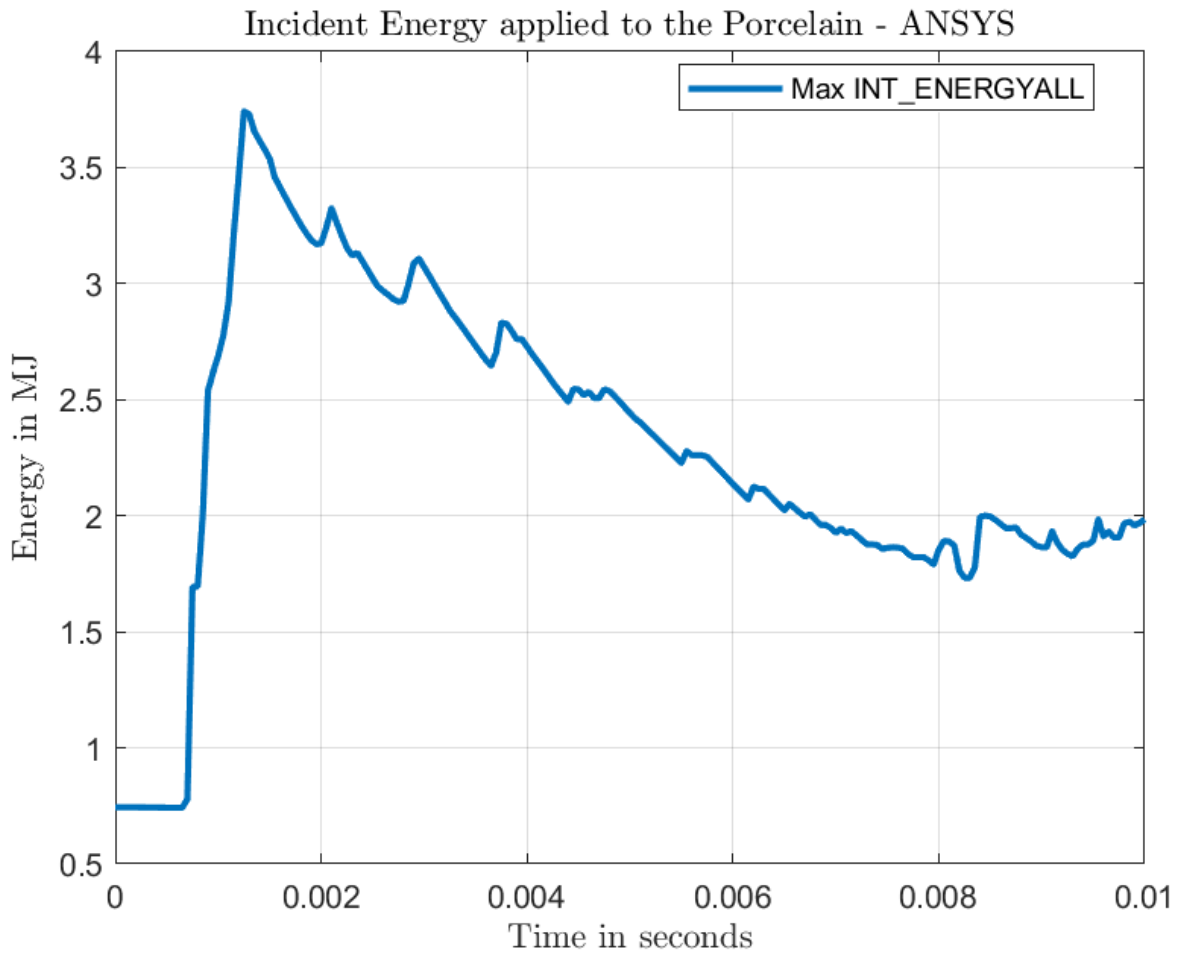

Figure 6 - 5: The maximum incident energy of the simulated explosion.

Looking at the solution results for pressure in Figure 6 - 6 and more closely in Figure 6 - 7 there is a very large pressure spike of 2.5 MPa in 0.7 millisecond. This represents a release in pressure at that point in time. The pressure stabilises for a very short period at around 1.6 MPa before the pressure drops below initial conditions after 3 milliseconds. The entirety of the pressure event that is caused by the explosion occurred within a very short amount of time.

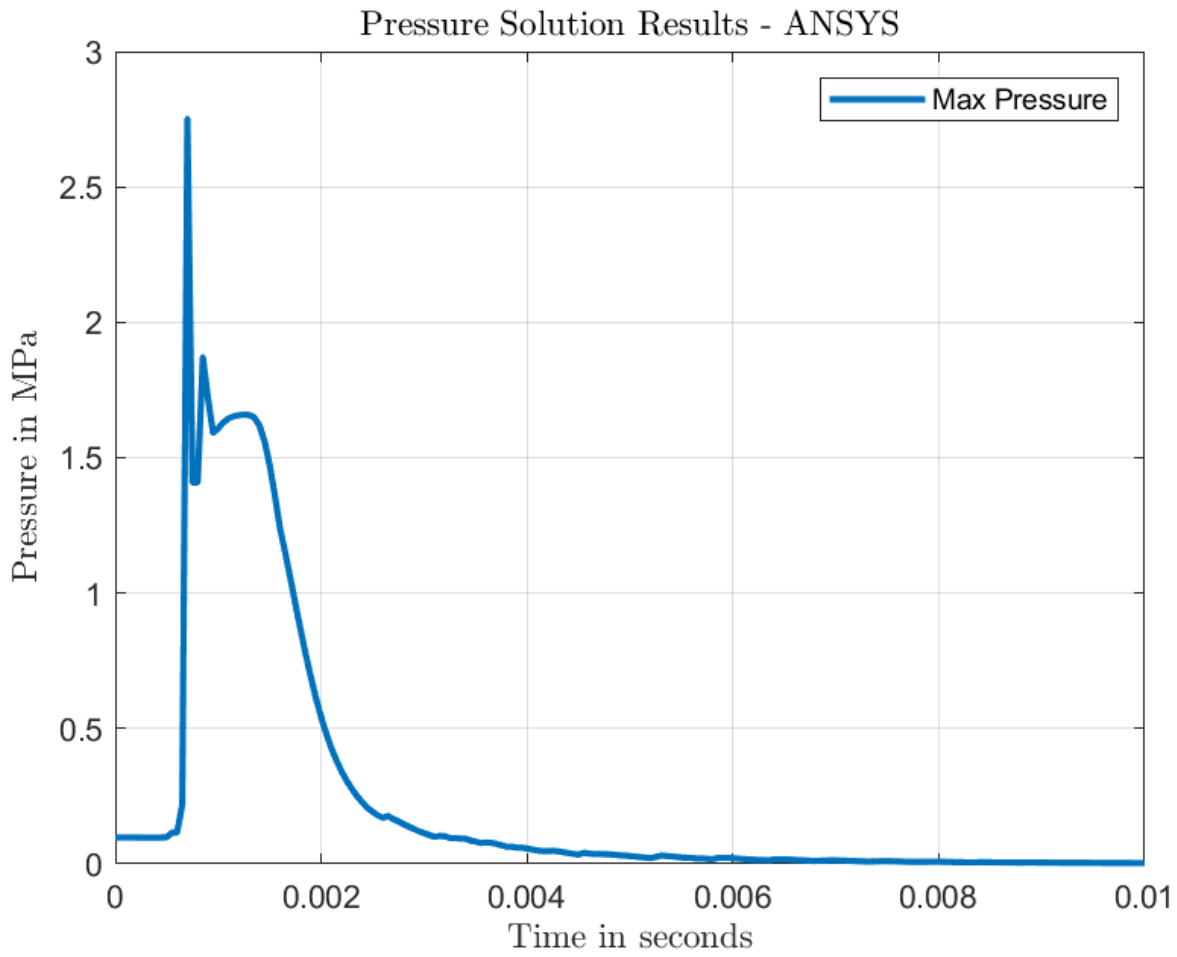

Figure 6 -6: The maximum pressure of the simulated explosion.

Figure 6 - 7 shows a higher resolution of the peak pressure from the Ansys models pressure solution. The data points on the plot provide a clearer view of the period from initial stress rise to the pressure peak. It is interesting to note that the initial rise to the peak occurs in 50 microseconds though the amount of pressure is less than the tensile strength of HV porcelain which is 55 MPa according to The Engineering ToolBox (2008).

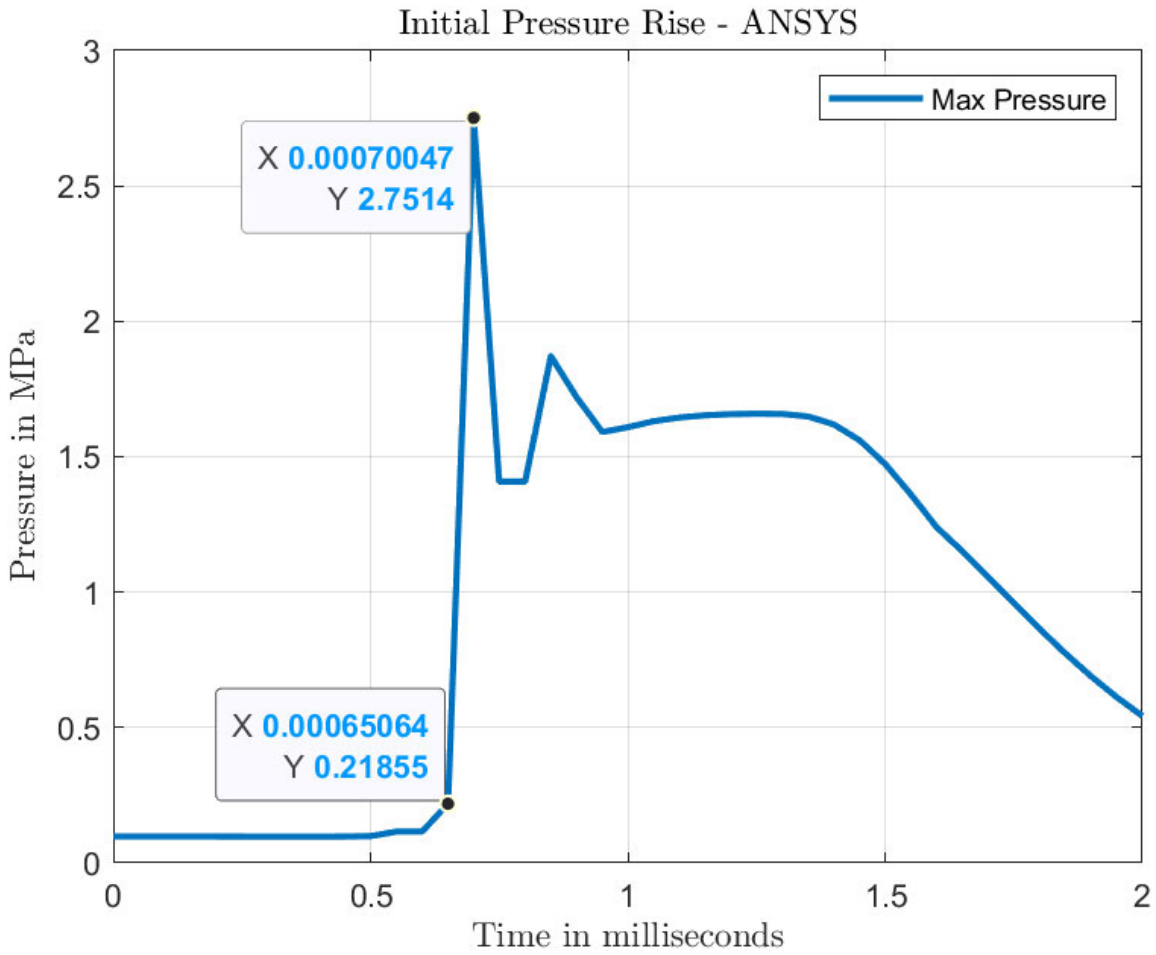

Figure 6 -7: The peak pressure points of the simulated explosion.

6.2.3 Conclusions of Ansys 2D and 3D modelling results

The explicit dynamics Ansys simulation package was able to provide model solutions of the explosion of a hollow cylinder with material properties from the available literature that could be considered conducive to HV porcelain. The total energy required to fragment the shell is high, which can be attributed to the simulation of the entire event not just the fragmentation and subsequent projectile phase. Modelling solutions of projectile distances of a brittle material was not successful due to its not being supported for fragmentation analysis. The pressure

solutions provided a potential insight into the time of the fragmentation phase though the amount of total pressure was significantly lower than the typical tensile strength values for HV porcelain.

6.3 PHYSICS BASED PROJECTILE MODELS

6.3.1 Projectile parameters

The projectile modelling script created in MatLab required the setting of the porcelain shell dimensions, the estimated size of the surge arrestor, and the Ansys fragmentation results. The mass and area of the three fragment sizes were calculated from these dimensions. These values were entered into the formula for terminal velocity and subsequently used in the derivation of the vertical component of velocity, with the results tabulated in Table 6 - 3. It was noted that the terminal velocity does not change with fragment size, as they have not yet been affected by air resistance.

Table 6 - 3. Porcelain Shell fragments and initial trajectory parameters.

Dimension	Mass (kg)	Area (m^2)	Terminal velocity (m/s)	Vertical component of velocity (kg/s)
Porcelain Total	11.406	0.6635	21.41	5.225
3 Fragments	3.8019	0.2212	21.41	1.742
5 Fragments	2.2811	0.1327	21.41	1.045
10 Fragments	1.1406	0.0664	21.41	0.5225

The initial velocity calculation using the derivation of equation 21, KE, is dependent on the amount of energy that is derived from the incident energy. The results of the Ansys solution and the energy calculation of the known events data using various times for energy transfer from the source to a projectile are tabulated in Table 6 - 4. It is important to note the influence variability of time has on the amount of energy available to the projectile, this will be analysed in the Discussion section.

Table 6 - 4. Energy calculations from simulations and computations

Data Source	Event time (m/s)	Energy (kJ)
Ansys Max	Max value	3400
Ansys Max less initial	Max value	2729
Known incident, typical fault clearing time	150	458
Known Incident, explicit time	1	3.056
Known Incident, initial stress rise - Pressure Ansys	0.65	1.986

The amount of energy available to a given fragment number or size for an estimated time of the initial blast phase can be viewed in Table 6 - 5. For comparison, the total amount of energy from the Ansys simulations Max INT_ENERGYALL was also included.

Table 6 - 5. Energy available to each fragment for time estimate.

Fragments	0.65ms (Joules)	1 ms (Joules)	150 ms (Joules)	Ansys Max Energy (Joules)
3	662	1,019	152,802	1,134,800
5	397	611	91,681	680,880
10	199	306	45,841	340,440

6.3.2 Projectiles modelling of height and distance.

The energy from the simulations and computations combined with the parameters for two trajectory angles of 25 degrees and 45 degrees are displayed in Figures 6 - 8 through to 6 - 11. The negative values on the y axis enable visualisation of where an ERF is installed off the ground. The total energy solution from Ansys is shown below in Figure 6 - 8. This amount of energy for any of the three fragment sizes cannot be differentiated for either trajectory angle shown by the two plot lines. The linear nature of the trajectories produced using the Ansys model does not match the parabolic path that is typical of projectiles affected by gravity and air resistance.

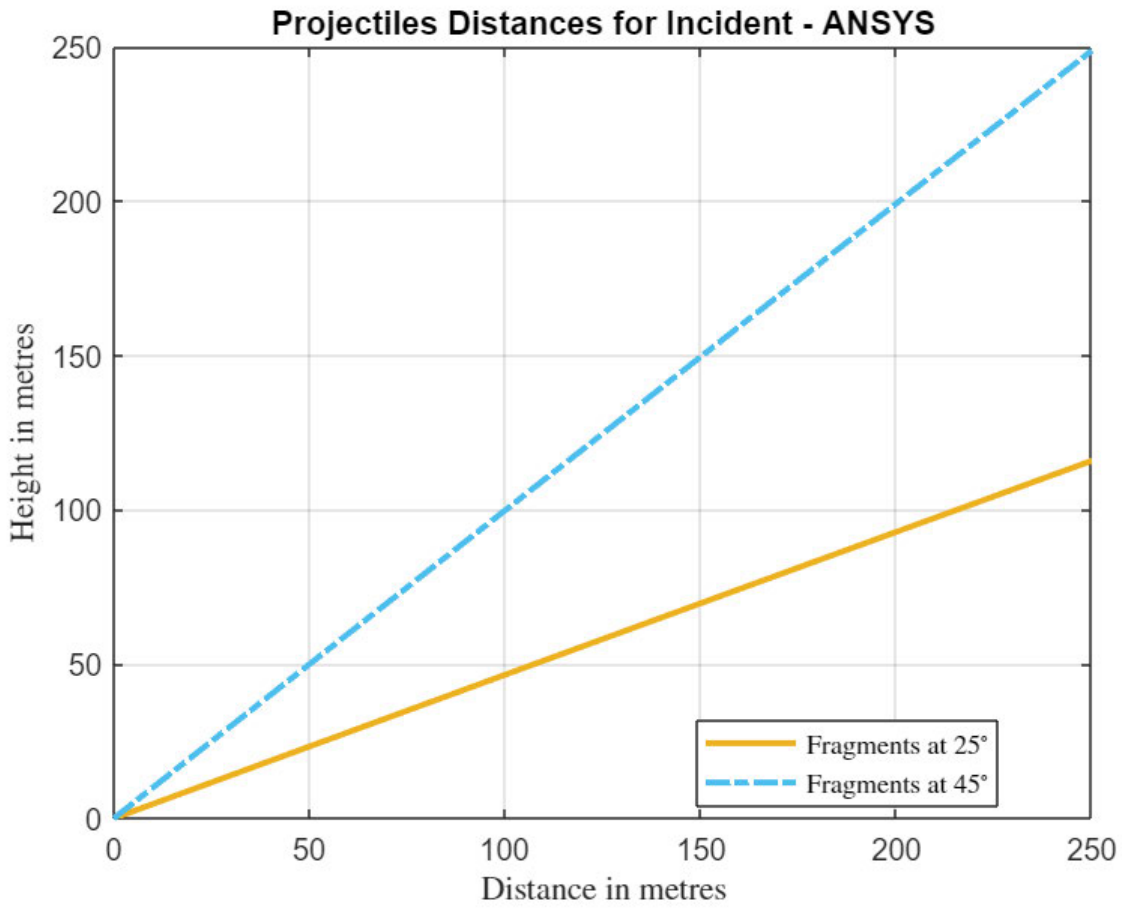

Figure 6 - 8: Projectile distances for INT_ENERGYALL maximum.

The projectile distances of the known incident energy using the total amount of time available, which is the Circuit Breaker (CB) clearing time of 150 milliseconds, is shown in Figure 6 - 9. The travel distances of the projectiles for both trajectory angles are beyond the limits of the plot's axis of 250 metres.

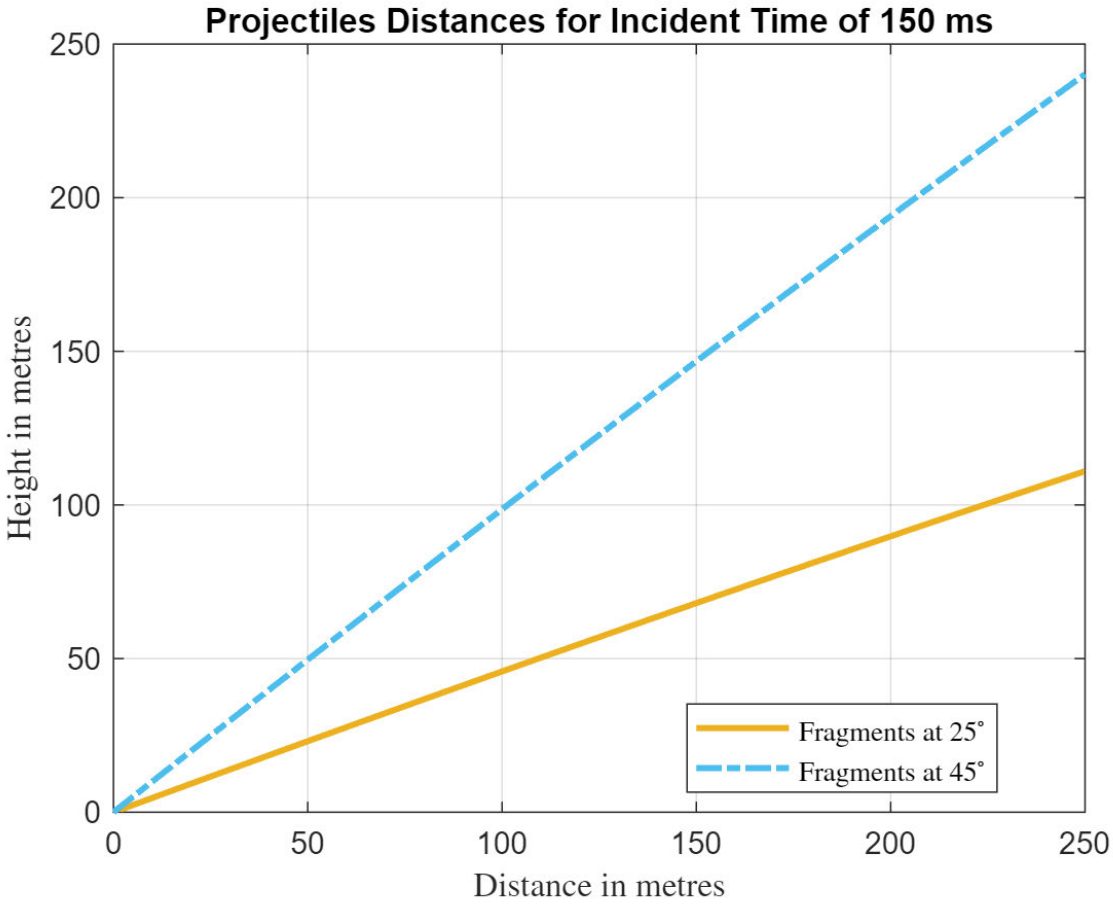

Figure 6 - 9: The projectile distances for a known incident energy transfer duration of 150ms.

Further modelling of the time available for energy transfer during the electrical arc blast was carried out. Figure 6 - 10 shows the estimated projectile distances using a 1 millisecond period and the known incident data. These results are comparable to historical events of ERF failure.

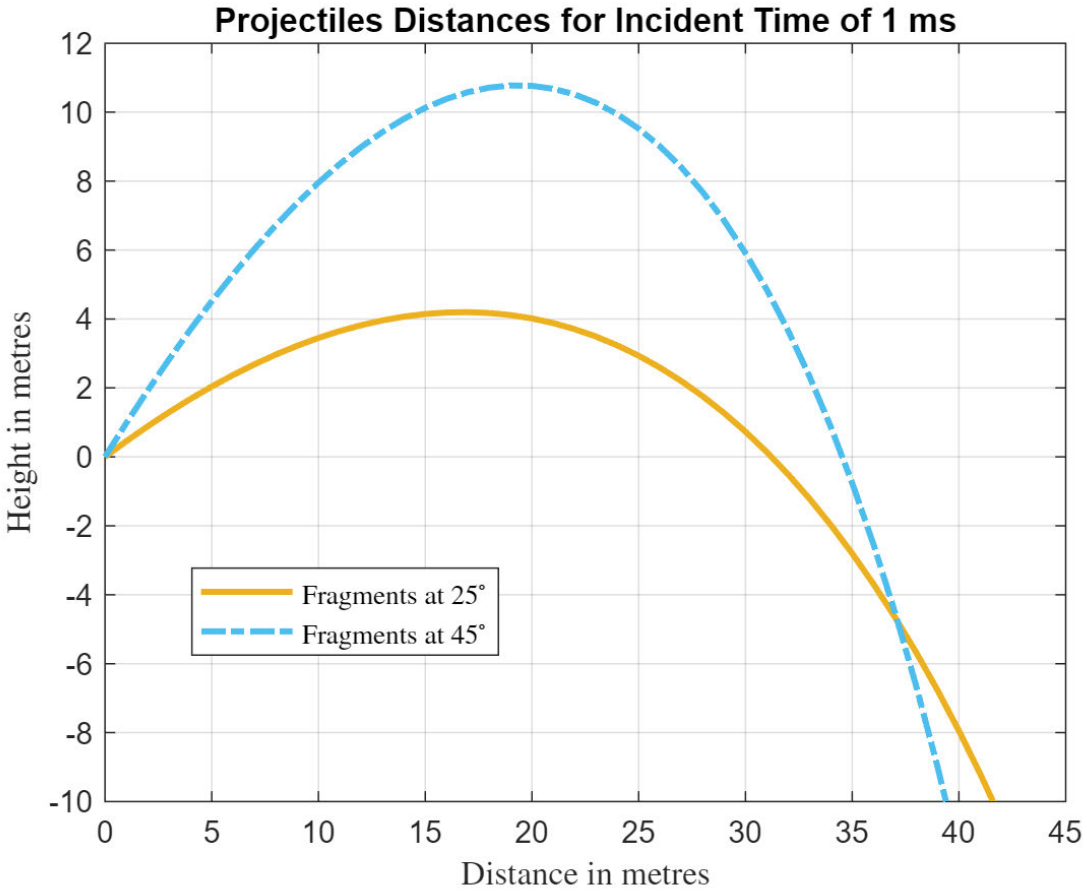

Figure 6 - 10: The projectile distances for known incident energy transfer duration of 1ms.

The observations of pressure and the time involved for the initial stress rise that was observed within the Ansys solution was modelled using the known incident and is shown in Figure 6 - 11. Reducing the time interval of the explosion to 0.65 milliseconds, in line with the expected time of fragmentation. This resulted in between a ten to twenty metre reduction in total distance travelled dependant on the trajectory angle and the height of the ERF installation.

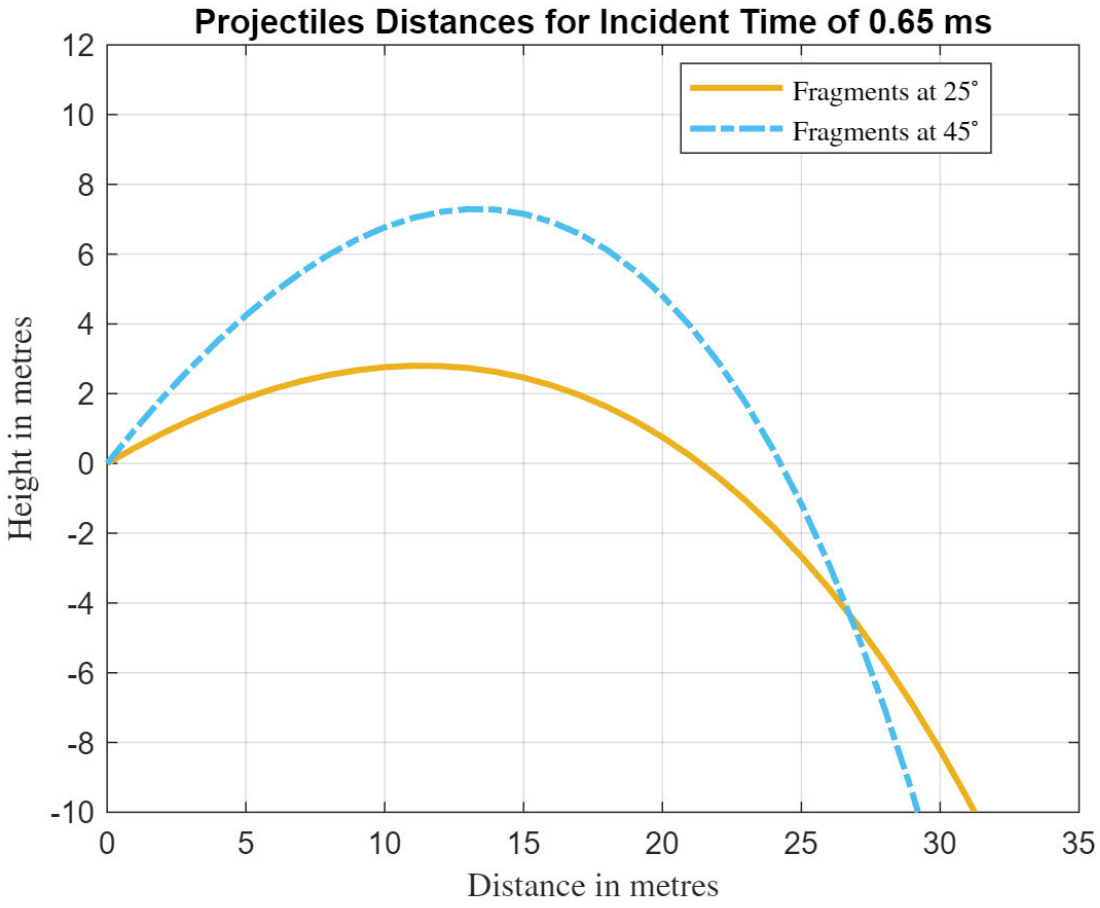

Figure 6-11: The projectile distances for known incident energy transfer duration of 0.65 ms.

6.3.3 Conclusion physics based projectile models

The comparison of Ansys solutions with formulae from literature for energy and projectiles identified that the estimated total amount of energy available from an electrical explosion or blast is significant. Analysis of the time available for the blast was also conducted. This required the time available for energy transfer to be reduced into the range between microseconds to less than a millisecond. The solutions derived using these shorter time periods produced an estimate of trajectory distances that aligned closely with historical event data.

6.4 CHAPTER SUMMARY

The results chapter provides a summary of the Ansys modelling, and the physics based projectile model results using the software program MatLab. The data from both Ansys solutions and the known incident were evaluated. This included changes to the projectile model's settings following initial results from Ansys solutions and the total energy available depending on time. It was shown that if either all the available incident energy, or an excessive amount of time was available for the explosion to occur, then a projectile is estimated to travel well beyond what is comparable with past events.

7 DISCUSSION

7.1 CHAPTER OVERIEW

This chapter will expand on the results that were achieved during this research project. Starting with the initial results from the Ansys and physics based projectile models, discussion will be expanded to address the phenomenon of material vaporisation and the effect of time and the total potential energy of the electrical arc blast in the open environment. These findings are contextualised to relate to the safety of individuals when exposed to the risks of an ERF. The key parameters for a determined calculation of the energy available for a given situation are presented for peer review.

7.2 ANSYS MODEL

The modelling of a porcelain cylinder explosion and subsequent fragmentation was studied to determine the characteristics of the event. The initial parameters that were assessed was the amount of TNT explosive that is required for fragmentation of the porcelain shell at various porcelain thicknesses. This allowed iterative analysis to be carried out using the INT_ENERGYALL solutions in conjunction with the built-in solution simulation package for both 2D and 3D models. The incident energy from the estimated surge arrester dimensions can be seen in Figure 6 - 1 for the event period of 10 milliseconds.

The 2D and 3D simulations that included an air gap between the porcelain shell and the TNT explosive identified that the model settings were limiting the test results. In these situations, the expansion of the explosive material was apparent in the simulations, but no fragmentation of the porcelain occurred as seen in Figures 6 - 1 and 6 - 2. For iterations where the air gap was removed the fragmentation parameters were identified. There were several potential causes for the air gap iteration failing to fragment, including material properties model settings, and the boundary conditions between material within the simulation model.

The Ansys simulations were continued with the air gap removed between the porcelain and the TNT explosive. The thickness of the porcelain shell was reduced over a series of iterations to identify the maximum thickness of the simulated porcelain shell, below which fragmentation

would occur. The results in Table 6 - 1 show that a thickness of 15mm was the maximum thickness beyond which fragmentation would not occur. For each successful fragmentation solution there were no noticeable change in the amount of incident energy required. This peaked at 3.7 MJ within 1.3 seconds before trending downwards over the remaining time simulation and can be viewed in Figure 6 - 5.

The pressure peak result, according to The Engineering ToolBox (2008), is significantly lower than the typical tensile strength for HV porcelain which is between 20 and 50 MPa. The potential cause for the simulated peak pressure being lower than what is typical is the rapid pressure change or the shock caused by the detonation of the explosive. It is argued by Rao et al. (2020) that dynamic loads from this detonation and the high speed outward directed forces would cause deformations of a casing or shell. The brittle nature of porcelain and the forming of cracks due to rapid deformation is considered a potential reason for this pressure peak result.

The initial peak in incident energy, according to Quan et al. (2006), is the phase of the event that includes the blast and the beginning of fragmentation which can be viewed in Figure 3 - 4 on page 15 within the literature review section. Analysing the pressure solutions for each iteration showed only a small difference in values or shape of the plot where fragmentation was successful. The initial peak was noticeable as shown in Figure 6-6. Closer examination of Figure 6-7 showed the initial pressure peak occurred at 0.65 milliseconds, and this could correlate to the point of the explosion. The pressure does not fully dissipate following this initial peak with pressure continuing to hold above half the peak pressure for approximately 1 millisecond before trending towards zero at the end of the simulation period. Of the simulations that were modelled in Ansys, all thicknesses of porcelain that fragmented showed an initial pressure peak at around two-thirds of a millisecond, similar to that shown in Figure 6-7. These findings are comparable to that argued by Tasdemirci and Hall (2007), being that the initial stress rise reaches its maximum at the point of failure, in the case of this research, the casing of the surge arrester.

After the initial pressure peak, the remaining pressure and kinetic energy released after that time would not be available to the fragments as they would have dispersed. Further analysis of the projectile and the explicit time associated with this phase was not successful due to the fracturing of porcelain not being supported by Ansys Autodyn. The Ansys solutions provide evidence that pressure build up within a cylinder can lead to fragmentation of the shell that has material properties modelled on ceramics. For all solutions the time for each peak in both

energy and pressure remained relatively constant. The solutions from the Ansys simulation raised additional questions that require further investigation using other means due to the limitations mentioned above.

7.3 PROJECTILE MODEL

The physics based projectile model was used to study the characteristics of fragments that can be expelled from an electrical explosion. The model utilised the dimensions of the estimated surge arrestor, the incident energy from a known event using equation 6, see page 7, the incident energy solution from Ansys for comparison. To produce suitable parabolic projectile curves for analysis, air resistance and gravity were also incorporated into the model. The location of the surge arrester installation was also included into the analysis by adjusting the y-axis to enable a negative height of 10 metres to represent the ERF being situated above the ground or zero point. With this data, an iterative analysis of the trajectory angles, fragment sizes and the amount of energy that could be transferred to a fragment was conducted.

The inclusion of drag within the computations required assumptions to be made in relation to the Coefficient of Drag (CD) which is included within the terminal velocity equation 21. The speed at which fragments are moving during the initial blast phase according to Ćatović et al. (2018) are well above the local sound velocity and due to this, the CD is considered to be constant for the entire trajectory computation. It can also be assumed that fragments will be exposed to turbulent air during the explosion or blast. For these reasons a CD of 0.2 was chosen. This value, according to by Cengel (2017), is for a sphere in turbulent air which could be considered a worst case scenario for a fragment during an electrical explosion.

The maximum possible incident energy available to all fragments created was modelled initially to estimate the furthest potential distance a fragment could travel. This was modelled using the simulations and computations from Ansys in Tables 6 - 4 and 6 - 5. As shown in Figure 6 - 8, fragments of all types were observed to follow a linear, and not parabolic, trajectory. As the trajectory was linear, fragments with maximum energy never approach zero on the x axis and therefore this makes this scenario impossible. This is because the amount of energy available for a given fragment is shown to be well beyond what could be considered realistic.

Three time periods for modelling of an ERF are considered. These are the typical clearing time for a CB of 150 milliseconds, 1 millisecond and 0.65 milliseconds, as seen in trajectory plots shown in Figures 6 - 9, 6 - 10 and 6 - 11 respectively. These time periods were chosen to align with the maximum possible time for an event to occur, which is limited by the CB, a nominal time of 1 millisecond, and 0.65 milliseconds to represent the initial peak pressure time observed in Ansys. The projected distances of fragments are comparable to the data collected for the known incident with the amount of energy available to each fragment in kilojoules or lower. Only in the plots with time periods of 0.65 and 1.0 millisecond did projectiles reach the ground at comparable distances to known historical events. This indicates that the energy available to a projectile during an electrical explosion is less than the MJ's estimated in the Ansys solutions.

The initial solutions from projectile modelling were used to identify what parameters could be considered when examining the phenomenon of an electrical explosion. The inclusion of drag on the projectiles allowed for practical representations of trajectories supporting this discussion. These computations have raised several questions around the time that is available for energy transfer to projectiles and the amount of energy that is involved, including the energy that is lost over the trajectory distance.

7.4 PROJECTILE MODEL EXTENDED

To extend the analysis of the blast and subsequent porcelain projectiles, the energy over the distance of the trajectory was considered. This modelling estimates the total potential energy that an individual could be exposed to, if within the path or hazardous zone of a projectile. Rearranging equations 11 through 21 to calculate a result for energy over a distance, provides an estimate of the energy released for the known event, giving an initial velocity (V_0) for each fragment size by rearranging KE.

Expanding V_{x0} and V_{y0} with V_0:

$$t = \frac{m}{b}\ln\left(\frac{mV_0\cos\theta}{mV_0\cos\theta - bx}\right) \tag{32}$$

$$V_x(t) = V_0 cos\ \theta * e^{-\frac{bt}{m}} \tag{33}$$

$$V_y(t) = \left(\frac{mg}{b} + V_0\sin\theta\right)e^{-\frac{bt}{m}} - \frac{mg}{b} \tag{34}$$

Kinetic Energy for time:

$$KE(t) = \frac{1}{2}\,m\left[{V_x}^2(t) + {V_y}^2(t)\right] \tag{35}$$

These formulae enable the energy over a distance to be estimated for a given fragments mass (m) and angle (θ). This assists in the identification of the potential energy that is available as the projectile travels away from the source of the event. Three ERF installation heights were analysed to replicate typical locations where surge arrestors are installed in the outdoor environment. The kinetic energy of a projectile (projectile energy) at any given point is graphed in Figures 7 - 1 through 7 - 4.

The estimated potential energy from an ERF installed on the ground can be seen in Figure 7 - 1. The amount of energy available at the point of explosion is the same regardless of angle for a given number of fragments. At ground level all fragments at 25 degrees impact the ground at the same distance, and fragments at 45 degrees travel further. This can be attributed to the additional height afforded by the trajectory angle which leads to longer flight time. For fragment trajectory at 25 degrees their projectile energy at any given point after the explosion is greater than the equivalent 45 degree fragments.

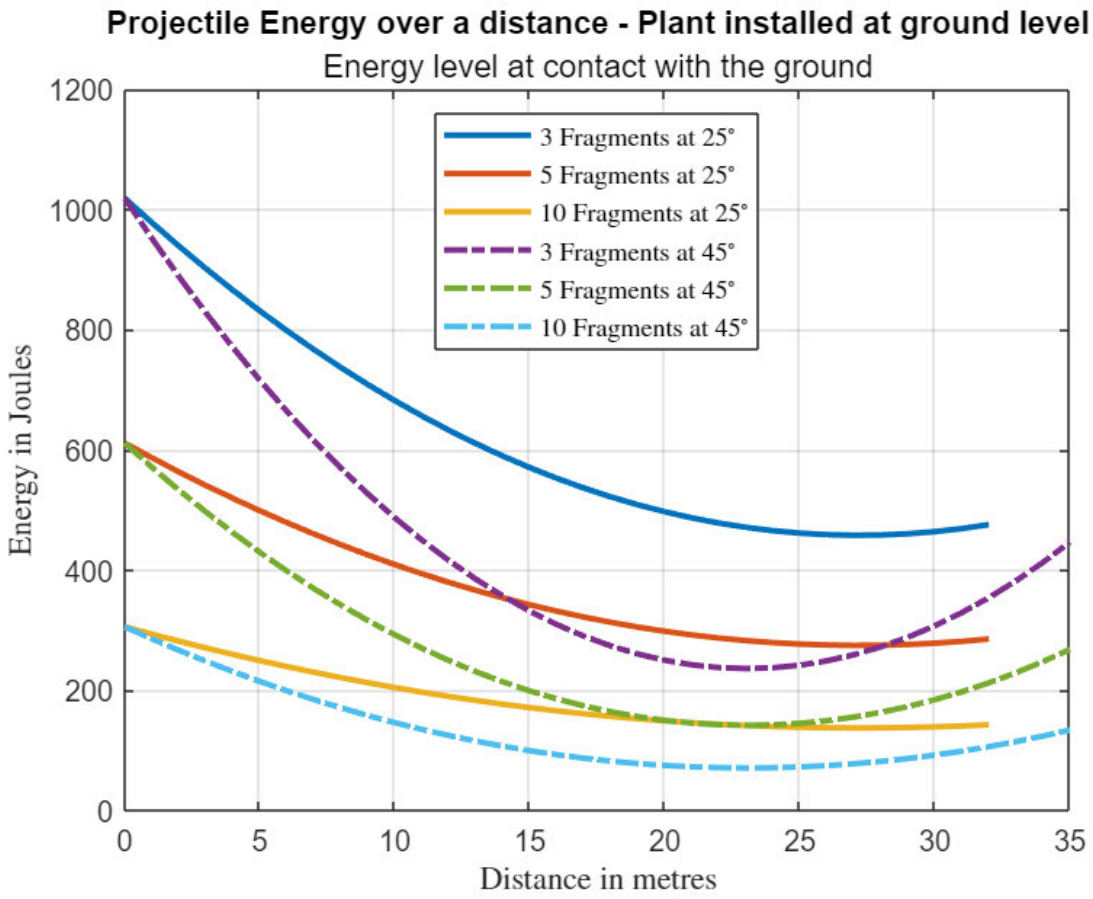

Figure 7 - 1: Estimated projectile energy over a distance for ERF installed at ground level.

The available energy over a distance for ERF installed 5 metres above the ground level can be seen in Figure 7 - 2. In this scenario all fragment sizes, independent of their trajectory angles contact the ground at the same distance from the explosion and with similar impact energy. At 5 metres above ground level, both 25 and 45 degree fragments travel further, and with more projectile energy at impact, than they do for an ERF at ground level.

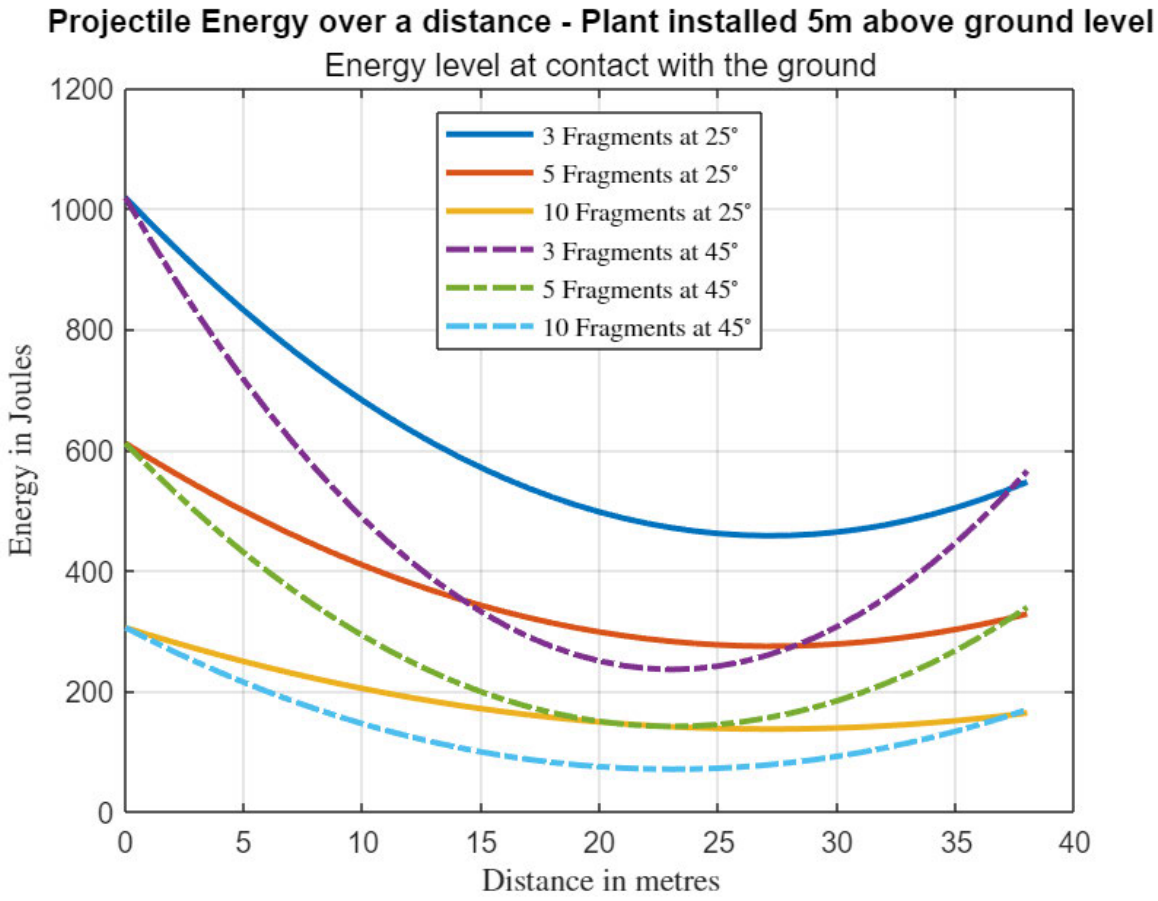

Figure 7 - 2: Estimated projectile energy over a distance for ERF installed height 5 metres.

When the ERF is installed 10 metres above the ground level, projectile energy over a distance can be viewed in Figure 7 - 3. In this scenario, the energy that a projectile would have when it impacts the ground would be the largest of all height installations modelled. Fragments that leave at 45 degrees now impact the ground earlier than those at 25 degrees, and with greater projectile energy.

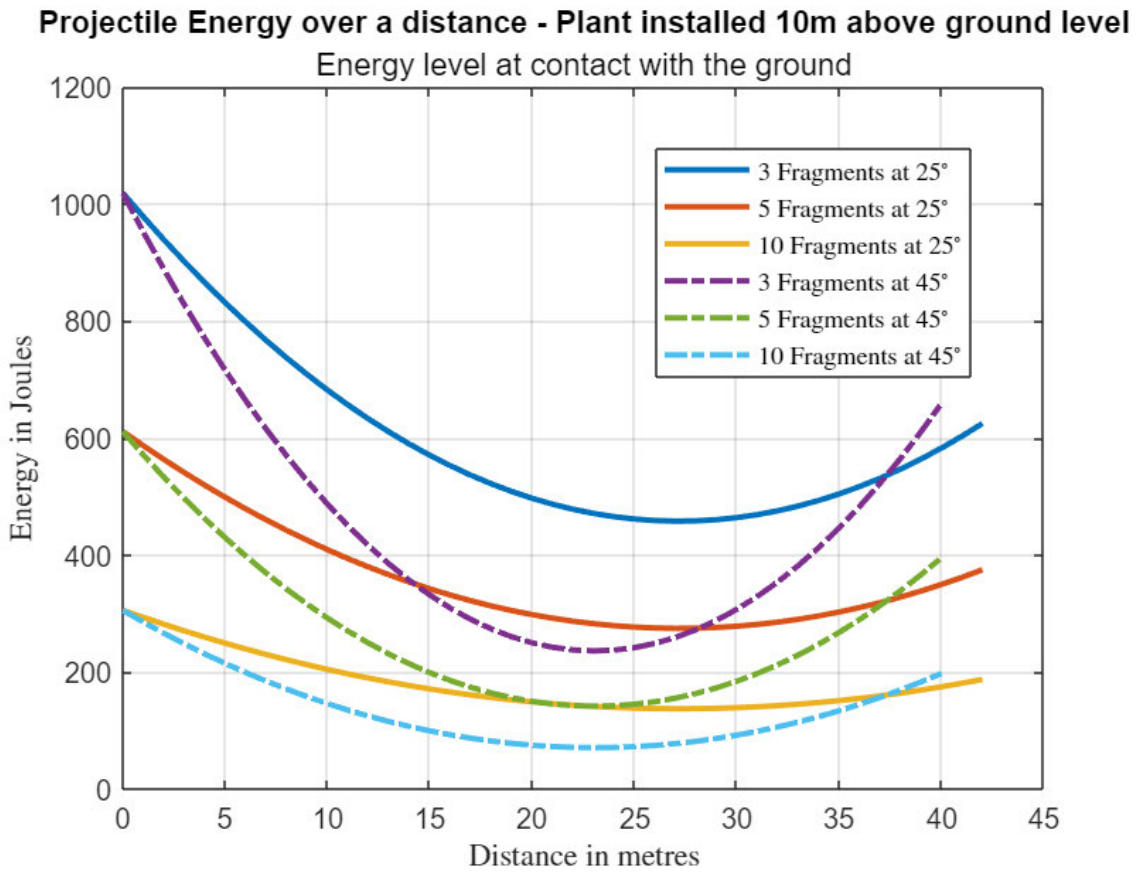

Figure 7-3: Estimated Projectile energy over a distance for ERF installed height 10 metres.

Each simulation of the projectile energy fragments produced in an electrical explosion of a surge arrestor showed that the installation height of the ERF influences the distance that a projectile will travel. This is due to fragments having further to fall along their trajectory before reaching the ground. The point of impact to the ground is given by the height of the installation y, and the distance x, as can be seen in Figure 6 – 10 on page 48. The plots provide visual representation of the available energy at a given distance from an electrical explosion. The energy at the point of impact with the ground for each height installation of the ERF can be seen in Table 7 - 1.

Table 7 - 1. Estimated projectile energy at point of impact with the ground.

Angle	Fragments	0 metres (Joules)	+5 metres (Joules)	10 metres (Joules)
25 Degrees	3	475	547	625
	5	285	328	375
	10	143	164	187
45 Degrees	3	446	565	659
	5	268	339	395
	10	134	170	198

All plots produced showed the same parabolic path for 3, 5 and 10 fragments respectively at the two trajectory angles studied. This shows that regardless of angle that a fragment leaves the explosion, its initial projectile energy is only dependant on how many fragments are produced and not its angle. Once expelled, the angle of the fragments projection now affects its flight path. All fragments lose energy in their flight path towards their peak, and then begin to gain energy again as they start to fall as gravity now works to increase their speed and therefore available projectile energy This shows that energy loss due to friction in air is less than that of gravity. Those leaving at the higher angle, 45 degrees, have more energy directed upwards against the force of gravity and so travel higher before falling to the ground. At closer distances, those fragments leaving the explosion at 25 degrees have more projectile energy as they are less effected by gravity. At a further distance, in this case at 37 metres, the flight paths of the 2 trajectory angles cross and the 45 degree fragments past this point have more available projectile energy.

We can infer that, in a real-life scenario, an electrical explosion would produce fragments of multiple sizes expelled at differing trajectory angles, and consequently that fragments would impact the ground at a spread of distances. Fragments of any size will all travel the same distance if they have the same trajectory angle. However, smaller fragments would have less initial projectile energy available to them and so would impact the ground with a lower impact force than larger fragments. Therefore, it is the angle that dictates the distance travelled before impacting the ground, and it is the fragments size that dictates its projectile energy at impact.

The impact energy that is available from these computations are shown to be in the range of hundreds of joules. To provide some context to these energy values and their ability to cause property damage or injury, a comparative analysis was undertaken to understand what being struck by a fragment is equivalent to. For example, the impact energy available from a baseball thrown by a professional pitcher is approximately 140 joules according to Windpact (2023). Another is the amount of KE a 0.02kg bullet has when travelling at 300 m/s, which is 900 joules. Both examples can be seen in Figure 7 - 4 with a comparison to 3 fragments starting on a 45 degree trajectory.

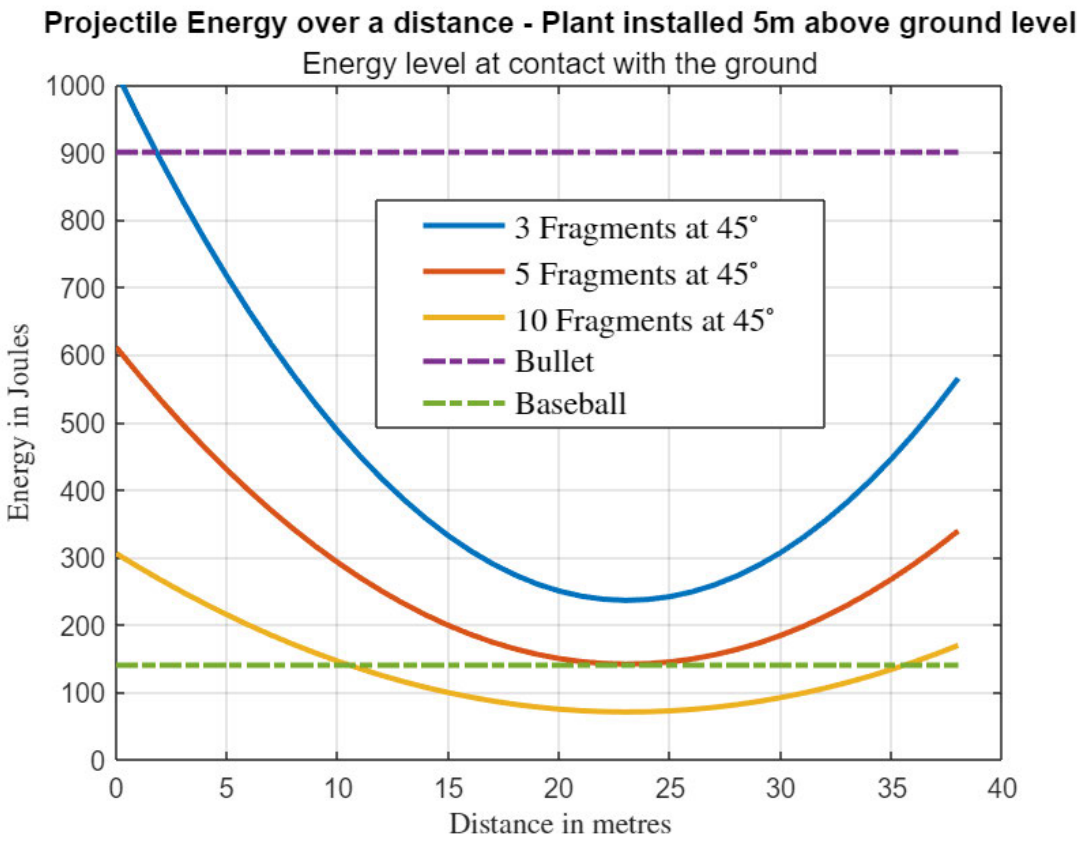

Figure 7 - 4: ERF installed 5 metres above ground level compared to a baseball and a bullet.

Hallowell et al. (2017) showed that energy forces experienced above 100 joules in all cases required at minimum first aid care, with most requiring higher medical care, see Figure 7 - 5. Energy magnitudes above 500 joules have resulted in fatalities. The projectile energy of the fragments, when in close proximity to the ERF, aligns with the energy found of a bullet at impact TotalShield (2022).

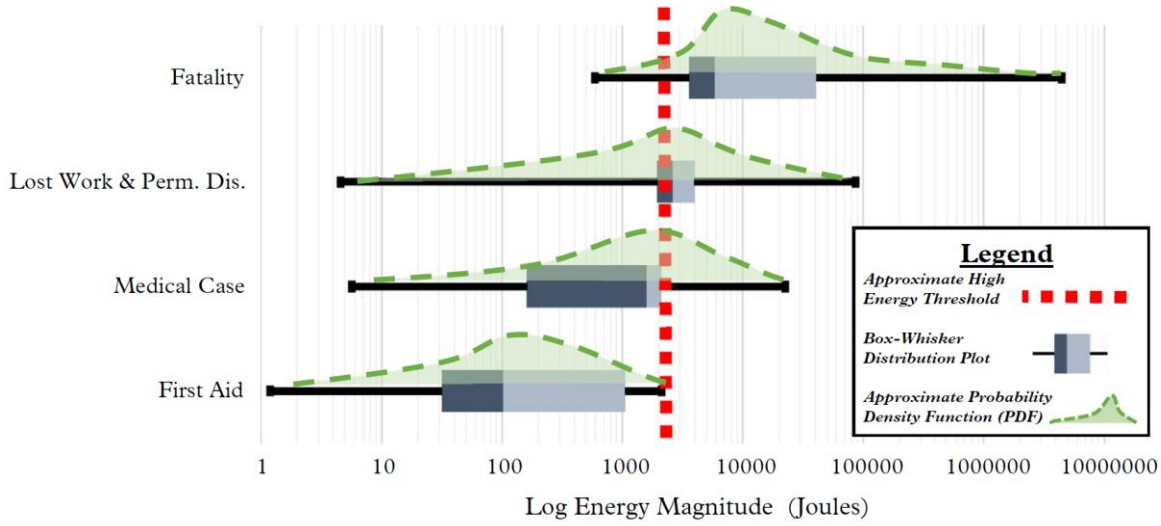

Figure 7 - 5: Boxplot distributions of energy magnitude with respect to injury severity.

The high amount of energy that is available from an electrical explosion initially reduces over distance due to gravity and drag, before increasing as fragments fall to the ground. The projectile was also found to be affected by the trajectory angle and height of the ERF installation. When considering the ERF in this research, it is worth noting that some fragments would still have a projectile energy of 461 joules at 25 metres, which is the typical RMHZ distance setting for similar construction types. Larger fragments held the most projectile energy and could be more dangerous and likely to cause serious injury or fatality across most of their trajectory path.

7.5 VAPORISATION ANALYSIS

In consideration of possible causes of the increase in pressure associated with the electrical arc explosion, vaporisation of metal components was considered. Examinations of historic electrical incidents identified that, in addition to fragmentation of ERF, in some instances metal components, often the electrical conductor, have been observed to have experienced partial melting or vaporisation. This is important as this phenomenon affects the amount of energy available in the event of an electrical explosion and may directly cause the fragmentation itself.

As previously identified, surge arrestors have several internal components, including Aluminium and ZnO, that have the potential to experience some amount of vaporisation, see Figure 7 - 6. A copper conductor was chosen for this analysis due to the ease in obtaining the parameters required for computation of the phase changes, and its widespread use in HV electrical equipment generally. This assisted in determining if there was a significant change to the pressure inside the enclosed porcelain shell caused by vaporisation. The computational modelling of energy and pressure changes caused by the vaporisation of copper utilised the measurement units for copper, found in Table 7 - 2.

Figure 7 - 6: 33kV Gapless surge diverter with pressure relief and sectioned view EQL (2019).

Table 7 -2. Measurement units for vaporisation of copper.

Name	Value	Units
Ambient Temperature – 25ºC	298.15	Degrees K
Universal gas constant	8.134	
Copper Atomic	63.546	u
R - Copper	0.128	kJ/kg. K
Density of 1kg of copper	8830	Kg/m3
Tensile strength of HV Porcelain	55	MPa
Specific Heat - Copper		
Solid	0.385	kJ/kg. K
Liquid	571.7118	kJ/kg. K
Solid to liquid - Temperature		
Fusion Temperature Copper	1358.2	Degrees K
Liquid to vapor - Temperature		
Vaporisation Temperature - Copper	2868.2	Degrees K
Latent Heat of Fusion - Copper	206	kJ/kg. K
Latent Heat of Vaporisation - Copper	5068.8	MJ/kg. K

These units were utilised to estimate the energy required for vaporisation, and the pressure changes for various amounts of copper. Equations 36 through 38 are used to calculate the phase changes associated with converting a solid to a vapor. To estimate the amount of copper vaporised also required considering the volume that the copper occupied prior to its vaporisation. This enabled pressure concentration to be localised using the density of copper in equation 40 resulting in more realistic computational solutions.

$$Energy = Q \tag{36}$$

$$Q_{Specific} = mC\ \Delta T \tag{37}$$

$$Q_{Latent} = mL \tag{38}$$

Ideal gas law,

$$PV = mRT \tag{39}$$

Solving using the density of copper before the explosion,

$$P = \rho RT \tag{40}$$

The amount of metallic material that has been identified as missing, and therefore melted or vaporised, is relatively small in observation made in previous incident reports. Computational analysis found the requisite energy to vaporise copper, graphed in Figure 7 - 7. The plot also shows the amount of energy that could be available for vaporisation of copper if porcelain shell had not fragmented by the time the CB operated. At the tensile strength of porcelain 18 grams of copper was estimated to be vaporised, equivalent to less than 100kJ. For comparison, an Australian $1 coin has a diameter of 25mm, weight of 9 grams and is made up of 92% copper (Royal Australian Mint 2023).

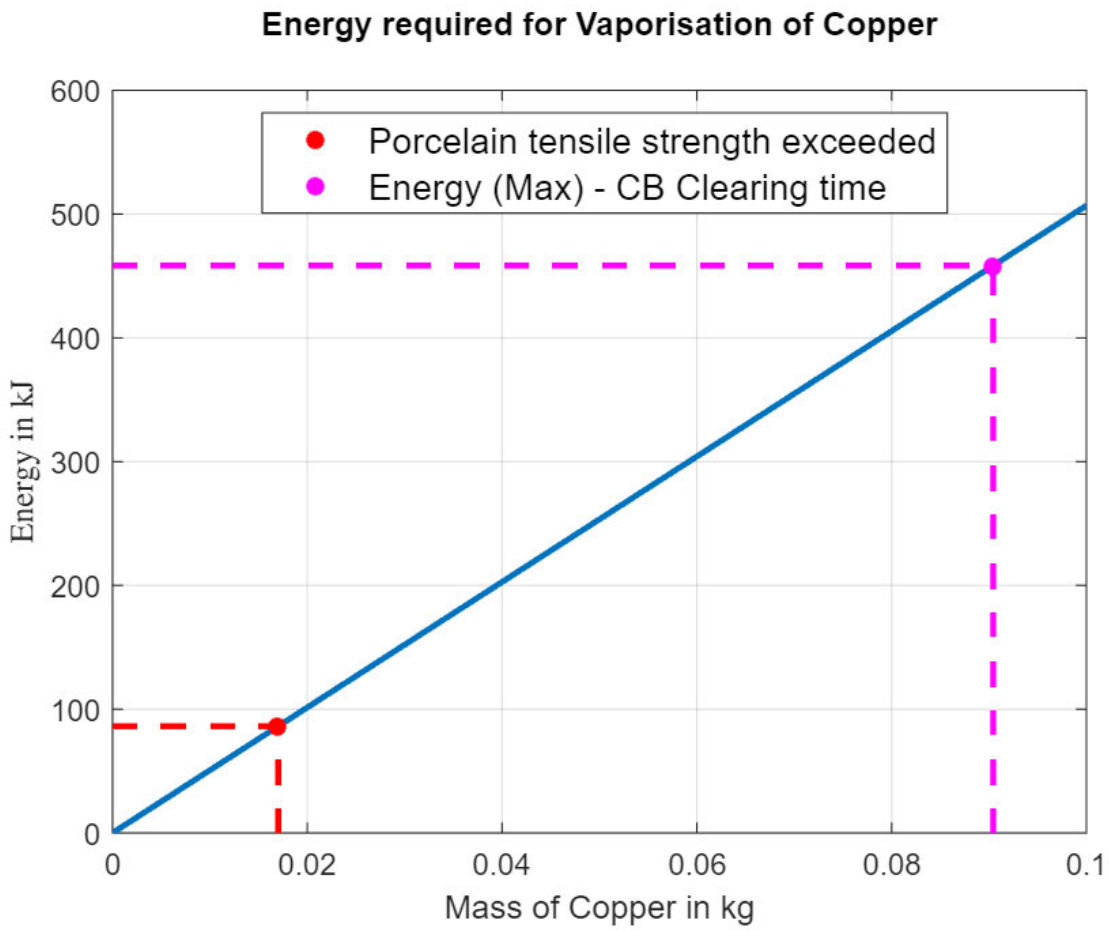

Figure 7 - 7: The energy required to vaporise an amount of copper.

Considering the amount of copper that could be involved in the initial phase of the electrical explosion, analysis of the pressure changes associated with the two-phase changes required for vaporisation was conducted. The solutions of these computations can be seen below in Figure 7 - 8 with the pressure increasing by a magnitude of 2 once the copper reaches the vaporisation phase, compared to the fusion or liquid. These changes in pressure are significant when considering the brittle material properties of porcelain.

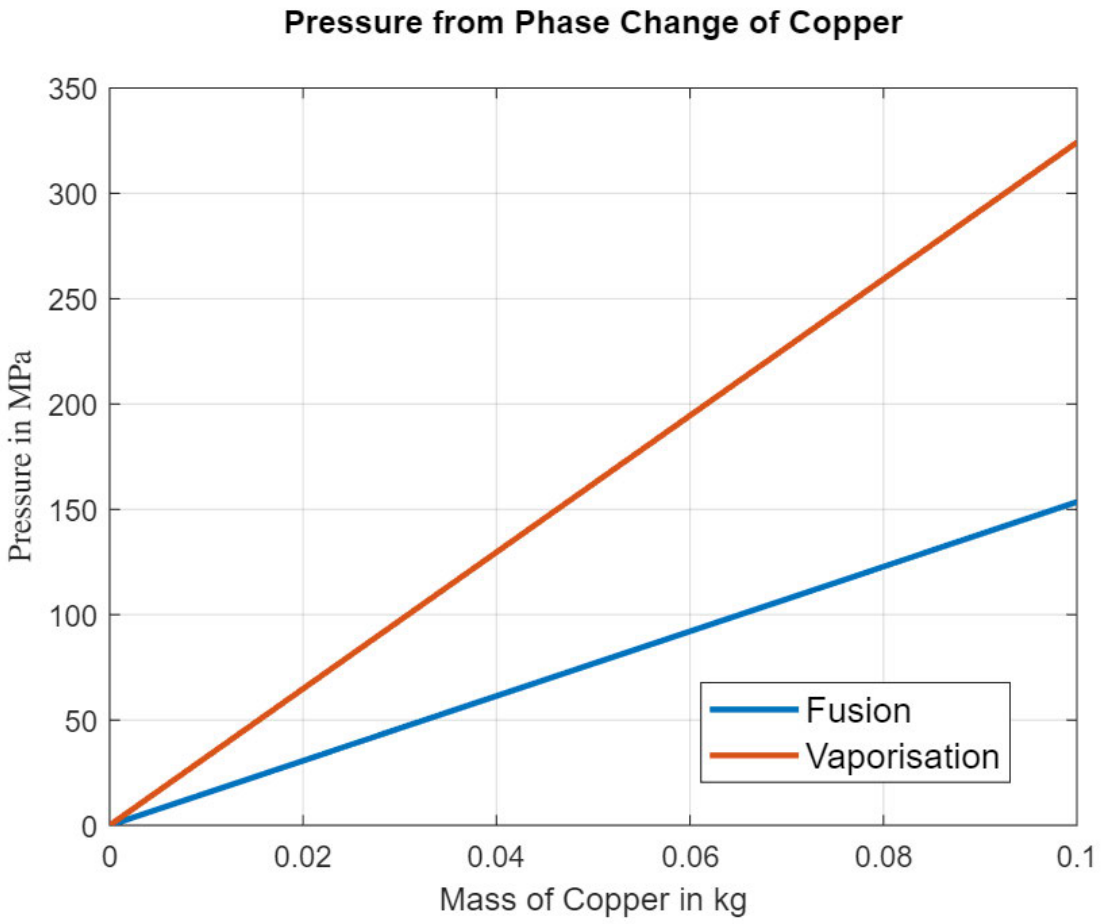

Figure 7 - 8: Pressure changes with phase changes of copper.

This increase in pressure from copper expansion is argued by Hoagland et al. (2016) to have less of an affect because vaporisation would not occur in a uniformed way. They suggest that the melting process could cause droplets of copper that is expelled as part of the arc before the full vapor pressure is achieved. This expelling of copper as part of the arc blast would still increase the potential of fragmentation of the brittle porcelain shell.

The internals of an ERF consist of various materials that could be exposed to extremely rapid temperature change during an electrical explosion. Often, the remains of the internal metallic materials from the ERF post failure have been observed to have experienced behaviour consistent with melting. The two-phase vaporisation process was found to reduce the amount of energy supplied to the fragments, which proved consistent with the literature reviewed. The resultant pressure increases observed placed additional forces on the porcelain shell.

7.6 FINDINGS

Multiple modelling techniques were utilised to provide estimates of the energy associated with ERF during an explosion and the potential distances that fragments could travel. The results for each method were used to further the understanding of the key parameters of the electrical explosion. There are multiple factors that can have a major impact on the outcome of the event. This required theoretical predictions to be made for some of the key parameters.

The time involved in the blast and fragmentation phases of the electrical explosion was estimated to be between 0.65 and 1 millisecond. The potential distances using these estimated times were between 20 – 45 metres depending on the time, angle of the trajectory, and the height above ground of the ERF installation. The pressure change associated with exceeding the tensile strength of HV Porcelain from vaporisation of copper was calculated to be less than 20% of the energy available for the whole event when considering the typical CB clearing times of 150ms. At the point of impact with the ground, fragments were estimated to have a projectile energy of between 134 and 625 joules for a given scenario. There is a potential for fragments to fall outside the 25 metre RMHZ distance typically used for this type of ERF, and projectiles at this distance have been estimated to have an energy up to 461 joules. This indicates that anyone within the flight path would potentially be exposed to lethal projectiles.

7.7 RESEARCH LIMITATION

The research into the electrical explosion of an ERF has been carried out using the available information from industry sources, literature, simulation packages and physics-based computations. Each of these resources have had limitations that have affected this research, which in some cases were not easily identifiable until a considerable amount of work had been

conducted. Additional analysis was performed to overcome these where possible. This had a flow on effect to the project timeline and associated deadlines.

The initial limitation was the steep learning curve that was required to become suitably proficient with Ansys and its very powerful modelling software. The Explicit Dynamic package included the Autodyn solver, though it did not support the advanced brittle material fragmentation analysis required once the element or node detached from the body of the cylinder. It did provide an excellent environment to conduct the simulations, though the complexity of the model setup was an issue.

There were limitations when setting material properties of porcelain required to model its behaviour during an explosion within Ansys. The massive material library that is available from Ansys, Granta, requires a licence which was not available during this research. To minimise this limitation an extensive literature search was conducted to determine the material properties of the model settings. These properties were set to reflect HV porcelain as close as possible, though this did influence the quality of the Ansys solutions.

The modelled cylinder restricted the accuracy of the modelling solutions, as the internals of a surge diverter were not included. This was to focus on the initial task of the simulation of the fragmentation using TNT explosives. Overcoming the tensile strength of the porcelain shell, while including the internal components, would enable more creditable modelling solutions. However, it would be a challenge to achieve results using the chosen software package.

There were also several limitations found when carrying out the physics based computational modelling. One was the comparison of the modelling methods between the scripted projectile distance model and the Ansys Autodyn fragmentation analysis, due to there being no fragmentation analysis solution available from Ansys. The pressure solutions from Ansys were also deemed to be unreliable, which limited the analysis of the time available for energy transfer to a projectile before it leaves the ERF. This created a reliance on the physics based projectile model for determining the potential energy transfer and distance that a projectile could travel. All these limitations stated above have restricted any work that was planned for improvements to the automated NAR tool that is under development.

7.8 CHAPTER SUMMARY

The discussion chapter provides detailed explanation of the findings of each method of analysis that was conducted. This included the Ansys modelling technique, the initial physics based projectile model, and then extended into the modelling of impact energy and the energy required for vaporisation of copper. From these modelling methods, the key findings are defined, followed by the limitations of this research.

8 CONCLUSION

8.1 RESEARCH OUTCOMES

The purpose of this dissertation was to further support the EQL NAR process by quantifying the potential distances that projectiles could travel and the safety hazard that they pose during an arc blast event. Multiple modelling techniques were utilised to develop a clearer understanding of the electrical arc explosion. The extensive use of published works also supported both the development of these models and associated solutions. Each of these methods were imperfect for various reasons, though through comparison they enabled a conclusion to be formed.

The initial modelling focused on the incident energy that was available during the explicit time event of an explosion. This was conducted using the Ansys explicit dynamic software and the formulae from literature. The amount of energy that was available from these simulations and computations were in the mega joules of energy range, when the entire event period of 150 milliseconds was modelled. It was determined that the time available for energy transfer was significantly less than the circuit breaker clearing time.

Using the projected period of the fragmentation phase of 1 millisecond or less, the potential distance of a given projectile was estimated. The trajectory angles of 25 and 45 degrees for each fragment size allows the maximum distance to be determined. The potential distance a given projectile could travel when exposed to 1 millisecond of incident energy was between 20 – 45 metres depending on the angle of the trajectory and the height of the ERF. The larger fragments were shown to have more energy at any given distance from the explosion at the same angle.

The cause of the fragmentation was associated with the extremely rapid pressure buildup inside the porcelain cylinder. The amount of energy that is available during the initial arc was enough to cause vaporisation of material inside. Using copper, which is a common component in ERFs, the energy required for vaporisation of a given mass was calculated. The results indicated that the amount of energy required to create deformation of HV porcelain from vaporisation was less than 100 kJ, and 18 grams of copper.

Looking at the projectile hazard from an impact perspective, the projectile energy of the fragments over the entire flight path and impact with the ground was calculated. This required the modification of the initial projectile modelling script to determine the amount of energy that could be available over the distances identified. The available energy was estimated to be extremely hazardous, along the fragments flight path, with the impact with ground calculated to be between 134 and 625 joules. The upper limit of 625 joules kinetic energy of the projectiles is above the 500 joules which has been shown to have the potential to cause fatality. In conclusion, this dissertation has identified that the energy available to a porcelain projectile during an electrical arc explosion can be extremely hazardous to anything within the flight path.

8.2 FUTURE RESEARCH

The research conducted during this dissertation has developed theorical predictions using several modelling methods and the support of published literature. This has enabled estimations to be established in relation to the explicit time. These predictions provide a reasonable estimate when considering the resources that were available.

Further refinement of electrical explosion research, specifically Ansys modelling, and including the internal components of the surge diverter, has the potential to improve modelling solutions. Gaining access to the exact material properties of all modelling components would also improve simulation results. If successful, then it would be rational to expand this research to other ERF types.

The next logical step into the research of porcelain projectiles would be physical testing in a controlled environment. Specifically, looking at the theorical predictions of time and the pressure during the event. This would require the establishment of test arrangements that could produce repeatable electrical arc blasts. The findings of this research would enable the theoretical predictions to be verified.

Beyond the expansion of physical testing, further research into the probability of the electrical arc explosion of an ERF would provide a more complete understanding of all elements involved. Probability was not considered within the scope of this dissertation, though would further support the engineering decisions when determining whether it is safe to leave an ERF in service.

Ultimately, this future research into ERF would support the calculation of the potential projectile hazards and enable them to be brought down to ALARP using an automated NAR tool. The control measures would also be able to be designed in a consistent manner while being tailored to the specific site location. Having this ability to predict the projectile distances more accurately from an electrical arc explosion will benefit both HV workers and the public.

9 REFERENCES

ANSYS, I 2023, *Ansys Engineering Simulation Software*.

ARCAD_INC 2019, *Arc blast Tri-Nitro-Toluene (TNT) / Trotyl equivalent*, viewed 28/09/2022, <https://arcadvisor.com/faq/arc-blast-explosive-equivalent>.

Australian Energy Council 2019, *ELECTRICAL ARC FLASH HAZARD MANAGEMENT GUIDELINE*, Guideline 30, <https://www.energycouncil.com.au/media/15808/eafhm_guideline_30_25-03-2019_web.pdf>.

Ćatović, A, Herzegovina & Kljuno, E 2018, 'Prediction of aerodynamic coefficients for irregularly shaped body using numerical simulations', *International Journal of ADVANCED AND APPLIED SCIENCES*.

Cengel, Y, Cimbala, J, Turner, R 2017, *Fundamentals of Thermal-Fluid Sciences* 5th edn, McGraw-Hill Education, New York.

Century-Dynamics 2005, *AUTODYN Explicit software for Nonlinear Dynamics*, vol. Theory Manual, Researchgate, Online, viewed 06/04/2023, <https://www.google.com/search?q=AUTODYN%2C+Theory+Manual%2C&sxsrf=APwXEdeoXihZF_25WxjnHWVfwBZxlwak7Q%3A1680743462404&ei=JhwuZL-qGMnk4-EP84iSyAU&ved=0ahUKEwi_1aOoiZT-AhVJ8jgGHXOEBFkQ4dUDCA8&uact=5&oq=AUTODYN%2C+Theory+Manual%2C&gs_lcp=Cgxnd3Mtd2l6LXNlcnAQAzIGCAAQHhANMgYIABAWEB4yBggAEBYQHjIGCAAQFhAeMgYIABAWEB4yCAgAEIoFEIYDOgoIABBHENYEELADSgQIQRgAUJkFWJkFYIYVaAFwAXgAgAHaAYgB2gGSAQMyLTGYAQCgAQKgAQHIAQjAAQE&sclient=gws-wiz-serp> >.

Doughty, RL, Neal, TE & Floyd, HL 2000, 'Predicting incident energy to better manage the electric arc hazard on 600-V power distribution systems', *IEEE transactions on industry applications*, vol. 36, no. 1, pp. 257-69.

EQL 2019, *Gapless Surge Diverter* Energy Queensland Limited.

EQL 2022, *DMPs and NARs*, Energy Queensland Limited, EQL SharePoint site, viewed 1/10/2022, <https://energyqonline.sharepoint.com>.

Expii, I 2016, *Phase Change Diagrams — Overview & Examples*, Website, viewed 5/9/2023, <https://www.expii.com/t/phase-change-diagrams-overview-examples-8057>.

Guide to Preparing Network Access Restriction Documentation, 2015, Ergon Energy Asset Investigations Group, Brisbane, Qld.

Gulski, E, Smit, JJ, Quak, B & Groot, ERS 2005, 'Decision support for life time management of HV infrastructures'.

Hallowell, MR, Alexander, D & Gambatese, JA 2017, 'Energy-based safety risk assessment: does magnitude and intensity of energy predict injury severity?', *Construction Management and Economics*, vol. 35, no. 1-2, pp. 64-77.

Hays, J 2014, 'Resistance is Futile', Student project thesis, College of the Redwoods.

Hoagland, H, Maurice, C, Haines, A & Maurice, A 2016, 'ARC flash pressure measurement by physical method, effect of metal vapor on ARC blast', *2016 IEEE IAS Electrical Safety Workshop (ESW)*, pp. 1-9.

IEEE Std 1584-2018 (Revision of IEEE Std 1584-2002): IEEE Guide for Performing Arc-Flash Hazard Calculations, 2018, IEEE.

INMR 2014, *Safety is Key Driver In Selection of Hollow Core Composite Insulators*, Website, https://www.inmr.com/safety-is-key-driver-for-growth-of-hollow-composite-insulators/>.

Jahangir, M, Iqbal, ST, Shahid, S, Siddiqui, IA & Ulfat, I 2020, 'MATLAB simulation for teaching projectile motion', *Adv J Sci Eng*, vol. 1, pp. 59-61.

Jonsson, LH, R; Andersson, A; SKoogh2, H; Mindykowski, P; Forsth,M. 2009, 'Fire and safety aspects of flashovers in high voltage transfer bushings', *Centre Of Excellence For Transformers*: *Proceedings of the Centre Of Excellence For Transformers*.

Kadivar, A, Niayesh, K, Sasaki Støa-Aanensen, N & Abid, F 2021, 'Metal vapor content of an electric arc initiated by exploding wire in a model N2 circuit breaker: simulation and experiment', *Journal of Physics D: Applied Physics*, vol. 54, no. 5, p. 055203.

Keller, K 2010, 'Understanding Arc Flash and Arc Blast Hazards', in *Electrical Safety Code Manual - A Plain Language Guide to National Electrical Code, OSHA, and NFPA 70E*, Elsevier, pp. 1-4.

Lee, RH & Nailen, RL 1987, 'Pressures Developed by Arcs [with Discussion]', *IEEE transactions on industry applications*, vol. IA-23, no. 4, pp. 760-4.

Ludwig, W 2012, *Investigation of the Effect of Convergent Detonation on Metal Acceleration and Gurney*, Naval PostGraduate School, CORE, https://core.ac.uk/download/pdf/36700849.pdf>.

MakeItFrom.com 2021, *High Strength Aluminous Porcelain (IEC 60672 Type C-130)*, viewed 4/2/2023, <https://www.makeitfrom.com/material-properties/High-Strength-Aluminous-Porcelain-IEC-60672-Type-C-130>.

Mari, L 2020, 18/12/2020, 'Types of Surge Arresters', *EE Power*, viewed 3/3/2023,<https://eepower.com/technical-articles/types-of-surge-arresters/#>.

Muhr, M & Sumereder, C 2008, 'Applying Risk Management for High Voltage Equipment', pp. 592-5.

Neal, TE & Parry, RF 2005, 'Shrapnel, pressure, and noise', *IEEE Industry Applications Magazine*, vol. 11, no. 3, pp. 49-53.

Network Risk Framework, 2021, Energy Queensland Limited, Brisbane, Qld, EX 02083 Ver 6; EE NA000302R102 Ver 6.

Packel, EW & Yuen, DS 2004, 'Projectile motion with resistance and the Lambert W function', *The College Mathematics Journal*, vol. 35, no. 5, pp. 337-50.

Polking, J, Boggess, A & Arnold, D 2022, *Differential Equations with Boundary Value Problems*, 2nd Edition edn, Pearson Modern Classic.

Quan, X, Gerber, B, Cowler, M & Birnbaum, N 2006, 'Simulation of blast and fragment loading using a coupled multi-solver approach', vol. 12, pp. 182-7.

Rao, P, Painter, J, Appleby-Thomas, G, Critchley, R, Wood, D, Roberts, A & Hazael, R 2020, 'Fragmentation studies by non-explosive cylinder expansion technique', *International Journal of Impact Engineering*, vol. 146, p. 103714.

Reindel, A & Steger, H 2010, 'PECO Reaps Rewards of Diagnostic Maintenance', *Transmission & Distribution World*, vol. 62, no. 7, pp. 30-4.

Risk management : Principles and guidelines (AS/NZS ISO 31000:2009), 2004, Standards Australia, Sydney, NSW.

Royal Australian Mint 2023, *Investigating Australian Coins*, viewed 9/8/2023, <https://www.ramint.gov.au/sites/default/files/About%20our%20coins.pdf>.

Speight, JG 2019, '9 - Gas condensate', in JG Speight (ed.), *Natural Gas (Second Edition)*, Gulf Professional Publishing, Boston, pp. 325-58.

Tasdemirci, A & Hall, IW 2007, 'Numerical and experimental studies of damage generation in multi-layer composite materials at high strain rates', *International Journal of Impact Engineering*, vol. 34, no. 2, pp. 189-204.

Taylor, J 2023, 'Short circuit behaviour - Surge arresters and counters', *ABB Power Products*.

The Engineering ToolBox 2008, Website, viewed 3/7/2023, <https://www.engineeringtoolbox.com/ceramics-properties-d_1227.html>.

TotalShield 2022, *Calculating the Energy of a Ballistic Impact*, viewed 4/9/2023, <https://totalshield.com/blog/calculating-energy-of-ballistic-impact/>.

Ward, BaW, Thomas 2021, '"Online Partial Discharge Monitoring and Failure Analysis of a 132 kV Current Transformer," 2021 IEEE Electrical Insulation Conference (EIC)', *2021 IEEE Electrical Insulation Conference (EIC)*, pp. 373-6.

Windpact 2023, *What Is It Like Getting Hit With A Baseball In The Head?*, Windpact, Website, viewed 04/09/2023, <https://windpact.com/getting-hit-baseball/>.

Xue, Z-q, Li, S, Xin, C-l, Shi, L-p & Wu, H-b 2019, 'Modeling of the whole process of shock wave overpressure of free-field air explosion', *Defence Technology*, vol. 15, no. 5, pp. 815-20.

10 APPENDIX A

10.1 COMPUTATIONAL MODELLING SCRIPT

```
%.....................................................................%
%% ENG4111/2, Modelling for Thesis, Semester 1 & 2, 2023
%  Author        :   Chase Richardson
%  Student Number:   [redacted]
%  Date created  :   September 2023
%{
This program is for my research project, all functions are included at the
bottom/end of program code.

% Version final :P

    -   ANSYS data import and comparsions/analyses with known event data

    -   Projectile with drag model with Energy calculation formula

    -   Projectile energy reduction over the distance

    -   Energy and Pressure Calculations for both Fusion & Vaporisation

%}
%.....................................................................%
clc, clear,close all % Clear workspace ,close figure & clear the command
window
%.....................................................................%
set(0,'defaulttextinterpreter','latex') % pretty fonts and convenient text
commands
fig = 0;     % number of plot/graphs
%.....................................................................%
% Constants
g = 9.81;               % gravity.              m/s^2
aD = 1.2258;            % air Density.          kg/m^2
pD = 2.7 * 1e3;         % density of porcelain. kg/m^3
tntD = 1.65 * 1e3;      % density of TNT.       kg/m^3
tntEunit = 4.294*1e6;   % Energy per unit mass. J/kg
```

Import data

```
[Time, E_Min, E_Max, E_Avg, P_Min, P_Max, P_Avg] =
importfile_ANSYS("INT_ENERGY+PRESSURE.xlsx", "Sheet1", [4, 204]);
```

Dimensions, mass and energy of the TNT cylinder

$$V = \pi * r^2 * h$$

$$\text{mass} = \rho * \text{volume}$$

```
r_tnt = 6.1 * 1e-2;              % m
h_tnt = 57.0 * 1e-2;             % m
V_tnt = pi*h_tnt*r_tnt^2;        % m^3
mass_tnt = (V_tnt * tntD);       % kg
e_tnt = mass_tnt * tntEunit;     % J/kg
```

Conversion of INT_ENERGYALL from Joules/kg to Joules

```
MaxPTNT = E_Max*mass_tnt;
Ansys_maxJ = max(MaxPTNT)-MaxPTNT(1);
fig = fig+1;
plot(Time,(E_Max*mass_tnt),'LineWidth',2)
xlabel('Time in seconds')
ylabel('Energy in MJ')
yticklabels({'0.5','1','1.5','2','2.5','3','3.5','4'})
title('Incident Energy applied to the Porcelain - ANSYS')
grid on,
legend('Max INT\_ENERGYALL', 'Location','Best')
```

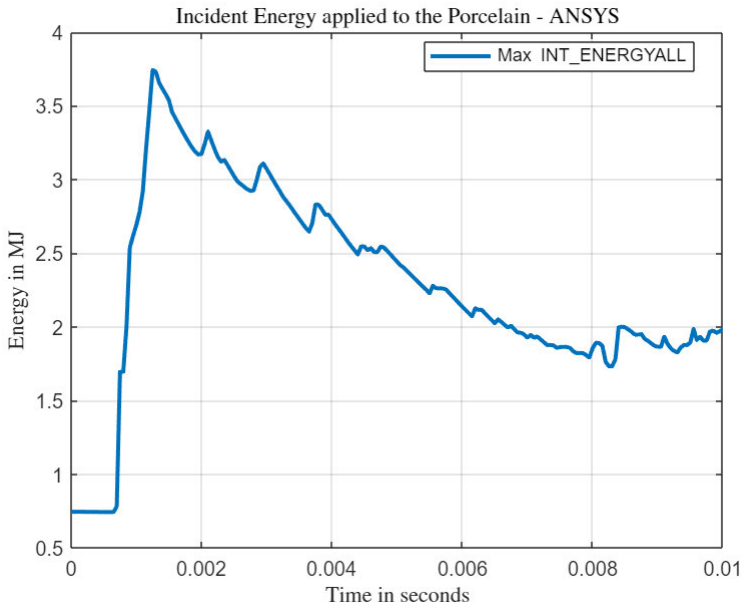


```
%}
all_E_Ansys = [E_Min, E_Max, E_Avg];
E_AnsysMax = max(E_Max);
e_int = min(E_Max);
E_AnsysMaxLessInitial = E_AnsysMax-e_int;
E_MaxLessInitial = E_Max-e_int;
%
fig = fig+1;
plot(Time,(E_Max*mass_tnt),'LineWidth',2)
xlabel('Time in milliseconds')
ylabel('Energy in MJ')
```

```
set(gca,'xticklabels',{'0.4','0.5','0.6','0.7','0.8','0.9','1'})
yticklabels({'0.5','1','1.5','2','2.5','3'})
title('Initial rise of Incident Energy applied to porcelain - ANSYS')
grid on,xlim([0.0004 0.001])
legend('Max INT\_ENERGYALL', 'Location','northeast')
```

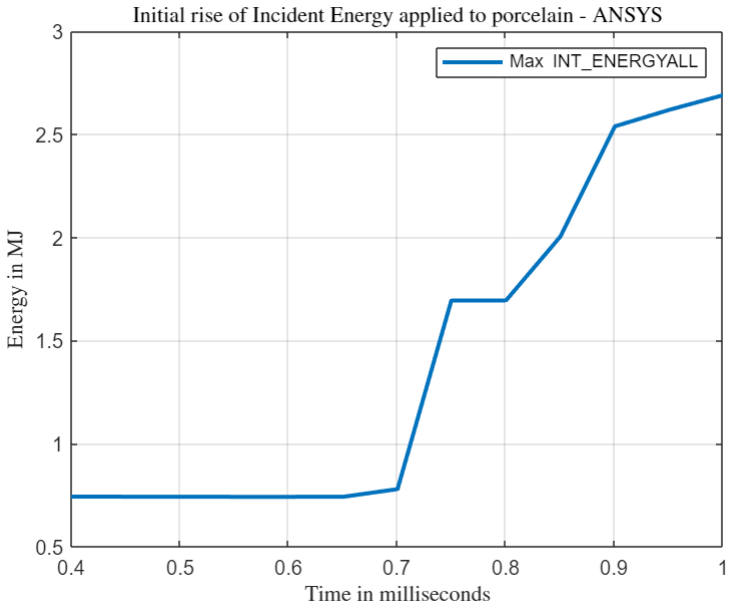


```
%}
```

Pressure results from ANSYS

```
%
df = max(P_Max)
```

```
df = 2.7514
```

```
fig = fig+1;
plot(Time,P_Max,'LineWidth',2)
xlabel('Time in seconds')
ylabel('Pressure in MPa')
grid on
title('Pressure Solution Results - ANSYS')
legend('Max Pressure', 'Location','northeast')
```

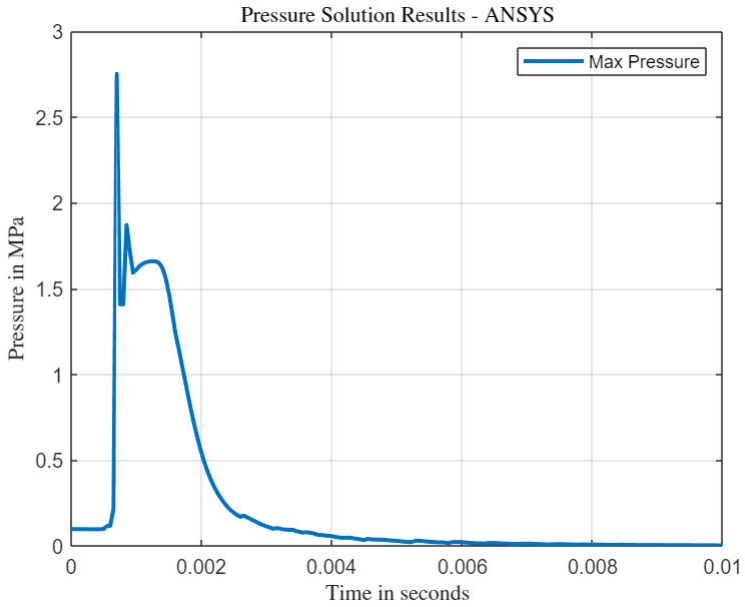


```
%
fig = fig+1;
plot(Time,P_Max,'LineWidth',2)
xlabel('Time in milliseconds','FontWeight','bold')
ylabel('Pressure in MPa','FontWeight','bold')
set(gca,'xticklabels',{'0','0.5','1','1.5','2'})
title('Initial Pressure Rise -
ANSYS','FontWeight','bold','Interpreter','tex')
grid on,xlim([0 0.002])
legend('Maximum Pressure','interpreter','latex', 'Location','Best')
```

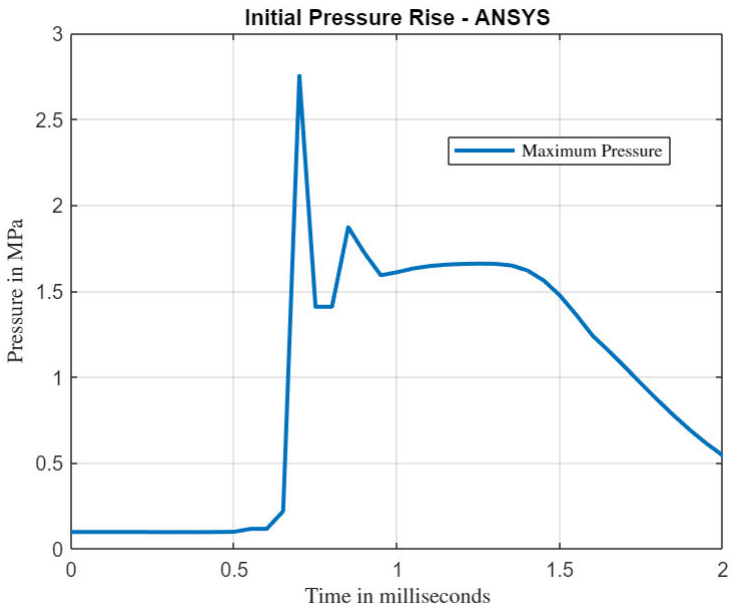

```
%{
ax2 = gca;
chart2 = ax2.Children(1);
%Recipe for pizza dough
%500g OO pizza flour
%62 percent hydration
%2.4 percent salt
%0.5 teaspoon of IDY
%5hr bulk RT, ball, 2hr RT
datatip(chart2,0.0006506,0.2185);

ax = gca;
chart = ax.Children(1);
datatip(chart,0.0007005,2.751);
%}
all_P_Ansy = [P_Min, P_Max, P_Avg];
%
fig = fig+1;
plot(Time,all_P_Ansy,'LineWidth',2)
xlabel('Time in seconds')
ylabel('Pressure in MPa')
title('ALL Pressure data - ANSYS')
grid minor,xlim([0.0005 0.002])
legend('Min Pressure','Max Pressure','Avg Pressure', 'Location','Best')
```

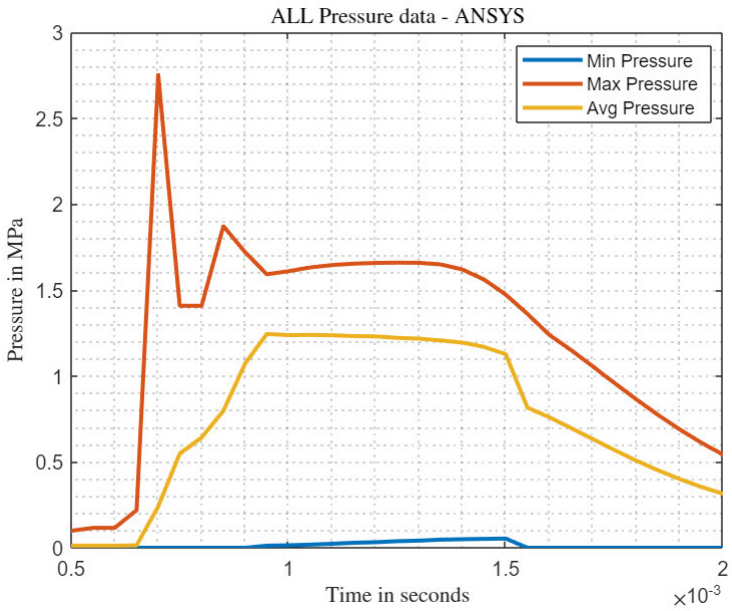


```
%}
```

Known Incident Data

Using fault data

Will need to do further analysis of the data in order to get more accurate values. This is a starting point.

```
singleF = 7684.17/sqrt(2);  % Phase to ground fault
singleV = 562.44;           % Voltage of phase to ground fault
doubleF = 8074.23/sqrt(2);  % Bolted Double inline fault
doubleV = 162.42;           % Voltage of double bolted
tfault = 0.18;              % time up until the second fault
```

Energy Calculations

Edata = V * I * t

```
t_int = 0.15;       % 150 milliseconds (typical clearing time)
t_Ansys = 6.5e-4;   % time estimate from ANSYS Pressure
t_milli = 1e-3;     % milliseconds
Edata_150 = singleV*singleF*t_int;          % Joules
Edata_AnsysTime = singleV*singleF*t_Ansys;  % Joules
Edata_milli = singleV*singleF*t_milli;
```

Energy Comparison

```
Energy_Form = ["TNT Cylinder";"Ansys Max";"Ansys Max Less initial";"Known Incident 150ms";"Known Incident 1ms"];
Joules = [e_tnt; E_AnsysMax; E_AnsysMaxLessInitial; Edata_150; Edata_milli;];
%
Energy_Comparison = table(Energy_Form,Joules)
```

Energy_Comparison = 5x2 table

	Energy_Form	Joules
1	"TNT Cylinder"	4.7210e+07
2	"Ansys Max"	3404400
3	"Ansys Max Less initial"	2729290
4	"Known Incident 150ms"	4.5841e+05
5	"Known Incident 1ms"	3.0560e+03

Dimensions of porcelain shell:

```
% When the porcelain will fragment in ANSYS
rOut = 7.6 * 1e-2;      % m
```

```
thick = 1.5 * 1e-2;     % m
rInner = rOut-thick;    % m
h = 60 * 1e-2;          % m
```

Mass calculations of porcelain shell:

Hollow cylinder:

mHollow = pi * height* (radius^2-(radius-thickness)^2)*porcelainDensity

End caps:

mCaps = pi*thickness*(radius-thickness)^2)*porcelainDensity

Total mass of the porcelain cylinder:

mTot = (mCaps*2)+mHollow

```
mHollow = pi*h*(rOut^2-(rOut-thick)^2)*pD;  % kg
mCaps = pi*thick*((rInner)^2)*pD;           % kg
mTot = (mCaps *2) + mHollow;                % kg
```

Total Volume including the porcelain shell

$$V_{\text{olume}} = \pi * r^2 * h_{\text{eight}}$$

```
Vout = pi*(rOut^2)*h;  % m^3
```

Area calculation of porcelain cylinder shell

Lateral Surface Area (LSA)

Exteral Surface Area (ESA)

Internal Surface Area (ISA)

$$\begin{aligned} \text{LSA} &= \text{ESA} + \text{ISA} \\ &= 2 * \pi * R_{\text{adius(Total)}} * \text{height} + 2 * \pi * r_{\text{adius(Inner)}} * \text{height} \\ &= 2\pi h(R + r) \end{aligned}$$

Areas of The Soild Bases (ASB) * 2

$$\text{ASB} = 2 * \pi * \text{height}_{\text{(Thickness of porcelain)}}\, r_{\text{adius(Inner)}} + 2 * \pi * r_{\text{adius(Inner)}}{}^2$$

Total Surface Area (TSA)

$$\begin{aligned} \text{TSA} &= (2 * \text{ASB}) + \text{LSA} \\ &= (2(2\pi \text{hr} + 2\pi r^2)) + 2\pi h(R + r) \end{aligned}$$

```
LSA = 2*pi*h*(rOut+rInner);
ASB = 2*pi*thick*rInner+2*pi*rInner^2;
TSA = 2*ASB+LSA;
```

```
% TSA1 = 2*pi*h*rOut+2*pi*rOut^2; % Using the external area of the cylinder
% only
```

Number of fragments: 3, 5, 10

```
% Mass of fragments
mfrag3 = mTot/3;       % kg
mfrag5 = mTot/5;       % kg
mfrag10 = mTot/10;     % kg
mfrag = [mfrag3 mfrag5 mfrag10];
%
% Area of fragment
afrag3 = TSA/3;    % m^2
afrag5 = TSA/5;    % m^2
afrag10 = TSA/10;  % m^2
```

Projectile Model Analysis

Terminal velocity formula

$$\mathrm{Vt} = \frac{\sqrt{2 * \mathrm{mass} * \mathrm{gravity}}}{\rho_{\mathrm{air}} * \mathrm{Area} * \mathrm{Cd}}$$

Coefficient:

flat surface = 1.0, sphere or cone = 0.5, Semicircular shell (curve facing the direction) = 1.2

Assumption for a porcelain projectile coefficient 0.2 - Cengel and Cimbala, ED. 5 - Fundaments of Thermal-Fluids sciences

Worst case scenario for sphere in turbulent air

```
Cd = 0.2;       % Drag coefficient
%
VTot = sqrt((2*mTot*g)/(aD*TSA*Cd));
Vt3 = sqrt((2*mfrag3*g)/(aD*afrag3*Cd));
Vt5 = sqrt((2*mfrag5*g)/(aD*afrag5*Cd));
% Vt10 = sqrt((2*mfrag10*g)/(aD*afrag10*Cd));
%%%% Terminal velocity is unchanged with fragment size %%%%
Vt10 = Vt3;  % m/s
VtKmh = Vt10*(3600/1000); % km/h
VtKms = Vt10/1000;  %km/s
```

Vertical component of velocity

$$0 = \mathrm{gravity} - \left(\frac{b * \mathrm{terminal\ Velocity}}{\mathrm{mass}}\right)$$

$$b = \frac{\mathrm{mass} * \mathrm{gravity}}{\mathrm{terminal\ Velocity}}$$

```
bTot = (mTot*g)/VTot;   % kg/s
```

```
b3 = (mfrag3*g)/Vt10;   % kg/s
b5 = (mfrag5*g)/Vt10;   % kg/s
b10 = (mfrag10*g)/Vt10; % kg/s
b = [b3 b5 b10];
```

Initial Velocity Calculation

Energy = Kinetic Energy

$$\mathrm{KE} = \frac{1}{2} * \mathrm{mass} * \mathrm{velocity}^2$$

$$\mathrm{velocity} = \sqrt{\frac{E}{\left(\frac{1}{2} * \mathrm{mass}\right)}}$$

```
% Energy options
numFrag = [3 5 10]; % Number of fragments
E_150_frag =  Edata_150./numFrag;
E_milli_frag =  Edata_milli./numFrag;
E_Ansys_frag = Edata_AnsysTime./numFrag;
E_AnsysMax_frag = E_AnsysMax./numFrag;

% E = Edata_150
% E = Edata_AnsysTime
E = Edata_milli
```

```
E = 3.0560e+03
```

```
% E = E_AnsysMax
% E = (E_AnsysMax*0.00065) %
%
v3 = sqrt((E/3)/((1/2)*mfrag3));    % m/s
v5 = sqrt((E/5)/((1/2)*mfrag5));    % m/s
v10 = sqrt((E/10)/((1/2)*mfrag10)); % m/s
v = [v3 v5 v10];
vKms =v/1000;    % km/s
```

Trajectory

```
distance = 0:1:250;         % metres
angleTest = 45*3.14/180;    % degrees in radians
ang = [25 45]*3.14/180;
%
Y = {length(b)};
y = nan(length(b),length(distance));
pail_0 = nan(1,length(b));    % Does what the name says :)
pail_5 = nan(1,length(b));
pail_10 = nan(1,length(b));
```

```
 % locating ground impact against the height of the plant install
 deck_0 = nan(length(ang),length(b));
 deck_5 = nan(length(ang),length(b));
 deck_10 = nan(length(ang),length(b));

 for k = 1:length(ang)   % Number of angles

     for i = 1:length(b) % Number of fragments

         for d = 1:length(distance) % Trajectory

             dump =
((mfrag(i)*g*sec(ang(k))/(b(i)*v(i)))+tan(ang(k)))*distance(d) +
((mfrag(i)^2*g)/b(i)^2)*log(1-
(b(i)*sec(ang(k))/(mfrag(i)*v(i)))*distance(d));

             if dump == real(dump) && dump >= -15
                 y(i,d) = dump;
             else        % Once well below zero remove imagary numbers
                 y(i,d) = nan;
             end
         end
         % locate first position below zero height
         pail_0(i) = find(y(i,:) < 0,1);
         pail_5(i) = find(y(i,:) < -5,1);
         pail_10(i) = find(y(i,:) < -10,1);
     end

     deck_0(k,:) = pail_0; % Once it hits the (variable name)
     deck_5(k,:) = pail_5;
     deck_10(k,:) = pail_10;
     %
     Y{k}=y; % Cell array storage centre
 end
 %
 fig = fig+1;
 plot(distance,Y{1},'LineWidth',2)
 xlabel('Distance in metres ')
 ylabel('Height in metres')
 title('Projectiles Distances for Incident Time 0.65ms at
25^{\circ}','Interpreter','tex')
 grid on%,ylim([-10 10]) %, xlim([0 140])
 h1 = legend('','','Fragments', 'interpreter','latex','Location','best');
```

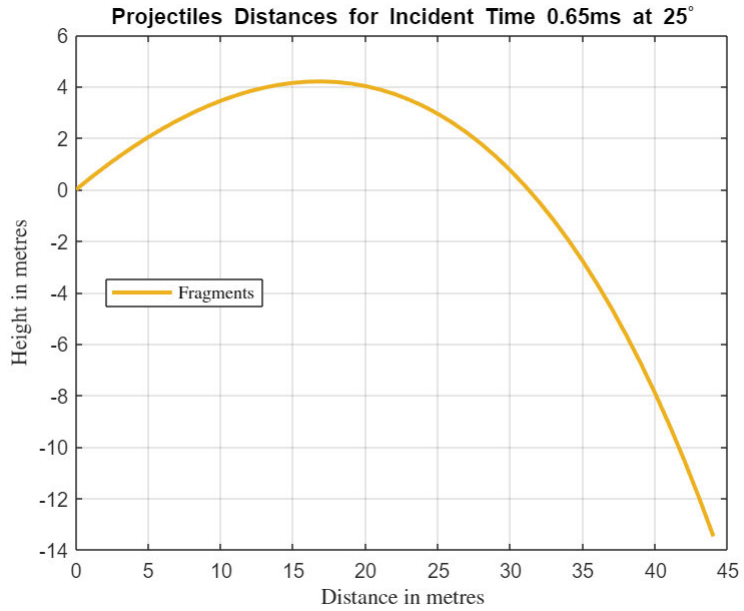


```
 fig = fig+1;
 plot(distance,Y(Jonsson),'LineWidth',2)
 xlabel('Distance in metres',FontWeight='bold')
 ylabel('Height in metres',FontWeight='bold')
 title('Projectiles Distance for Incident Time 0.65ms at
45^{\circ}','Interpreter','tex')
 grid on%,ylim([-5 60]),xlim([0 120])
 %
 h2 = legend('3 Fragments','5 Fragments', '10
Fragment','interpreter','latex','Location','northeast');
```

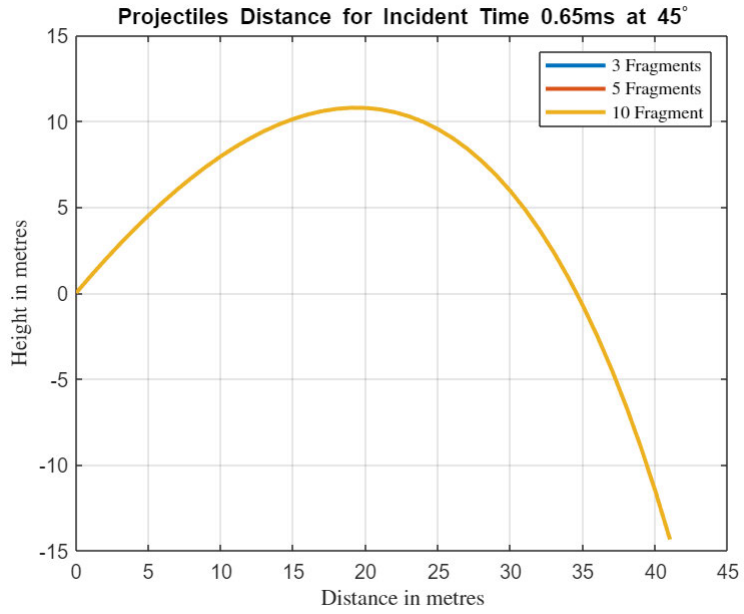


```
 fig = fig+1;
 gg = plot(distance,Y{1},distance,Y(Jonsson),'LineWidth',2);
 indi = {'-','-','-','-.','-.','-.'};
```

```
 [gg(:).LineStyle] = indi{:};
 xlabel('Distance in metres',FontWeight='bold')
 ylabel('Height in metres',FontWeight='bold')
 title('Projectiles Distances for Incident Time of 1 ms','
','Interpreter','tex')
 grid on,ylim([-10 12])%,xlim([0 45])
 h3 = legend('','','Fragments at $25^{\circ}$','','', 'Fragments at
$45^{\circ}$ ', 'interpreter','latex','Location','best');
 fontsize(h3,12,"points")
```

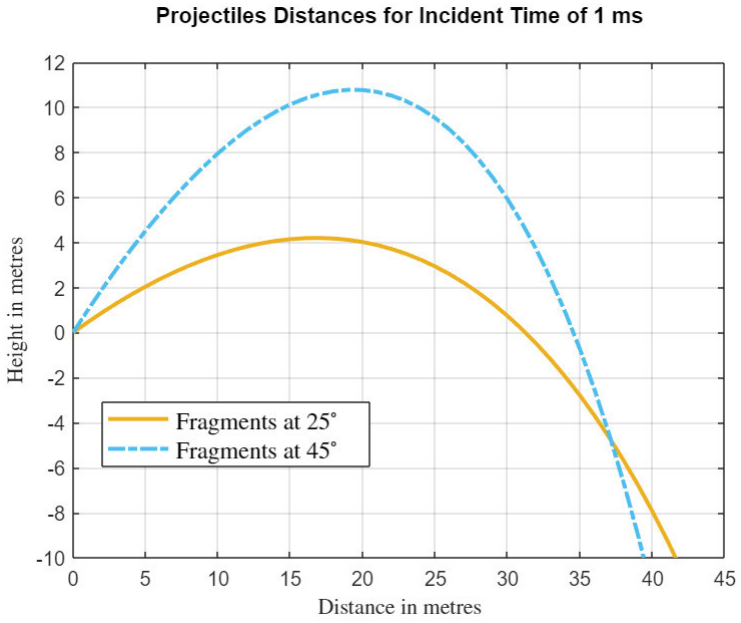

Energy reduction of distance

Using the equations derived for projectiles distances to find the energy reduction of time/distance

$$V_x(0) = V_{xo} = V_0 \operatorname{Cos}\theta \quad \& \quad V_y(0) = V_{yo} = V_0 \operatorname{Sin}\theta$$

Also using the calculated initial energy for at or just before the event, the initial velocity at t = 0 can be calculated.

$$E_{nergy} = \frac{1}{2} * m_{ass} * V_{elocity_{Initial}}{}^2$$

$$V_{elocity_{Initial}} = \sqrt{\frac{E_{nergy} * 2}{m_{ass}}}$$

Assumptions:

No energy loss.

Energy is split evenly between fragments

```
 e_initial = E./numFrag; % Joules  % Energy at time zero for each size of
fragments
 % Table
```

```
 Total_Energy_Divided_by_No_Fragements = ["3 Fragments";"5 Fragments";"10
Fragments"];
 Joules = [e_initial(1);e_initial(2);e_initial(3)];
 split = table(Total_Energy_Divided_by_No_Fragements,Joules)
```

split = 3×2 table

	Total_Energy_Divided_by_No_Fragements	Joules
1	"3 Fragments"	1.0187e+03
2	"5 Fragments"	611.2068
3	"10 Fragments"	305.6034

Using the energy divided by number of fragments and against the weight of 3 fragments

```
 V0_3 = sqrt(e_initial*2./mfrag); %Velocity is the same for each fragment
when the energy is also divided
 Vo_3 = V0_3(1);
 %
 Vx0 = Vo_3*cos(ang(1));
 Vy0 = Vo_3*sin(ang(1));
 %
 eTD = {length(b)};
 ee_D = nan(length(b),length(distance));
 jug_0 = nan(1,length(b));    % Does what the name says :)
 jug_5 = nan(1,length(b));
 jug_10 = nan(1,length(b));
 eTdeck_0 = nan(length(ang),length(b));
 eTdeck_5 = nan(length(ang),length(b));
 eTdeck_10 = nan(length(ang),length(b));

 for ko = 1:length(ang)          % Number of angles

     for io = 1:length(b)        % Number of fragments

         Vx0 = v(io)*cos(ang(ko));    % Initial X velocity for a given angle
         Vy0 = v(io)*sin(ang(ko));    % Initial Y velocity for a given angle

         for do = 1:length(distance)    % number of time steps

             t_posi = mfrag(io)/b(io)*log((mfrag(io)*Vx0)/((mfrag(io)*Vx0)-
(b(io)*distance(do))));
             VxX = Vx0*(exp(-(b(io)*t_posi)/mfrag(io)));
             VyY = (((mfrag(io)*g)/b(io))+Vy0)*exp(-
(b(io)*t_posi)/mfrag(io))-(mfrag(io)*g)/b(io);
             ee_D(io,do) = (1/2) * mfrag(io) * ((VxX^2)+(VyY^2));
         end
```

```
        jug_0(io) = real(ee_D(io,deck_0(ko,io)));
        jug_5(io) = real(ee_D(io,deck_5(ko,io)));
        jug_10(io) = real(ee_D(io,deck_10(ko,io)));
    end

    eTdeck_0(ko,:) = jug_0; % Energy once it hits the ground in Joules
    eTdeck_5(ko,:) = jug_5;
    eTdeck_10(ko,:) = jug_10;
    %
    eTD{ko}=real(ee_D);  % Cell array storage centre
end

% Table
Projectiles = ["3 Fragments at 25 Deg";"5 Fragments at 25 Deg";"10 Fragments
at 25 Deg";"3 Fragments at 45 Deg";"5 Fragments at 45 Deg";"10 Fragments at
45 Deg"];
Plant_H_0m_Joules =
[eTdeck_0(1,1);eTdeck_0(1,2);eTdeck_0(1,3);eTdeck_0(2,1);eTdeck_0(2,2);eTdeck
_0(2,3)];
Plant_H_5m_Joules =
[eTdeck_5(1,1);eTdeck_5(1,2);eTdeck_5(1,3);eTdeck_5(2,1);eTdeck_5(2,2);eTdeck
_5(2,3)];
Plant_H_10m_Joules =
[eTdeck_10(1,1);eTdeck_10(1,2);eTdeck_10(1,3);eTdeck_10(2,1);eTdeck_10(2,2);e
Tdeck_10(2,3)];

Contact =
table(Projectiles,Plant_H_0m_Joules,Plant_H_5m_Joules,Plant_H_10m_Joules)
```

Contact = 6×4 table

	Projectiles	Plant_H_0m_Joules	Plant_H_5m_Joules	...
1	"3 Fragments at 25 Deg"	475.4845	546.8334	
2	"5 Fragments at 25 Deg"	285.2907	328.1001	
3	"10 Fragments at 25 Deg"	142.6453	164.0500	
4	"3 Fragments at 45 Deg"	446.3690	565.1904	
5	"5 Fragments at 45 Deg"	267.8214	339.1142	
6	"10 Fragments at 45 Deg"	133.9107	169.5571	

```
% Remove energy below ground level
[E0] = impact(eTD{1},eTD(Jonsson),deck_0);
[E5] = impact(eTD{1},eTD(Jonsson),deck_5);
```

```
 [E10] = impact(eTD{1},eTD(Jonsson),deck_10);
 %
 % Require for presentation plot
 baseball = nan(1,length(E5));
 bullet = baseball;
 baseball(1:39) = 140;
 bullet (1:39) = 900;
 e_m5_45 = [E5(4,:);E5(5,:);E5(6,:);bullet;baseball];
 %
 fig = fig+1;
 gf = plot(distance,E0,'LineWidth',2);
 indi = {'-','-','-','-.','-.','-.'};
 [gf(:).LineStyle] = indi{:};
 grid on%,ylim([-10 300]),xlim([0 30])
 % ylim([-10 5000]),xlim([0 30])
 xlabel('Distance in metres',FontWeight='bold')
 ylabel('Energy in Joules',FontWeight='bold'),% xlim([0 30])
 title('Projectile Energy over a distance - Plant installed at ground
level','Energy level at contact with the ground','Interpreter','tex')
 h7 = legend('3 Fragments at $25^{\circ}$',  '5 Fragments at $25^{\circ}$',
'10 Fragments at $25^{\circ}$',  ' 3 Fragments at $45^{\circ}$', '5 Fragments
at $45^{\circ}$',  ' 10 Fragments at $45^{\circ}$ ',
'interpreter','latex','Location','north');
```

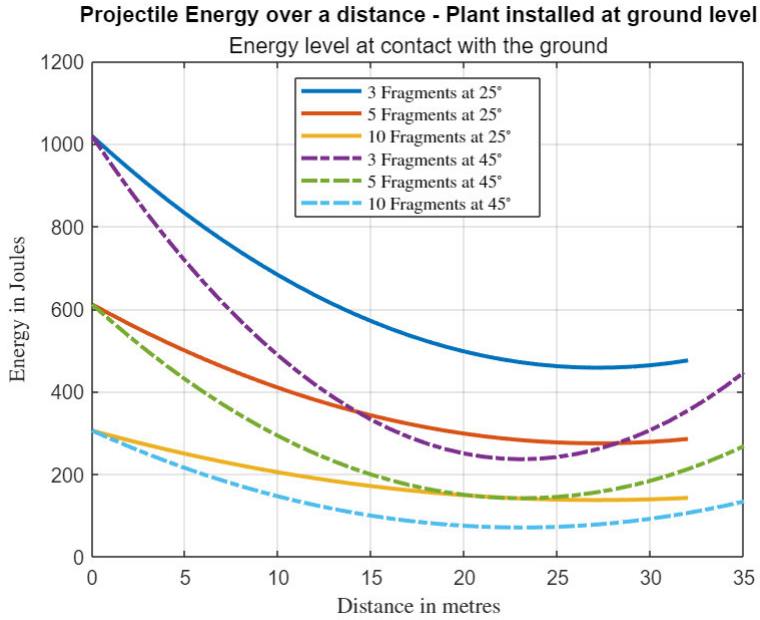


```
 fig = fig+1;
 gg = plot(distance,E5,'LineWidth',2);
 indi = {'-','-','-','-.','-.','-.'};
 [gg(:).LineStyle] = indi{:};
 grid on
 xlabel('Distance in metres',FontWeight='bold')
 ylabel('Energy in Joules',FontWeight='bold')
```

```
 title('Projectile Energy over a distance - Plant installed 5m above ground
level','Energy level at contact with the ground','Interpreter','tex')
 h8 = legend('3 Fragments at $25^{\circ}$',  '5 Fragments at $25^{\circ}$',
'10 Fragments at $25^{\circ}$',  ' 3 Fragments at $45^{\circ}$', '5 Fragments
at $45^{\circ}$',  ' 10 Fragments at $45^{\circ}$ ',
'interpreter','latex','Location','north');
```

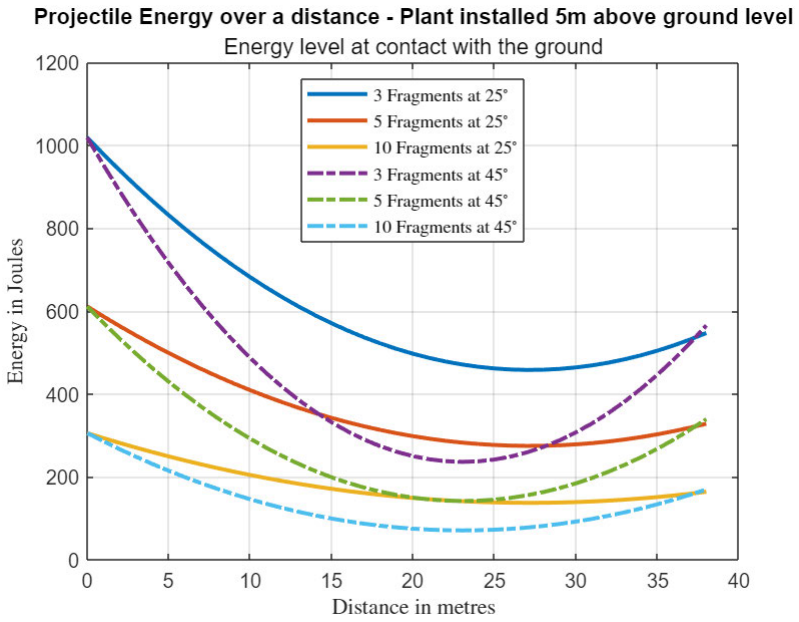


```
 fig = fig+1;
 gg = plot(distance,e_m5_45,'LineWidth',2);
 indi = {'-','-','-','-.','-.'};%,'-.'};
 [gg(:).LineStyle] = indi{:};
 grid on,ylim([0 1000]),xlim([0 40])
 xlabel('Distance in metres',FontWeight='bold')
 ylabel('Energy in Joules',FontWeight='bold')
 title('Projectile Energy over a distance - Plant installed 5m above ground
level','Energy level at contact with the ground','Interpreter','tex')
 h9 = legend(' 3 Fragments at $45^{\circ}$', '5 Fragments at $45^{\circ}$',
' 10 Fragments at $45^{\circ}$ ','Bullet','Baseball',
'interpreter','latex','Location','southwest');
 fontsize(h9,12,"points")

 legend("Position",[0.35724,0.49724,0.39286,0.26667])
```

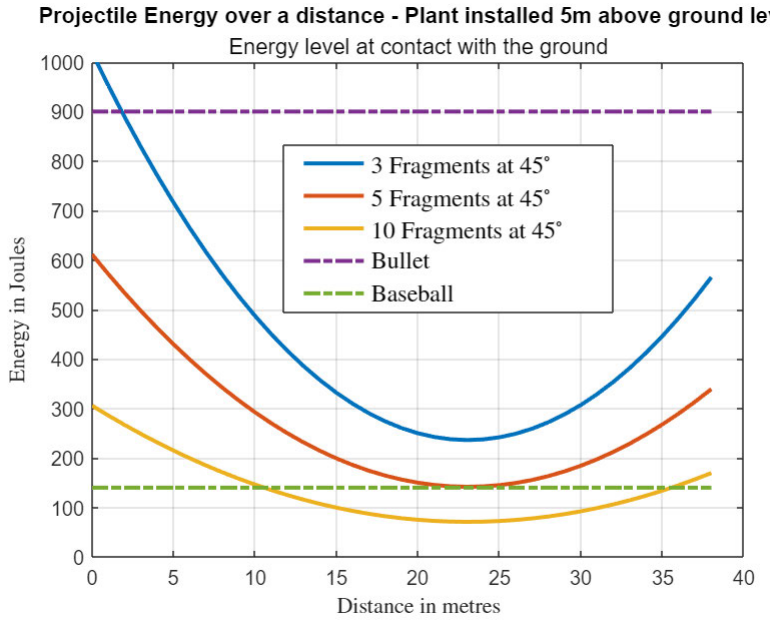


```
 % h8 = legend('3 Fragments at $25^{\circ}$',  '5 Fragments at $25^{\circ}$',
'10 Fragments at $25^{\circ}$',  ' 3 Fragments at $45^{\circ}$', '5 Fragments
at $45^{\circ}$',  ' 10 Fragments at $45^{\circ}$ ',
'interpreter','latex','Location','best');
 fig = fig+1;
 gh = plot(distance,E10,'LineWidth',2);
 indi = {'-','-','-','-.','-.','-.'};
 [gh(:).LineStyle] = indi{:};
 grid on%,ylim([-10 300]),xlim([0 30])
 xlabel('Distance in metres',FontWeight='bold')
 ylabel('Energy in Joules',FontWeight='bold')
 title('Projectile Energy over a distance - Plant installed 10m above ground
level','Energy level at contact with the ground','Interpreter','tex')
 h9 = legend('3 Fragments at $25^{\circ}$',  '5 Fragments at $25^{\circ}$',
'10 Fragments at $25^{\circ}$',  ' 3 Fragments at $45^{\circ}$', '5 Fragments
at $45^{\circ}$',  ' 10 Fragments at $45^{\circ}$ ',
'interpreter','latex','Location','best');
```

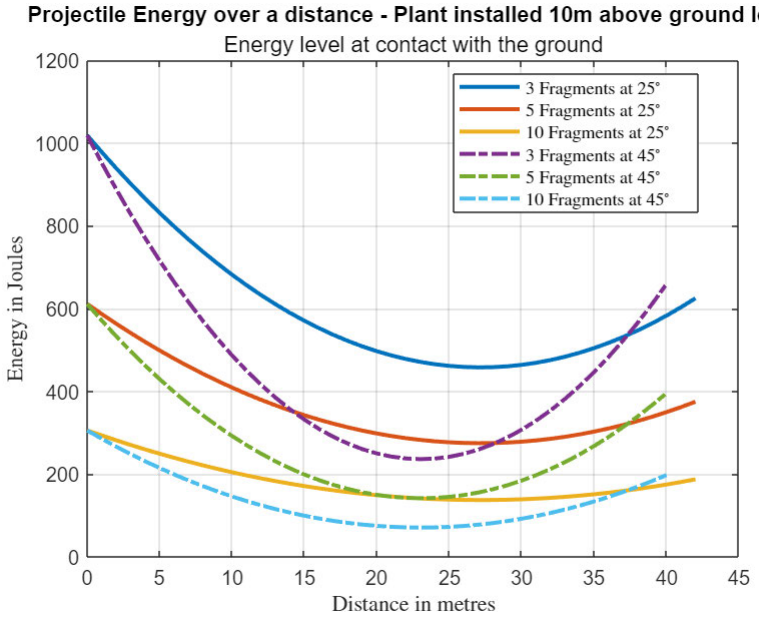

Energy & Pressure change caused by phase change

Assumption for ambient temperature $25^{o}C$

```
% Constants
K = 273.15;                     % Kelvin
T_amb = 25 + K;                 % Ambient Temperature in Kelvins
R = 8.134;                      % Universal gas constant
CU_Atomic = 63.546;             % u
R_CU = R/CU_Atomic*1e3;         % J/kg.K
%
Vinner = 0.0067;                %m^3 - Inner volume of the cylinder
%
CU_SpecificHeatCapacitySolid = 0.385;                           % kJ/kg.K
CU_SpecificHeatCapacityLiquid = 36.33 * (1/CU_Atomic) * 1e3;    % kJ/kg.K
%
CU_Temp_Fusion = 1085 + K;  % Kelvin - solid to liquid
CU_Temp_Vap = 2595 + K;     % Kelvin - liquid to gas
%
CU_LatentHeatFusion = 206;                                      % kJ/kg
CU_LatentHeatVap = (322.1 * 1e3) * (1/CU_Atomic) * 1e3;     % MJ/kg -
Enthalpy
CU_mass= 0.001;    % Copper mass in kilograms
CU_range = (0:0.001:0.1);
```

Energy = Q

Specific Heat transfer :

$$Q_{\text{Specific}} = m * C * \Delta T$$

Latent Heat :

$$Q_{\text{Latent}} = m * L$$

```
 E_tot = nan(1,length(CU_range));
 E_fus = E_tot;
 E_vap= E_tot;

 for qq = 1:length(CU_range)

     Q_Specific_Fusion = CU_range(qq) * CU_SpecificHeatCapacitySolid *
(CU_Temp_Fusion-T_amb); % kJ
     Q_lat_Fusion = CU_range(qq) * CU_LatentHeatFusion;  % kJ
     Q_Specific_Vap = CU_range(qq) * CU_SpecificHeatCapacityLiquid *
(CU_Temp_Vap - CU_Temp_Vap); % kJ
     Q_lat_Vap = CU_range(qq) * CU_LatentHeatVap;        % kJ
     E_fus(qq) = Q_Specific_Fusion + Q_lat_Fusion;       % E_Fusion in kJ
     E_vap(qq) = Q_Specific_Vap + Q_lat_Vap;             % E_Vapor in kJ
     E_tot(qq) = E_fus(qq) + E_vap(qq);                  % Totals row 3 in kJ

 end
 % points of interest
 tot_Xpoint = 0.090427175;
 tot_Ypoint = 458.410;
 g_Xpoint = 0.0170149;
 g_Ypoint = 86.255047887;
 %
 fig = fig + 1;
 plot(CU_range,E_tot*1e-3,'LineWidth',2)
 hold on
 plot(g_Xpoint,g_Ypoint,'r*',tot_Xpoint,tot_Ypoint,'m*','LineWidth',2)
 plot([tot_Xpoint,tot_Xpoint],[0.09,tot_Ypoint], 'm--','LineWidth',2)
 plot([0,tot_Xpoint],[tot_Ypoint,tot_Ypoint], 'm--','LineWidth',2)
 plot([g_Xpoint,g_Xpoint],[0.015,g_Ypoint], 'r--','LineWidth',2)
 plot([0,g_Xpoint],[g_Ypoint,g_Ypoint], 'r--','LineWidth',2)
 lgd = legend('','Porcelain tensile strength exceeded','Energy (Max) - CB
Clearing time','','Location','best');
 fontsize(lgd,12,"points")
 hold off
 xlabel('Mass of Copper in kg','Interpreter','tex')
 ylabel('Energy in kJ')
 title('Energy required for Vaporisation of Copper',' ','Interpreter','tex')
 grid on
 legend("Position",[0.24899,0.76682,0.54464,0.10595])
```

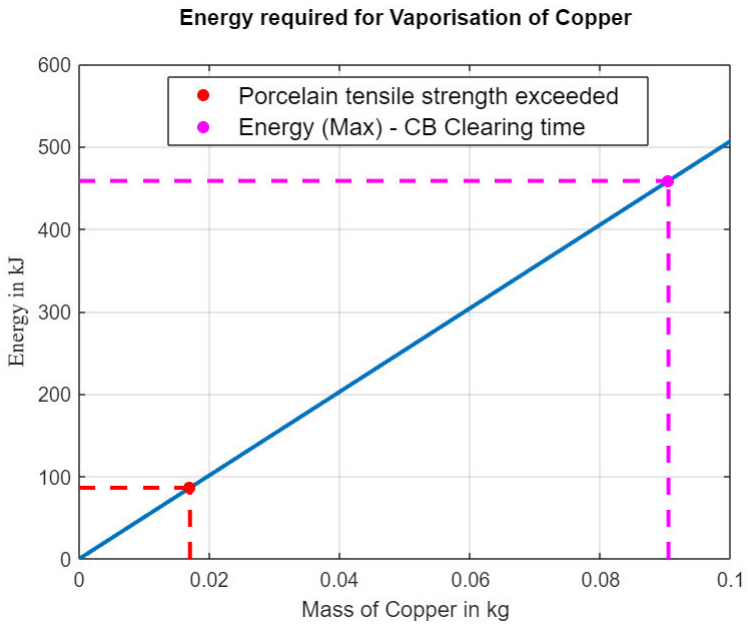

Ideal Gas

$$\text{PV} = \text{mRT}: \quad \frac{P_{\text{ressure}}}{m_{(\text{per gram})}} = \frac{R_{\text{constant}} * T_{\text{emperature}}}{V_{\text{olume}}}$$

Pressure using gradient and the density of kg of copper

$$P = \rho RT$$

```
PressureVap_PerGram = (R_CU*CU_Temp_Vap)/(Vinner);       % Pa/g or J/m^3 /g
% arc blast pressures research
% using 150 milli seconds = 458410

Tesn = 55.15806*1e6; %  Mpa
density_CU = 8830; %kg/m3
fastVapPressureWave = density_CU*R_CU*CU_Temp_Vap; % Pa/kg of copper (1000 X
atmosphere)
fastFusPressureWave = density_CU*R_CU*CU_Temp_Fusion;
df = Tesn/fastVapPressureWave; % number of kg of copper to reach the 55 mpa
dg = Tesn*1e3/fastVapPressureWave; % To melt a gram of copper
PressureFusion_PerGram = (R_CU*CU_Temp_Fusion)/(Vinner); % Pa/g or J/m^3 /g

P_tots = nan(2,length(CU_range));

for pp = 1:length(CU_range)
    %   Pressure of fusion per kg
    P_tots(1,pp) =  (R_CU*(density_CU*CU_range(pp))*CU_Temp_Fusion); % Pa/kg
    %   Pressure of Vaporisation per kg
    P_tots(2,pp) = (R_CU*(density_CU*CU_range(pp))*CU_Temp_Vap);% Pa/kg

end
```

```
% RT/V :   is the grad
fig = fig + 1;
plot(CU_range,P_tots*1e-6,'LineWidth',2)
xlabel('Mass of Copper in kg','Interpreter','tex')
ylabel('Pressure in MPa')
title('Pressure from Phase Change of Copper',' ','Interpreter','tex')
lgd1 = legend('Fusion','Vaporisation','Location','best');
fontsize(lgd1,12,"points")
grid on
legend("Position",[0.60333,0.15558,0.24821,0.10595])
```

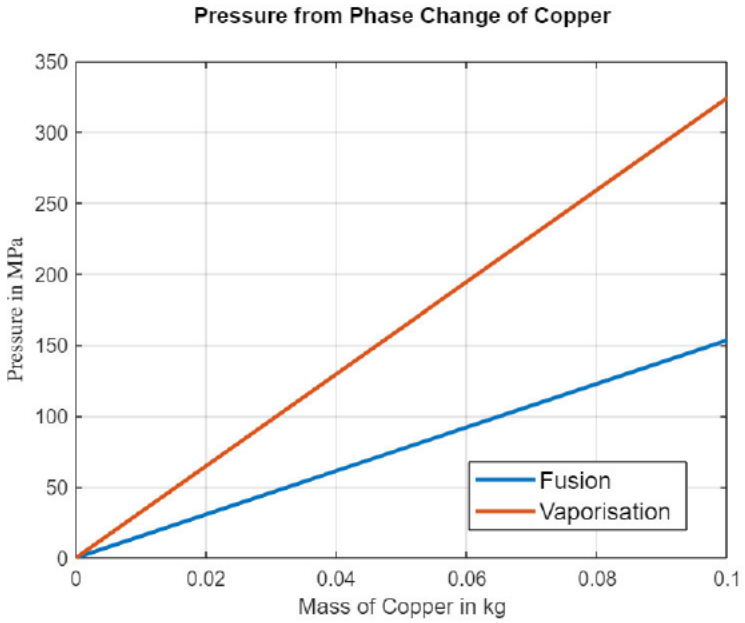


```
% Table
Energy_Phase_Per_g = ["Energy_Fusion";"Energy_Vaporisation";];
Pressure_Phase = ["Pressure_Fusion";"Pressure_Vaporisation"];
kJ = [E_fus(2); E_vap(2);];
Pa_Per_kg = [P_tots(1,2); P_tots(2,2)];
%
Phase = table(Energy_Phase_Per_g,kJ,Pressure_Phase,Pa_Per_kg)
```

Phase = 2×4 table

	Energy_Phase_Per_g	kJ	Pressure_Phase	Pa_Per_kg
1	"Energy_Fusion"	0.6141	"Pressure_Fusion"	1.5351e+06
2	"Energy_Vaporisation"	5.0688e+03	"Pressure_Vaporisation"	3.2417e+06

```
%.....................................................................%
%%
fprintf('\n%0s\n','End of Computations, :)')
```

```
End of Computations, :)
```

```
%.....................................................................%
%% End of Program
```

The function "impact" creates a solution for ploting the amount of energy at point of impact by removing the remaining values below the height of ground.

Date created : August 2023

```
function [pool] = impact(d1,d2,deck)
    d1(1,deck(1,1)+1:end) = nan;
    d1(2,deck(1,2)+1:end) = nan;
    d1(3,deck(1,3)+1:end) = nan;
    d2(1,deck(2,1)+1:end) = nan;
    d2(2,deck(2,2)+1:end) = nan;
    d2(3,deck(2,3)+1:end) = nan;
    pool = [d1;d2];
end
```

11 APPENDIX B

11.1 TIMELINES

The timelines of the project have been developed for each individual task while ensuring the progress can be easily quantified. When considering the time required to complete a task a buffer of a few weeks is also included. This allowed some flexibility for the completion of a given task and limit the possible knock-on effects that can occur with tight schedules. The initial project requirement started with the development of the research proposal document, with the final activity being the submission of the thesis. To reach the final milestone required several activities to be completed over the life of the research project. A brief overview of the activities are as follows:

- An exhaustive literature review forms a crucial part of quality research and needs to be properly documented. This activity was commenced as part of the research proposal and continued right up to the final writeup of this dissertation paper.
- The collection of historical incidents as well as the typical values for voltage, fault currents, clearing times. This process commenced at the beginning of 2023 and was successfully completed within the allotted two-month period.
- The simulation and computational analysis of both the electrical arc flash, pressure waves and projectile distances was conducted in line with the allotted perioded. The writing of the program code for the mathematical model calculations as well as the design of the Ansys simulation models. Refinement of the simulated model was conducted as required to progress the research.
- Analysis of the data from the simulation and computation was expected to be completed within a month. Further analysis was carried out during the automation activities as required.
- The creating of the automated program with a suitable user interface was allocated three months due to the amount of coding and testing that will be required. A working prototype has required additional time beyond the initial estimate.
- It was expected that the dissertation paper would be in various forms of draft as the project developed. The main writing components of the dissertation commenced

following the completion of the simulations and computations. A 3-month timeline was allocated to complete this.

- Thesis presentation was conducted in the semester 2 break period as part of Professional Practice 2. This required a suitable amount of time to prepare slides and talking points with a 4-week timeline allocated and was carried out in conjunction with the completion of this thesis.
- The submission of the thesis was the only deadline within the final month of the project. This allowed a buffer of a couple of weeks for any holdups or over runs that occurred during the research period.

The project's full timeline can be viewed in Table 1 and was reviewed weekly over the project's life. Amendments were made to Table 11.1 as required to ensure the final submission was achieved.

Table 11-1 Proposed research timeframe

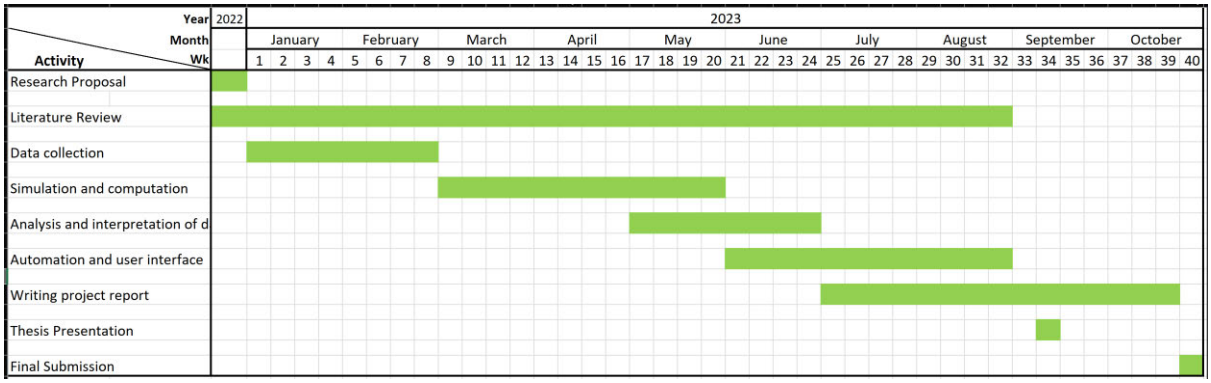

12 APPENDIX C

12.1 RISK ASSESSMENT

As part of this project a detailed risk assessment has been conducted to determine the risk associated with this research. Most of the work that will be undertaken is theoretical using computing machines. These machines will be accessed at both the university laboratories and at the researcher's residence. All work will be conducted in the indoor environment with most of the safety risks being associated around workspace ergonomics. As part of this assessment, work areas were also inspected to ensure electrical equipment inspection tags were in date and the workstation and associated equipment was fit for purpose.

Other risks to the project are based on the limited time allotted to complete the research. There are a number of unknowns associated with carrying out this research especially on the chosen topic. Successful simulation of the event being one of the highest risks. The use of Ansys Explicit Dynamics and Autodyn suites is the primary analysis tool and is believed to be the software program that could provide the best results for this research. It is a nonlinear explicit dynamics analysis tool that has many complexities that requires expertise in modelling which the researcher may not be able to develop to the required level in the available timeframe.

To both support the Ansys simulation and provide another option if the simulation was not able to meet the requirement a simplified physics based mathematical model is developed using calculated energy, velocity, time, and standard projectile formulae that are supported by a number of assumptions. This will allow for comparison between a suitable simulation solution from Ansys and redundancy if a suitable model is not able to be developed.

12.2 SAFETY RISK MANAGEMENT PLAN

University of Southern Queensland **Offline Version**

USQ Safety Risk Management System

Note: This is the offline version of the Safety Risk Management System (SRMS) Risk Management Plan (RMP) and is only to be used for planning and drafting sessions, and when working in remote areas or on field activities. It must be transferred to the online SRMS at the first opportunity.

Safety Risk Management Plan – Offline Version			
Assessment Title:	Undergraduate Research into pressure waves distances	Assessment Date:	2/03/2023
Workplace (Division/Faculty/Section):	School of Engineering	Review Date:(5 Years Max)	2/02/2024

Context			
Description:			
What is the task/event/purchase/project/procedure?	Simulations and Computations studies of electric discharges and resultant pressure wave		
Why is it being conducted?	Chase Richardson		
Where is it being conducted?	Toowoomba - Z Block Level 2, Room 213, Level 3, Room 308 and Off Campus		
Course code (if applicable)	ENG4111	Chemical name (if applicable)	Na
What other nominal conditions?			
Personnel involved	Chase Richardson		

Equipment	Computing Machines
Environment	Indoors
Other	Na
Briefly explain the procedure/process	Computational analysis will be conducted on the theoretical distances that shockwaves of a hazadous nature can travel. This will be conducted on a variety of computing machines at the locations within a number of the university's laboratories within the Zblock building as stated above and the residence of the researcher.
Assessment Team - who is conducting the assessment?	
Assessor(s)	Chase Richardson
Others consulted:	Terry Bynre, Head of the electical laboratories within ZBlock

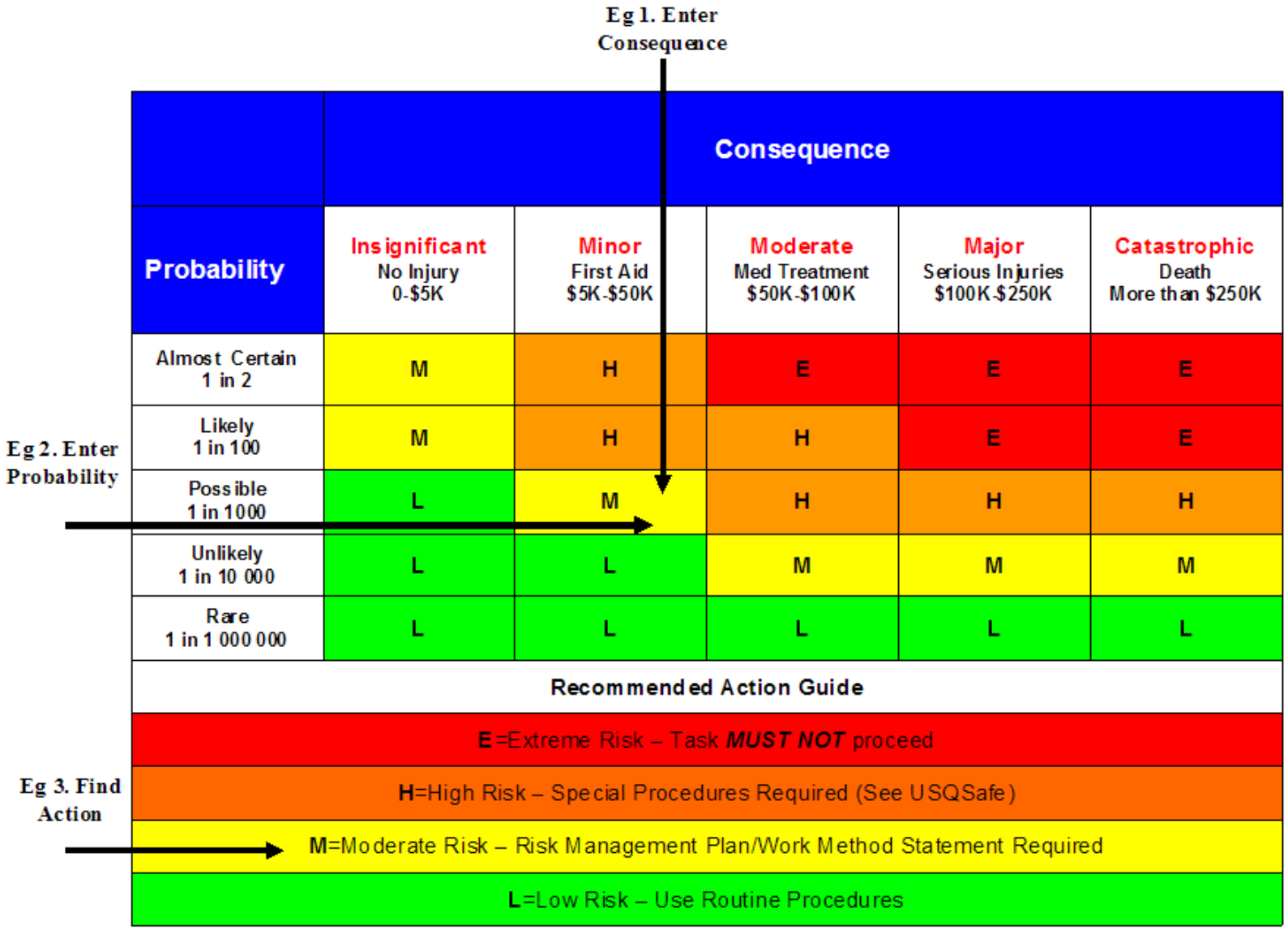

Probability	Consequence				
	Insignificant No Injury 0-$5K	Minor First Aid $5K-$50K	Moderate Med Treatment $50K-$100K	Major Serious Injuries $100K-$250K	Catastrophic Death More than $250K
Almost Certain 1 in 2	M	H	E	E	E
Likely 1 in 100	M	H	H	E	E
Possible 1 in 1000	L	M	H	H	H
Unlikely 1 in 10 000	L	L	M	M	M
Rare 1 in 1 000 000	L	L	L	L	L

Recommended Action Guide

E=Extreme Risk – Task ***MUST NOT*** proceed

H=High Risk – Special Procedures Required (See USQSafe)

M=Moderate Risk – Risk Management Plan/Work Method Statement Required

L=Low Risk – Use Routine Procedures

Step 1 (cont)	Step 2	Step 2a	Step 2b	Step 3			Step 4				
Hazards: From step 1 or more if identified	*The Risk:* What can happen if exposed to the hazard without existing controls in place?	*Consequence:* What is the harm that can be caused by the hazard without existing controls in place?	*Existing Controls:* What are the existing controls that are already in place?	*Risk Assessment:* Consequence x Probability = Risk Level			*Additional controls:* Enter additional controls if required to reduce the risk level	*Risk assessment with additional controls:*			
				Probability	**Risk Level**	**ALARP? Yes/no**		**Consequence**	**Probability**	**Risk Level**	**ALARP? Yes/no**
Example											
Working in temperatures over 35^0 C	Heat stress/heat stroke/exhaustion leading to serious personal injury/death	catastrophic	Regular breaks, chilled water available, loose clothing, fatigue management policy.	possible	high	No	temporary shade shelters, essential tasks only, close supervision, buddy system	catastrophic	unlikely	mod	Yes
Chair	Incorrect positioning or use of chair results in a fall or pain including back and or neck. Use of equipment which does not meet the Australia Standards	Major	Inspection of chair prior to use to ensure it is good working order.	Unlikely	Low	Yes or No	Chair is be removed from service if the chair is not in sound working order or allow an ergonomic seated position to be obtained. Set the seat height so that: - Feet are comfortably flat on the floor; -knees are positioned at approximately 90 degrees; and -elbows are positioned approximately 90 degrees Back Support: - ensure the back rest is positioned to meet the curve of the lower back Armrests: - If fitted ensure they do not prevent user from reaching the required distance from the desk.	Major	Rare	Low	Yes
Desk	Incorrect position of desk and use over long periods causing pain and fatigue.	Moderate	Check and adjust seating position to suit desk height. Organise desk to aviod over reaching at the workstation. Position frequently used items near by. Take regular breaks or if possible use multi height desks to allow for both standing and seating work	Unlikely	Low	Yes or No	Multi height workstation or sit-stand desk in used: Manage tranisation by checking monitor heights to ensure head is in a neutral position and adjust according to each situation.	Minor	Rare	Low	Yes

Step 1 (cont)	Step 2	Step 2a	Step 2b	Step 3			Step 4				
Hazards: From step 1 or more if identified	*The Risk:* What can happen if exposed to the hazard without existing controls in place?	*Consequence:* What is the harm that can be caused by the hazard without existing controls in place?	*Existing Controls:* What are the existing controls that are already in place?	*Risk Assessment:* Consequence x Probability = Risk Level			*Additional controls:* Enter additional controls if required to reduce the risk level	*Risk assessment with additional controls:*			
				Probability	**Risk Level**	**ALARP? Yes/no**		**Consequence**	**Probability**	**Risk Level**	**ALARP? Yes/no**
Example											
Working in temperatures over 35^0 C	Heat stress/heat stroke/exhaustion leading to serious personal injury/death	catastrophic	Regular breaks, chilled water available, loose clothing, fatigue management policy.	possible	high	No	temporary shade shelters, essential tasks only, close supervision, buddy system	catastrophic	unlikely	mod	Yes
			activities to be carried out at the workstation.								
Monitors	Incorrect position of monitor at the workstation cause pain and fatigue due to twisting to view screens and not maintaining a neutral head position	Moderate	Position monitors to allow neutral posture to minimise the need to bend the neck or lift the chin.	Unlikely	Low	Yes or No	Dual and multiple monitors arrangment are to arrange to reduce the need to twist. Orientate dual monitor in a 'V' shape	Moderate	Unlikely	Low	Yes
Posture	Seated or standing poorly causing phyical pain and fatigue	Moderate	Rest breaks from the computing machine and the workstation.	Unlikely	Low	Yes or No	Incorporate a short walk as part of a (2-3 minute) break where possible	Minor	Rare	Low	Yes
Electricity	Exposure to live wires can cause shock, burns or death from electrocution. Use of equipment which does not meet Australian Standards.	Catastrophic	Examples of types of controls: Ensure that all equipment is compliant with Australian Standards and fit for purpose. If unsure, verify compliance with an electrician before use.	Unlikely	Moderate	Yes or No	If for example, the equipment is provided and doesn't meet Australian Standards, the equipment must be certified to Australian Standards prior to use.	Catastrophic	Rare	Low	Yes

Step 1 (cont)	Step 2	Step 2a	Step 2b	Step 3			Step 4				
Hazards: From step 1 or more if identified	*The Risk:* What can happen if exposed to the hazard without existing controls in place?	*Consequence:* What is the harm that can be caused by the hazard without existing controls in place?	*Existing Controls:* What are the existing controls that are already in place?	*Risk Assessment:* Consequence x Probability = Risk Level			*Additional controls:* Enter additional controls if required to reduce the risk level	*Risk assessment with additional controls:*			
				Probability	**Risk Level**	**ALARP? Yes/no**		**Consequence**	**Probability**	**Risk Level**	**ALARP? Yes/no**
Example											
Working in temperatures over 35^{0} C	Heat stress/heat stroke/exhaustion leading to serious personal injury/death	catastrophic	Regular breaks, chilled water available, loose clothing, fatigue management policy.	possible	high	No	temporary shade shelters, essential tasks only, close supervision, buddy system	catastrophic	unlikely	mod	Yes
			Follow manufacturers instructions. Ensure all equipment is connected to an RCD and tagged/tested within the required timeframes								
Project over due	Simulation in complete	Major	Develop other types of models including a simplified projectile script	Possible	Moderate	Yes		Select a consequence	Select a probability	Select a Risk Level	Yes or No
Limited computer power	Access to HPC	Moderate	Request access and permissions early in the project	Select a probability	Select a Risk Level	Yes or No		Select a consequence	Select a probability	Select a Risk Level	Yes or No
		Select a consequence		Select a probability	Select a Risk Level	Yes or No		Select a consequence	Select a probability	Select a Risk Level	Yes or No
		Select a consequence		Select a probability	Select a Risk Level	Yes or No		Select a consequence	Select a probability	Select a Risk Level	Yes or No
		Select a consequence		Select a probability	Select a Risk Level	Yes or No		Select a consequence	Select a probability	Select a Risk Level	Yes or No
		Select a consequence		Select a probability	Select a Risk Level	Yes or No		Select a consequence	Select a probability	Select a Risk Level	Yes or No
		Select a consequence		Select a probability	Select a Risk Level	Yes or No		Select a consequence	Select a probability	Select a Risk Level	Yes or No
		Select a consequence		Select a probability	Select a Risk Level	Yes or No		Select a consequence	Select a probability	Select a Risk Level	Yes or No

Step 1 (cont)	Step 2	Step 2a	Step 2b	Step 3			Step 4				
Hazards: From step 1 or more if identified	*The Risk:* What can happen if exposed to the hazard without existing controls in place?	*Consequence:* What is the harm that can be caused by the hazard without existing controls in place?	*Existing Controls:* What are the existing controls that are already in place?	*Risk Assessment:* Consequence x Probability = Risk Level			*Additional controls:* Enter additional controls if required to reduce the risk level	*Risk assessment with additional controls:*			
				Probability	**Risk Level**	**ALARP? Yes/no**		**Consequence**	**Probability**	**Risk Level**	**ALARP? Yes/no**
Example											
Working in temperatures over 35^0 C	Heat stress/heat stroke/exhaustion leading to serious personal injury/death	catastrophic	Regular breaks, chilled water available, loose clothing, fatigue management policy.	possible	high	No	temporary shade shelters, essential tasks only, close supervision, buddy system	catastrophic	unlikely	mod	Yes
				Select a probability	Select a Risk Level	Yes or No		Select a consequence	Select a probability	Select a Risk Level	Yes or No
				Select a probability	Select a Risk Level	Yes or No		Select a consequence	Select a probability	Select a Risk Level	Yes or No
				Select a probability	Select a Risk Level	Yes or No		Select a consequence	Select a probability	Select a Risk Level	Yes or No
				Select a probability	Select a Risk Level	Yes or No		Select a consequence	Select a probability	Select a Risk Level	Yes or No
				Select a probability	Select a Risk Level	Yes or No		Select a consequence	Select a probability	Select a Risk Level	Yes or No

Step 5 - Action Plan (for controls not already in place)			
Additional controls:	*Resources:*	*Persons responsible:*	*Proposed implementation date:*
			Click here to enter a date.
			Click here to enter a date.
			Click here to enter a date.
			Click here to enter a date.
			Click here to enter a date.
			Click here to enter a date.
			Click here to enter a date.
			Click here to enter a date.
			Click here to enter a date.
			Click here to enter a date.
			Click here to enter a date.
			Click here to enter a date.

Step 6 - Approval			
Drafter's name:	Chase Richardson	Draft date:	1/10/2022

Drafter's comments:				
Approver's name:		Approver's title/position:		
Approver's comments:				
I am satisfied that the risks are as low as reasonably practicable and that the resources required will be provided.				
Approver's signature:			Approval date:	Click here to enter a date.